

H4. SMR/1247
Lecture Note: 23

**WORKSHOP ON PHYSICS OF
MESOSPHERE-STRATOSPHERE-TROPOSPHERE
INTERACTIONS WITH SPECIAL EMPHASIS ON MST
RADAR TECHNIQUES**

(13 - 24 November 2000)

GRAVITY WAVES IN THE EARTH'S ATMOSPHERE

Prof. W. K. Hocking

Dept. of Physics
University of Western Ontario
London, Ontario
CANADA

GRAVITY WAVES IN THE EARTH'S ATMOSPHERE.

We now turn our attention to
more "organized" dynamical
motions in the Earth's atmosphere.

GRAVITY WAVES IN THE EARTH'S ATMOSPHERE.

We now turn our attention to
more "organized" dynamical
motions in the Earth's atmosphere.

MST STUDIES OF GRAVITY WAVES AND TURBULENCE

W.K. Hocking

6.1. INTRODUCTION

On horizontal scales of a few hundreds of kilometres and less, and vertical scales of less than a few tens of kilometres, the main dynamical motions in the upper atmosphere are those due to gravity waves and turbulence. These two types of motions have important implications for the energetics of the whole region. Gravity waves in particular affect the winds at larger scales, and even the latitudinal temperature distribution. In this lecture, we will discuss the techniques used to measure these motions, particularly with regard to radar applications.

In this section, we discuss the theory and nature of gravity waves.

6.1.1 An introduction to gravity waves

It is generally believed that gravity waves (also called buoyancy waves) are the main cause of wind and temperature fluctuations with periods of a few hours and less, down to a few minutes. There is a school of thought which suggests that at least some of these motions are due to two-dimensional turbulence, but this is a minority view. We will nevertheless discuss this approach briefly in the section on turbulence, but for the moment let us begin with an account of what gravity waves are, and a brief summary of their role in atmospheric dynamics.

Gravity waves are atmospheric waves which propagate in the free air. Individual waves cause velocity, pressure and density fluctuations of a sinusoidal nature, and these waves carry momentum flux and energy with them as they propagate. The waves are observed as quasi-sinusoidal oscillations in wind velocity and temperature as a function of both time and height; an example of the vertical velocity component of the wind is shown in fig. [1]. They are generated in a multitude of ways, but the simplest way to visualize them is as the waves generated by flow of air over a corrugated boundary. The air begins to oscillate over the corrugations, and in so doing generates propagating waves. The waves have the curious property that the phase velocity and group velocity are almost perpendicular to each other, and when the phase group velocity is upward, the phase velocity is downward. If such a wave loses no energy as it propagates, then the exponential decrease of atmospheric density with increasing height results in an exponential increase of amplitude with increasing height, so that waves which start at ground level with amplitudes of a few centimetres per second attain amplitudes of several tens of metres per second at altitudes of 70 km and above. In reality the waves do in fact lose some energy and momentum as they rise in height, but the most dramatic losses are in the regions above 70 km altitude. The waves are important in the atmosphere because of this loss of momentum and energy which occurs as they propagate; the momentum and energy are deposited in the atmosphere and affect both the mean winds and the temperature distribution. In particular, the momentum deposited by the waves acts to alter the mean eastward (zonal) winds, in some cases even reversing them compared to the direction expected on the basis of radiative theory alone. This

changed zonal wind then drives a north-south (meridional) wind circulation, and this in turn causes upwelling at some latitudes and down-welling at others. As a result, the temperatures in the upper mesosphere are also substantially altered relative to their radiative situation, and one dramatic result of note is the phenomenon of the polar summer mesopause becoming much colder than even the winter polar mesopause. More detail about the way in which these waves modify the mean wind circulation and thence the latitudinal temperature distribution can be found in Holton (1982, 1983), and will be elaborated upon later in this article.

The waves show other interesting properties. For example, although there are seasonal variations in wave intensity, there is also a remarkable degree of consistency in wave activity. From summer to winter the variation in amplitude is less than a factor of 3, and the variations as a function of latitude are also relatively small. The distribution of wave power densities as a function of period and wave number also seems to be somewhat independent of latitude and season. It seems the waves can be described by a common "universal" spectrum of almost invariant shape and amplitude, and the term "universal spectrum" is often encountered in the literature (Van Zandt, 1982). We will consider this universality in more detail in due course.

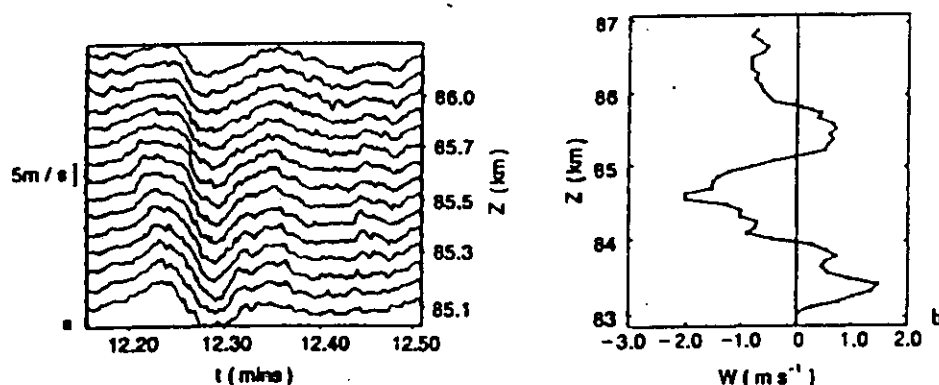


Fig. 1. Example of vertical velocity fluctuations w as a function of a time t and b height z in the mesosphere. (Czechowsky et al. 1989)

6.2. GENERAL THEORY

In the following section, we will discuss just how gravity waves arise from the fluid dynamical equations, and then consider the various quantities which can be measured in connection with these motions. Discussion of typical scales will be left to a later section which deals with experimental results.

6.2.1 The fluid dynamical equations of motion.

The equations considered are the standard fluid-dynamical equations

$$\frac{D\mathbf{u}}{Dt} + 2\mathbf{\Omega} \times \mathbf{u} + \mathbf{g} + \frac{1}{\rho} \nabla p - \nu \nabla^2 \mathbf{u} = 0 \quad (1)$$

$$\frac{D\rho}{Dt} = \frac{1}{c_s^2} \frac{Dp}{Dt} \quad (2)$$

$$\frac{D\rho}{Dt} + \rho \nabla \cdot \mathbf{u} = 0 \quad (3)$$

$$\frac{D\Theta}{Dt} = \frac{\kappa}{\rho} \nabla^2 \Theta \quad (4)$$

where D/Dt represents differentiation following the motion. The total velocity is \mathbf{u} , the density ρ , $\mathbf{\Omega}$ is the Earth's angular rotation rate, \times means cross product, \mathbf{g} is the acceleration due to gravity $= (0,0,-g)$, p is the pressure, c_s^2 is the speed of sound squared, ∇ represents the gradient differential operator and " \cdot " means the dot product. Θ represents potential temperature, κ the heat diffusion coefficient, and ν is the kinematic viscosity coefficient.

In the following sections, it will be briefly shown how these equations are modified for dealing with gravity waves and turbulence, and the important parameters required in any useful study will be defined.

6.2.2 The approximations of the equations of motion for gravity wave studies

The above equations describe the motions for all fluids, but it is often useful to simplify them somewhat to study particular types of flow. One example is the study of wave events, in which the equations are linearized and solved for solutions of the type $\exp\{i(\mathbf{k} \cdot \mathbf{x} - \omega t + \phi)\}$. Examples of such solutions include planetary waves, tides, buoyancy (gravity) waves and vortical modes (e.g. Houghton, 1977; Gossard and Hooke, 1975; Hines, 1960; Dong and Yeh, 1988; Yeh and Dong, 1989). These are all important for the upper atmosphere, and some of them carry momentum and energy from source regions like the troposphere to the stratosphere and mesosphere. Gravity waves are particularly important, and indeed the momentum flux deposited in the mesosphere by these waves is enough to completely alter the mean flow state at those heights (Matsuno, 1981; Holton, 1982, 1983).

In the case of gravity waves, one assumes solutions of the form $\varphi = \varphi_0 \exp\{i(\mathbf{k} \cdot \mathbf{x} - \omega t + \phi)\}$, (where φ can be any one of the velocity components, the pressure, the density or temperature), and then substitutes into the equations of motion, retaining only first order terms. As a result, one finds that various waves can indeed exist, but they must also satisfy particular relations between the wave frequency and wavenumbers; the so-called "dispersion relation". In particular, waves are confined to have intrinsic frequencies in the range between the "Vaisala-Brunt" frequency (the natural frequency of oscillation of a displaced air parcel in the atmosphere - typically in the range 5 to 10 mins below 100 km altitude) and the "inertial frequency", the lower frequency limit set by the Coriolis parameter. The relations between wave velocity amplitudes and the temperature, density and pressure amplitudes are also defined uniquely by these equations, and these relations are called "polarization relations". There are also different levels of approximation, depending on whether particular terms are ignored or retained in the linearized approximations of the equations of motions, and the dispersion relations and the polarization relations differ slightly depending on the form of the equations used. Examples include the "Boussinesq" approximation (the simplest), the "hydrostatic" approximation, and the "anelastic" approximation.

We begin our treatment by "linearizing" the afore-mentioned equations, as well as ignoring the term $\nu \nabla^2 \underline{u}$. (The latter term represents viscous dissipation effects, which are usually unimportant at the scales of interest to us). This means we consider only small perturbations, and ignore second-order terms.

The general form of the equations is then

$$\frac{\partial u'}{\partial t} - f v' = -\frac{\partial \psi'}{\partial x} \quad (5)$$

$$\frac{\partial v'}{\partial t} + f u' = -\frac{\partial \psi'}{\partial y} \quad (6)$$

$$\frac{\partial w'}{\partial t} + r' g = -\left(\frac{\partial}{\partial z} \psi' - \frac{\psi'}{H}\right) \quad (7)$$

$$\frac{\partial r'}{\partial t} - w' \frac{N^2}{g} = \frac{1}{c_s^2} \frac{\partial \psi'}{\partial t} \quad (8)$$

$$\frac{\partial r'}{\partial t} + \frac{\partial u'}{\partial x} - \frac{w'}{H} + \frac{\partial w'}{\partial z} = 0 \quad (9)$$

Equations (5) through (7) are the momentum equations, (8) is a form of the first law of thermodynamics, and (9) is the continuity equation. The complex velocity amplitude is (u', v', w') . Additionally, we use the definitions $\psi' = p'/\bar{\rho}$, and $r' = \rho'/\bar{\rho}$. N is the Brunt-Väisälä frequency given by

$$N^2 = \frac{g}{\bar{T}} \frac{\partial \bar{T}}{\partial z} + \kappa \frac{g}{\bar{H}} \quad (10)$$

Here \bar{H} is the scale height given by

$$\bar{H} = \frac{R \bar{T}}{g} \quad (11)$$

g is the acceleration due to gravity, ρ is density, p is pressure, c_s^2 is the speed of sound, and $\kappa = R/c_p$, where R is the gas constant for air and c_p is the specific heat of air at constant pressure.

The quantity f is the Coriolis parameter. Overbars refer to time-averaged quantities and primes refer to deviations therefrom.

The governing equations describe two-dimensional nonhydrostatic compressible flow on an f plane. We have taken variable as the sum of a mean and fluctuating component $\bar{\varphi}_0 + \varphi'_0$.

We now assume solutions of the form $\varphi'(x, z, t) = \varphi'_0 \exp\{i(kx + mz - \omega t)\}$, where ^{we} ~~we~~ redefine the x axis to be along the horizontal direction in the plane of propagation of the wave. We recognize that we have dropped terms involving second-order quantities, and whilst these will not drastically alter things like the relation between wavelengths and frequencies (the so-called dispersion relations), they can cause wave-damping. Inclusion of them complicates the equations, so we often take an intermediate approach to consideration of their effects. We do this by assuming that all these terms can be lumped together as a so-called *Rayleigh drag*; in other words, we write these dissipative terms as equal to a constant multiplied by the wind speed. Thus in the x -component, we add a term " $-\alpha u$ ", and so forth. We often do not bother with this term for vertical fluctuations.

Thus by using complex exponential (sinusoidal) solutions, and including Rayleigh drag, we produce the following resultant algebraic equations (note that we have assumed that $\bar{u}_0 = 0$):

$$-i\omega u' - f v' = -ik\psi' - \alpha u' \quad (12)$$

$$-i\omega v' + f u' = \alpha v' \quad \left(\frac{d\psi'}{dy} = 0 \text{ for our wave}\right) \quad (13)$$

$$-i\omega w' + r'g = -(im\psi' - \psi'/\bar{H}) \quad (14)$$

$$-i\omega r' - w'\bar{N}^2/g = \frac{1}{c_s^2}(i\omega\psi') \quad (15)$$

$$-i\omega r' + iku' - w'/\bar{H} + imw' = 0. \quad (16)$$

These are the basic equations one normally works with in dealing with gravity wave theory. There are also various simplifications of these equations which are also employed.

We will leave these equations here, and now turn to simplifications of the equations to highlight the effects of turbulence. We will then return to a more detailed solution of the equations as they relate to both gravity waves and turbulence.

6.3 SOLUTIONS

6.3.1 Solution of the gravity wave equations

We now return to our equations for gravity wave motion (equations (12) - (16)).

These are actually an algebraic matrix equation. When it is solved, one finds relations between the various quantities like p' , ρ' , u' etc., as well as an *additional* expression which relates the frequency and wavelengths. This latter term is called the *dispersion relation*.

The dispersion relation for this system is

$$\bar{m}(\bar{m} + i/\bar{H}) = \frac{\omega_*}{\omega} \cdot \frac{(N^2 - \omega^2)}{(\omega_*^2 - f^2)} k^2 + \frac{\omega^2}{c_s^2} \quad (20)$$

where $\bar{m} = m - i2/\bar{H}$ and ω_* is defined as $\omega + i\alpha$ (Hines 1960; Pitteway and Hines 1963). If $\alpha = 0$, then $\bar{m}_i = -1/2H$.

The associated polarization relations are listed below:

$$v' = -(if/\omega_*)u' \quad (21)$$

$$w' = - \left\{ \frac{\omega(\omega_*^2 - f^2)}{\omega_*(N^2 - \omega^2)k} \left[\bar{m} + i \left(\frac{1}{\bar{H}} - \frac{g}{c_s^2} \right) \right] \right\} u' \quad (22)$$

$$\psi' = [(\omega_*^2 - f^2)/(\omega_*k)]u' \quad (23)$$

$$r' = \frac{k}{\omega}u' + \left(\frac{\bar{m}}{\omega} + \frac{i}{\omega\bar{H}} \right) w'. \quad (24)$$

Under various assumptions, these can be simplified even further. For example, we might assume zero damping, and small phase speeds relative to the speed of sound. The simplest (Boussinesq) dispersion relation then takes the form

$$\frac{m^2}{k^2} = \frac{N^2 - \omega^2}{\omega^2 - f^2} \quad (25)$$

For a wide range of frequencies, somewhat larger than f and somewhat smaller than N , this dispersion relation can be reasonably well approximated by

$$\frac{m}{k} \simeq \frac{N}{\omega} \quad (26)$$

In the above and following relations, the following symbols apply:- (u' , v' , w') = velocity perturbations, $i = \sqrt{-1}$, ω = angular frequency, k is the horizontal wavenumber in the direction of wave propagation, m is the vertical wavenumber, Θ' = potential temperature perturbation, ρ' = density perturbation of a parcel of air displaced by the wave relative to the surrounding air (although the air is assumed incompressible, density fluctuations due to the vertical displacement of air are allowed), ρ_0 = mean density, p' is the pressure fluctuation due to the wave, N is the Vaisala-Brunt frequency, and f is the inertial frequency = $2\Omega \sin \theta_L$, where θ_L is the latitude. The term \bar{u} refers to the mean horizontal wind at the height of observation, and c is the horizontal phase speed of the wave as seen

from the ground. Hence $c - \bar{u} = \omega/k$ is the so-called "intrinsic phase speed" of the wave, or the wave phase speed with respect to the mean wind at the height of the wave.

The following equations serve as useful approximations to the polarization relations. These are not all exact, but nevertheless they are often useful because they are extremely simple, yet still apply fairly accurately over a wide range of frequencies. They are particularly good at frequencies of more than about 3 times the "Vaisala-Brunt" frequency.

$$w' = -(k/m)u' \quad (27)$$

$$v' = i f u' / \omega \quad (28)$$

$$\Theta' = \frac{-i u'}{m(\bar{u} - c)} \cdot \frac{d\bar{\Theta}}{dz} = \frac{-i u'}{\omega} \frac{d\bar{\Theta}}{dz} = -\frac{i w'}{\omega} \frac{N^2}{g} \bar{\Theta} \quad (29)$$

$$\Theta' / \bar{\Theta} = -\rho' / \rho_0 \quad (30)$$

$$p' = -u' \rho_0 (c - \bar{u}) \quad (31)$$

The first two equations (for v' and w') are exact for the Boussinesq approximation, whilst the last three are really only valid for $f \ll \omega \ll N$; they do, however, apply quite well over most of the range of observed frequencies.

Some of the most important parameters required in studies of gravity waves are the velocity fluctuations, and the temperature, density and pressure fluctuations. The wave periods (or frequencies), the vertical and horizontal wavelengths, and the direction of propagation are also sought-after quantities; so are the momentum flux terms. Examples of the latter include terms like $\overline{\rho u' w'}$, where the overbar may be either a space or time average (see the discussion relating to the fluid equations for turbulence (section 6.2.3)). This particular term refers to the vertical flux of eastward momentum, and also the eastward flux of vertical momentum. Terms like $\overline{p' w'}$ refer to the flux of energy - in this case vertical. One other useful quantity is the preferred direction of wave propagation.

The momentum flux terms can also be used to determine body forces in the atmosphere, and it is these forces which can act on and change the mean flow, as discussed earlier. For example, $d/dz(\overline{\rho u' w'})$ gives the drag force per unit volume. This force acts on the atmosphere in which the wave is dissipating, and can substantially alter the mean wind. The drag force per unit mass is obtained by dividing by ρ .

232

6.3.1.1 Special circumstances for gravity waves - critical levels, turning levels.

As a wave propagates up into the atmosphere, the background wind may change. The frequency and horizontal wavelength as viewed from the ground stay unchanged, so the ground-based horizontal phase speed c_g stays unchanged. Thus the *intrinsic* phase speed must change as \bar{u} changes. Since the horizontal wavelength stays unchanged, then ω , the intrinsic frequency (ie the frequency as seen from the frame of reference of the mean wind) must also change. This means that the vertical wavelength must also change as the wave propagates upward, as evidenced by the various dispersion relations we have seen. If we take the simplest form as given by equation (25) viz.

$$\frac{m^2}{k^2} = \frac{N^2 - \omega^2}{\omega^2 - f^2} \quad (32)$$

then we see that there are some critical "special cases".

First, we note that if ω tends towards f (low frequencies, approaching zero) then $\omega^2 - f^2$ tends to zero and m tends to infinity. Thus the vertical wavelength approaches zero. This also corresponds to the case of the intrinsic phase speed tending towards zero. In this case, the *vertical component of the group velocity* of the wave tends to zero too, and the wave starts to "pile up" on itself. This produces large amplitudes, as the wave energy from below enters the region at a faster rate than that at which the energy leaves above. As a result, the wave achieves large amplitudes and generally breaks down. If the wave actually reaches the region where $(c - \bar{u})$ equals zero, this is called a *critical level*. In reality, waves usually break down before they reach this level.

Secondly, we note that the frequency may approach N (ie high values). When this happens, m tends to zero. The vertical wavelength tends to a very large value, and as it happens the group velocity tends towards vertical. The phase velocity tends towards horizontal, and the wavefronts become nearly vertical. Waves in this situation can "turn around" and head back down (if they were originally moving up), so this situation is called a *turning level*. Waves in the upper atmosphere can often be "ducted", which means they bounce back and forth between two turning levels at different heights in the atmosphere, whilst also traveling horizontally. Waves can travel for thousands of kilometres in this mode - and many observations of waves with large vertical wavelengths are in fact ducted waves. Ground-based ^{active} optical instruments are particularly susceptible to detection of ducted waves.

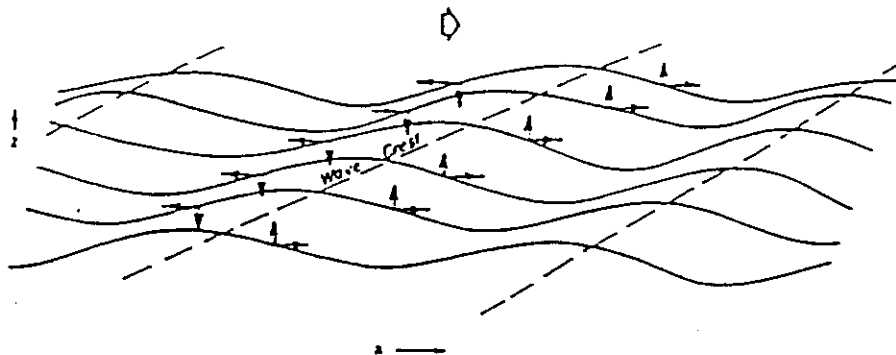
6.4 Visualization of the motions.

6.4.1 Visualization of gravity waves

Visualization of gravity wave motions is modestly straight-forward for anyone who is able to visualize wave motions. Fig. 5 shows a collection of useful diagrams. The key points which FIGS distinguish gravity waves from other waves are that

- (i) they grow exponentially with height
- (ii) their phase and group velocities are almost perpendicular.

The attached diagrams demonstrate these points. (Dunkerton, Hines).



Parcel motion in untrapped wave system propagating to the right.

Fig. 5a.

DUNKERTON, JAS, 38, 281-297 (1961)

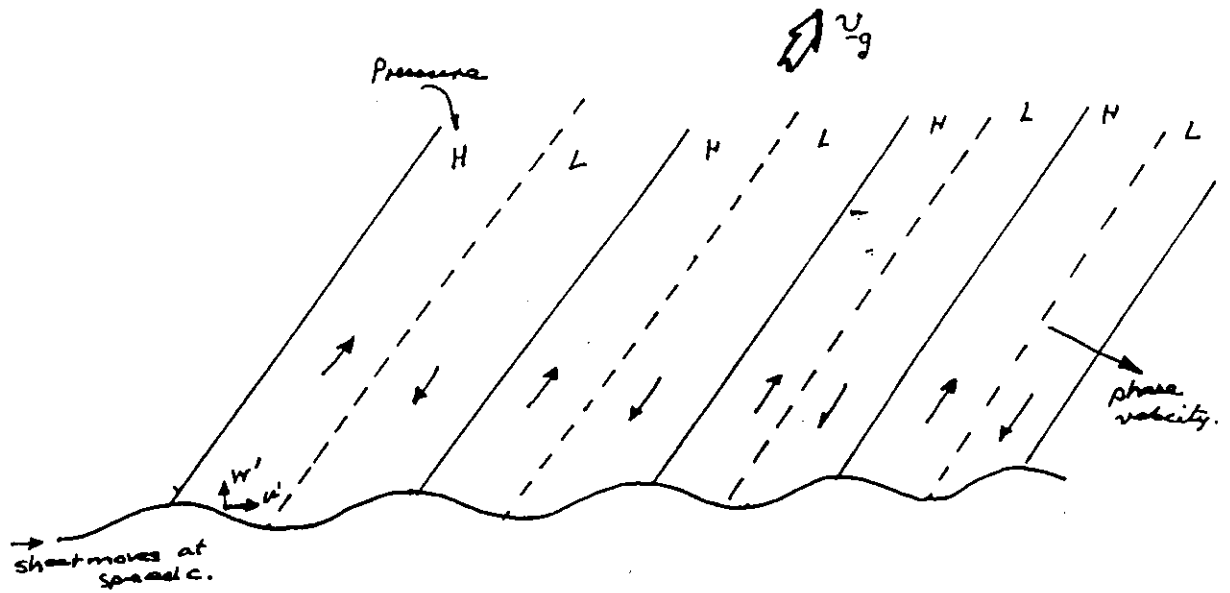


Fig. 5b.

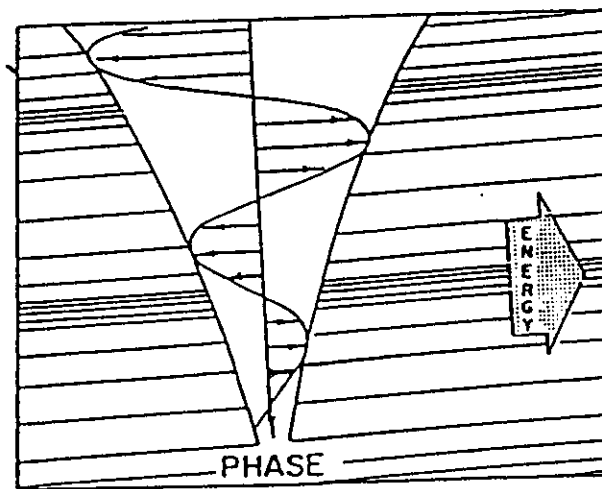


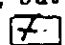
Fig 5c. Exponential growth with height.

6.5 SPECTRA

Both gravity wave and turbulence studies involve determinations of relevant spectra at some stage. The nature of these spectra, and the ways in which they are interpreted, are very different. In this section, we will consider these functions.

6.5.1 The "Universal Spectrum" and saturation theory

We first turn to a discussion about gravity waves and their relevant spectra. Previously we have considered single waves, and examined their polarization and dispersion relations. Many early studies concentrated solely on monochromatic events, but the recognition that the atmosphere contains a large number of waves at any one time forces us to consider spectral representation of these motions.

To begin this section, however, let us recourse to a little history on the subject of these motions. The concept of gravity waves as a major contributor to motions in the upper atmosphere was first introduced by Hines, (1960), and that paper has led to many publications describing wave motions in that region. Initially most studies concentrated on individual "sightings" of single quasi-monochromatic waves, and these have been discussed in various reviews (e.g. Rastogi, 1981; Fukao et al., 1979; Vincent and Ball, 1977, to list but a few). However a major change in the "monochromatic" approach to gravity wave studies came about in 1982 with the proposal by Van Zandt, (1982) that the spectral distribution of wave energies was not a strong function of latitude, longitude or time of year, but was in fact almost invariant. Van Zandt, (1982) described an empirical form for this spectrum, adopting a modification of the so-called "universal spectrum" originally proposed for internal waves in the oceans (Garrett and Munk, 1972; Garrett and Munk, 1975). It was found that not only were the spectral shapes independent of position, time and underlying terrain, but also the absolute values at any one altitude were fairly insensitive to position and time. Fig.  7 shows spectra of wave energy densities plotted as a function of frequency for wave motions at 85 km altitude, using data recorded at 35°S, 10°S and 65°N. Clearly the absolute spectral densities are similar at all 3 latitudes. The work by Van Zandt, (1982) noted similar agreement not only as a function of frequency but also as a function of wave number. The forms of the spectra proposed by Van Zandt, (1982) are:

$$E(k, \omega) = E_0 \frac{c^*}{[1 + k/k_*]^p} \cdot \frac{2}{\pi} \omega_i \frac{\omega^{-t}}{k_*} \quad (56)$$

and

$$E(m, \omega) = E_0 \frac{c^*}{[1 + m/m_*]^q} \cdot \frac{2}{\pi} \omega_i \frac{\omega^{-t}}{m_*} \quad (57)$$

Note that in this case, k and m are taken as inverse wavelengths ($1/\lambda_x, 1/\lambda_y$), rather than ($2\pi/\lambda_x, 2\pi/\lambda_y$), although this definition is somewhat unconventional.

If the spectrum is separable, then it can be shown that p must equal q . Van Zandt, (1982) proposed that $p=2.4$, $t=5/3$, $q=2.4$ and $c_*=1.4$ if m and k are in units of cycles per metre, but these determinations were based on a small amount of data, primarily data collected in the

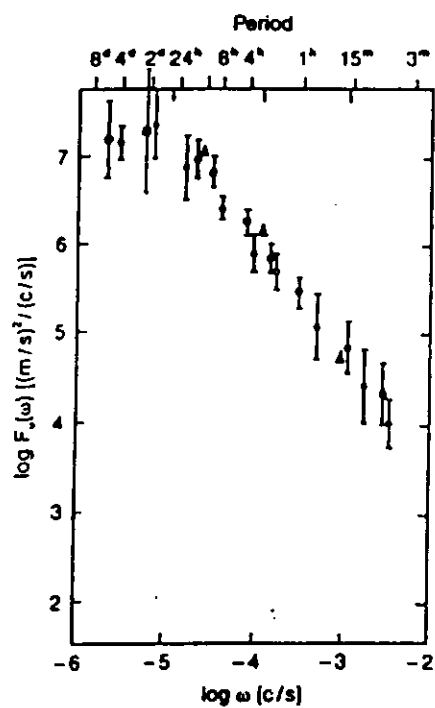


Figure 7. Some different spectra of horizontal velocity fluctuations as a function of frequency for an altitude of around 85 km. The data are for 65°N (triangles), 35°S (filled circles) and 10°S (open circles). (Van Zandt 1985)

FIG. 7

troposphere. More recent results suggest that t is around 1.5 - 2, while p and q may be about 2 - 3. Van Zandt, (1982) also took m_* to be about 10^{-4} cycles per metre, corresponding to a vertical wavelength of about 10 km. The quantities m_* and k_* represent typical values which separate the "high" wavenumber part of the spectrum (where the spectrum is almost of the form m^{-q} or k^{-p}) and the "low" wavenumber part (where E is almost independent of m or k). It should be emphasized that a value for $m_* = 10^{-4}$ cycles per metre applies only in the troposphere, and changes as a function of altitude. Sidi et al., (1988) have recently suggested refinements and improvements to the above model, but the concept of a universal spectrum still applies.

Further developments in this area have been to consider the assumption of separability (e.g. Gardner, 1997) and to try and develop a stronger theoretical explanation for the reasons for this spectrum (e.g. Dewan and Good??; Smith et al., 1987??; Hines, early 1990's). Dewan (GRL, 1997; JGR, 1997/8) has also further developed a similitude approach to understanding the spectrum, and has produced additional relationships between wave-numbers and frequencies over and above the standard dispersion relations. We will not dwell on these points here; they represent discussions beyond the scope of the current course. However, a true scholar of gravity wave studies should most certainly pursue and investigate these articles.

Many studies made in the 1980's and 1990's have concentrated on examining spectra of wave motions (e.g. Van Zandt, 1985; Scheffler and Liu, 1985; Smith and Van Zandt, 1985; Vincent, 1984; Nastrom et al., 1987; Fritts and Vincent, 1987; Meek et al., 1985; Dewan et al., 1984). Considerable progress has been made in determining to what degree the wave spectrum can be really described as "universal". In brief, it has been found that whilst there is some degree of "universality", there is still some departure from this, but not by more than a factor of 3 or 4 at any one height. For example, the GASP experiments (Nastrom et al., 1987, 1992??) found wave activity in the upper atmosphere to be 2-3 times greater over mountainous terrain than over flat land or the sea. Studies of wave activity as a function of season in the mesosphere have also shown variations of a factor of 2 or 3, and these will be reported later.

The spectra also tend to grow in spectral density with increasing height, but once above about 70 km altitude there is a tendency for the wave amplitudes to become more constant, as if the atmosphere is "saturated" with waves and cannot tolerate any more. For this to be so, the waves must lose energy as they propagate upwards, and it seems likely that as they grow, they become unstable, cause small amounts of turbulence, lose energy and thereby reduce their amplitude to become stable once again. This process repeats at various altitudes, with the actual altitudes at which breaking occurs depending on the way in which the waves add up. This is to say, at any one altitude the resultant velocity and temperature profiles are due to the sum of all contributing waves, and at some altitudes they will add in such a way as to give an unstable Richardson number (depending on the phases of the waves). At this altitude, turbulence will occur, while at other nearby altitudes the arrangement of phases may not result in instability. Desaubies and Smith, (1982) have studied processes of this type, and examined the statistics and expectation of regions of instability arising. These patches of turbulence occur in much the same way as whitecaps appear on the surface of the ocean. Similar studies in the atmosphere have been discussed by Hocking, (1991: JGG) and Fairall et al., (JAS. 1991), (Figure 8a)

The nett result of this process is that the mean wave amplitudes tend to be somewhat constant as a function of altitude above about 70 km and up to 100 km altitude. This "saturation theory" has been proposed and reported in several papers (Dewan and Good, 1986; Smith et al., 1987; Weinstock, 1984; Tsuda et al., 1989; Fritts and Chou, 1987). It is also found that there is a "rollover" vertical wavelength as a function of altitude, and at wavelengths much lower than this value the spectral shape is of the form m^{-q} , whilst at much longer vertical wavelengths the spectral shape is nearer to

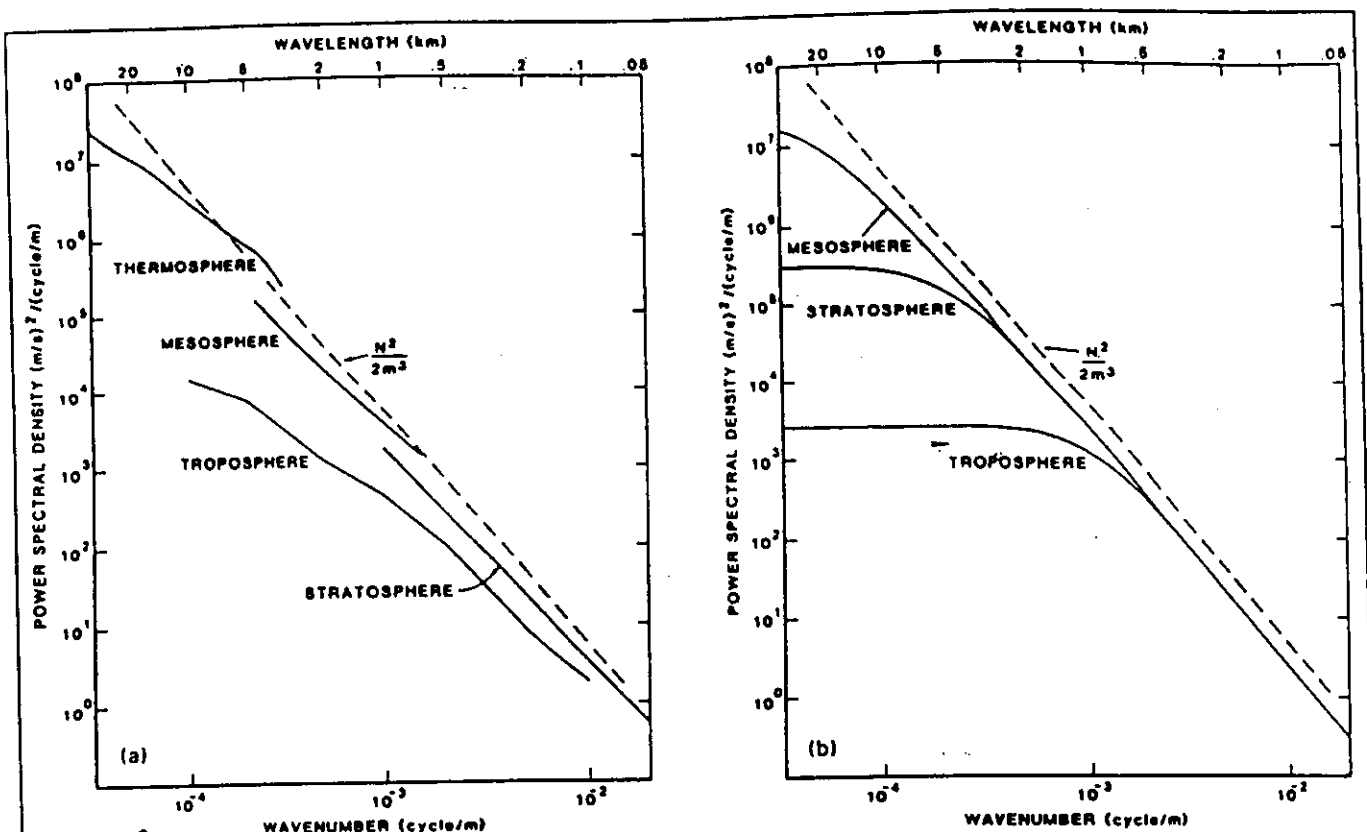
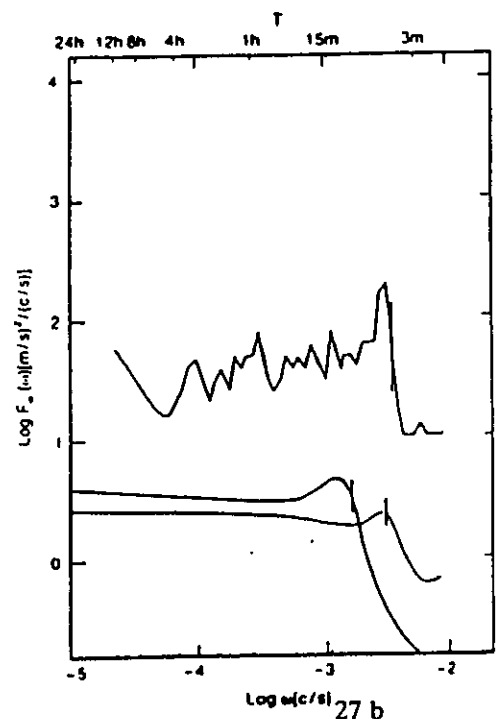



Fig 9a
 (a) A summary of typical experimental spectra of gravity wave horizontal motions as a function of vertical wave-number, for four different altitude regimes. (b) Schematic model of expected spectral shapes and magnitudes of gravity wave spectra of horizontal fluctuations. Note the similarity to Fig. 2(a), and also note the tendency for all spectra to overlap at high wave-numbers (the saturated part of the spectrum) but not at low wave-numbers (unsaturated part of the spectrum). The concept of saturated spectra is discussed further in the text (from Smith *et al.*, 1987).




Some typical frequency spectra of vertical velocity fluctuations under quiet conditions, emphasizing a spectral peak close to the Vaisala-Brunt frequency. The curves show the basic shape; absolute values are only meaningful for the lower two curves. (Van Zandt 1985). The upper curve refers to an altitude of 22.5 km, the middle one to about 11.5 km, and the lowest to about 5 km altitude

FIG. 9b

flat. The "rollover" vertical wavelengths are smallest at the lowest altitudes. Fig.  7a from Smith et al., (1987) illustrates these characteristics. It has also been found that the spectral densities depend on the Vaisala-Brunt frequency, and that the spectral density as a function of vertical wavenumber in the high wavenumber limit takes the form

$$P(m) \propto N^2/m^3 \quad (58)$$

Other variations of the universal theory include modifications to take account of Doppler shifting due to the mean wind (Van Zandt and Fritts, 1987), and variations in wave amplitude as a function of height due to variations in static stability (Van Zandt and Fritts, 1989).

The original studies concentrated on the horizontal wind fluctuations, but the vertical wind fluctuations have also been studied in some detail. The spectrum of these fluctuations shows a fairly flat spectrum, but in light wind conditions there is a peak in spectral density just before the Vaisala-Brunt frequency, and then a sharp cutoff at frequencies higher than the Vaisala-Brunt frequency. Fig.  7b shows an example.

It should once again be emphasized that the above discussions are all based on a theory of quasi-universality, and assume that the irregular motions are due to a spectrum of buoyancy waves. It was noted earlier that a few workers believe that the irregular motions are due to 2-dimensional turbulence, but it does appear that at least in the stratosphere and mesosphere the wave theory is quite compelling. For motions in the troposphere, the argument is still much more alive; two-dimensional turbulence will be discussed shortly in the section on turbulence. The actual reason that this spectral shape results is far from established, although wave-wave interactions may play an important role (e.g. Muller et al., 1986). As noted, Hines (1990's), Gardner (199?) and Dewan (1997?) have examined causes for this spectrum in the atmosphere.

6.6 EXPERIMENTAL STUDIES WITH RADAR - TECHNIQUES

6.6.1 Measurement techniques - gravity waves

Measurement of gravity wave parameters is usually a fairly straight-forward matter of measuring velocity and temperature fluctuations. The most common ways in which this is done are via experiments situated on rockets and balloons, or by radar and lidar techniques. The literature abounds with such measurements, and it would be impossible to discuss them in any detail here. We will simply note that rocket techniques may involve smoke trail releases (e.g. Dewan et al., 1984), falling spheres released at altitude (e.g. Jones and Peterson, 1968) or release of chaff (e.g. Widdel, 1987) to name a few. Balloons carry a variety of instrumentation, usually including an anemometer.

As far as radar experiments go, either tilted beams and Doppler measurements are used (e.g. Woodman and Guillen, 1974) or the spaced antenna method (e.g. Hocking et al., 1989). Lidar experiments usually infer temperature and the fluctuations in this parameter can then be used to study gravity wave motions (e.g. Chanin and Hauchecorne, 1981; Shibata et al., 1986; Hauchecorne et al., 1987).

This lecture is about radar techniques, and that is what we are about to discuss. But I will not dwell here on intimate details like how one uses radar to measure individual radial velocities - this is done elsewhere by other authors. However, we will consider some other "derived" techniques for measurement of gravity wave parameters, and chief amongst these is measurements of the so-called "momentum fluxes". We have already seen how important it is to know these terms; now we will see that in fact these can be directly measured by radar techniques.

6.6.1.2 Momentum Fluxes

- 1) Simplest method; if adequate spatial resolution available, measure u' , w' , v' accurately in a common volume

If not, use method of thermistors; Vincent & Reid. (Dual Beam)

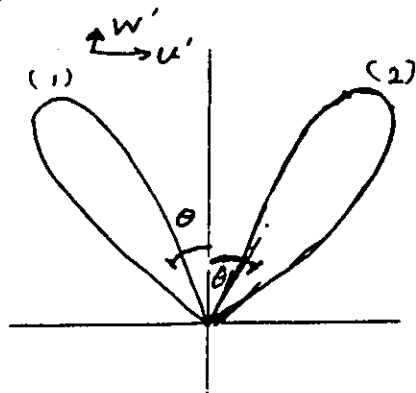


Fig. 11.

$$v_{rad(1)} = w' \cos \theta + u' \sin \theta$$

$$v_{rad(2)} = w' \cos \theta - u' \sin \theta$$

$$[v_{rad(1)}^2 - v_{rad(2)}^2] = 4 \overline{u'w'} \sin \theta \cos \theta$$

$$= 2 \overline{u'w'} \sin 2\theta$$

$$\overline{u'w'} = \frac{v_{rad(1)}^2 - v_{rad(2)}^2}{2 \sin 2\theta}$$

Provided one has sufficient resolution, determination of momentum fluxes is relatively straight-

forward. Nevertheless, such resolution is not always possible, and some other techniques have been developed which enable direct calculation of these fluxes. For example one technique, developed originally by Lhermitte, (1983), uses pairs of tilted beams to make direct measurements of the vertical flux of horizontal momentum. This method was also later used to good effect by Vincent and Reid, (1983) to make measurements of momentum flux and body drag in the upper atmosphere.

6.6.1.3 Other Gravity Wave Parameters

Measurements of wave periods and wavelengths are, surprisingly, still quite difficult. The vertical wavelengths are fairly straight-forward, but determination of horizontal wavelengths, phase velocities and intrinsic frequencies are more difficult. (The intrinsic frequency is the frequency which would be measured by an observer moving with the mean wind at the height of measurement.) At present, the only available methods are multi- station observations and (to a limited degree) radar beam-swinging methods (e.g. Vincent and Reid, 1983).


6.7 EXPERIMENTAL RESULTS AND IMPLICATIONS


We now turn to some brief details about our current knowledge of the distributions and values of gravity wave parameters, and ε and K , in the atmosphere. As usual, we will begin by examining gravity waves.

6.7.1 Results - gravity waves

We will concentrate in this section on studies of the characteristics of gravity wave spectra. Despite a large number of studies of gravity wave motions in the atmosphere, only recently has it been possible to examine in detail the "universality" of the spectra, and any seasonal variations. Thus some of the following results are somewhat tentative, but nevertheless they do seem to produce a self-consistent picture. Perhaps the first point to highlight is that there is no genuinely "universal spectrum", since there are indeed seasonal variations. Nevertheless in the height range of 80-100km over a large part of the globe and the whole year, the variations in total wave RMS amplitude seems to be less than a factor of 3 or so, which is still quite a small variation. Hence most workers in the field do still speak of a "universal" spectrum as a reference spectrum, and study deviations from this law.

6.7.1.1 Frequency and wave-number spectra, typical scales, and directions of propagation

Typical frequency spectra have already been discussed, and illustrated in fig. . Periods are generally in the range from about 5 mins up to the inertial period (generally 10 - 20 hours for most latitudes), and the spectra all tend to show similar shapes. The absolute integrated power under the spectra also tend to vary by less than a factor of 3 or 4. The spectral shape is generally a power law, of the type $P(f) \propto f^{-2}$, with f in the range between about 1.3 and 2. This has been confirmed using radars as well as other methods. Radiosonde data have also been used; e.g. Tsuda, Van Zandt etc.; Allen and Vincent, (1997) (JAS). F1

Likewise the power density as a function of vertical wavenumber m and horizontal wavenumber k are also power laws, but with a "roll-off" to flatter shapes at low m and k . Fig.  showed examples, and showed how this "roll-off" wavenumber changed as a function of altitude. This "roll-off" vertical wavelength $\lambda_{z0} (= 2\pi/m_{z0})$ varies from about 5 km in the lower stratosphere up to about 20 km in the upper mesosphere (Smith et al., 1987; Eckermann and Vincent, 1989). At wavelengths much longer than λ_{z0} , the spectrum is flat, and in the short wavelength limit the spectrum tends to be proportional to m^{-3} . F1.

There are also short-wavelength cutoffs in the spectrum, with shorter wavelengths not being found at all. The vertical wavelengths are generally confined to wavelengths greater than about 1.5 km at 60 km altitude, and greater than about 3 km at 100 km altitude (Vincent, 1987, Philbrick, 1981). It also appears that vertical wavelengths in excess of about 30 km are rare.

It should be noted that the estimates of "typical" scales outlined above were often made from studies of seemingly "monochromatic" waves, and although this is generally an allowable procedure, one must be careful. The dangers of studying "monochromatic" events in the presence of a spectrum of waves have been highlighted by Eckermann and Hocking, (1989).

Horizontal wave spectra can also be described by power laws, being typically proportional to k^{-2} (Fritts et al., 1989), with horizontal wavelengths ranging from about 5 km out to thousands of

kilometres (Reid, 1986). This typical power of -2 is not consistent with a power of -3 for the vertical wave-number spectra unless the spectra are not separable in ω , k and m . Nevertheless it should be noted that this k^{-2} power law is based on only a few observations made by Fritts et al., (1989), and there was large variability between the few spectra measured by these authors. Fritts et al., (1989) suggested that a "typical" horizontal scale is about 300 - 500 km. *Gardner (1992) has discussed non-separable effect*

Another important quantity is the relative contributions of upgoing and downgoing waves. It is believed by most workers in the field that the majority of gravity waves in the mesosphere have their sources in the troposphere, and studies of "rotary" spectra by Vincent, (1984) and Eckermann and Vincent, (1989) have supported this assertion, showing more than 65% of the wave energy was due to upward propagating waves. This may well be a lower limit. For example, an upward propagating elliptical wave will have both an upward and downward component if decomposed into circular modes. Nevertheless, the idea that gravity waves have a high percentage of sources in the troposphere does seem correct, and this in itself is an important result.

It is not only important to know whether waves propagate preferentially up or down, but also whether they have preferred senses of horizontal propagation. For example, Vincent and Stubbs, (1977), Vincent and Fritts, (1987) and Hocking, (1983b) found a preference for winter-time north-south propagation in the altitude region 80 - 100 km. A more detailed study by Eckermann and Vincent, (1989) in the region 30 - 60 km altitude showed an east-west preference in summer and a north-south preference in winter in southern Australia. Part of the reason for this north-south preference in winter may be related to filtering of gravity waves due to critical level interactions with the mean flow, but Eckermann and Vincent, (1989) suggests that the distribution of sources may also be important in establishing these preferred orientations. Ebel et al., (1987) have studied the effects on gravity waves of filtering by the mean wind.

The shapes of the spectra are only poorly known, but the situation is even worse when it comes to phase velocities. Typical horizontal phase velocities are in the range between 0 and 100 m s^{-1} , but experimental determinations of the distribution of phase velocities are sorely needed. A knowledge of this distribution is needed because it will help in describing how and where waves in the atmosphere break. The quantity $c - \bar{u}$ (where c is the horizontal phase speed and \bar{u} is the mean wind) is the speed of the wave relative to the mean wind, and is called the intrinsic phase speed. When this quantity approaches zero at any height, the vertical group velocity also tends toward zero, and the upward rising wave begins to "pile up" its energy on itself, resulting in very large amplitudes which then cause the waves to break (see our discussion of critical levels earlier in this paper). The waves may break by convective instability (Fritts and Rastogi, 1985), shear instability (usually in the presence of an already existing mean shear) (e.g. Fritts and Yuan, 1989; Reid et al., 1987), or slantwise instability (Hines, 1988). However, one must be careful in assuming that gravity waves always break into turbulence. For example, Klostermeyer, (1989) has proposed that waves may also lose energy by non-linearly converting to waves of other frequencies and wavenumbers, and even "cascade" down to waves of very short vertical wavelength.

6.7.1.2 Seasonal and latitudinal variations

The most thorough investigations of gravity wave variations as a function of time and latitude have been those due to Hirota, (1984), Meek et al., (1985), and Fritts and Vincent, (1987). Hirota, (1984) collated wind and temperature data recorded by meteorological rockets from a variety of stations situated around the globe, and fig. [26] from Hirota, (1985) shows a summary of their results. The data refer to RMS values of the second derivative of wind and temperature as a function of height and measured in the altitude range 30-70km. An annual oscillation exists in wave intensity as a function

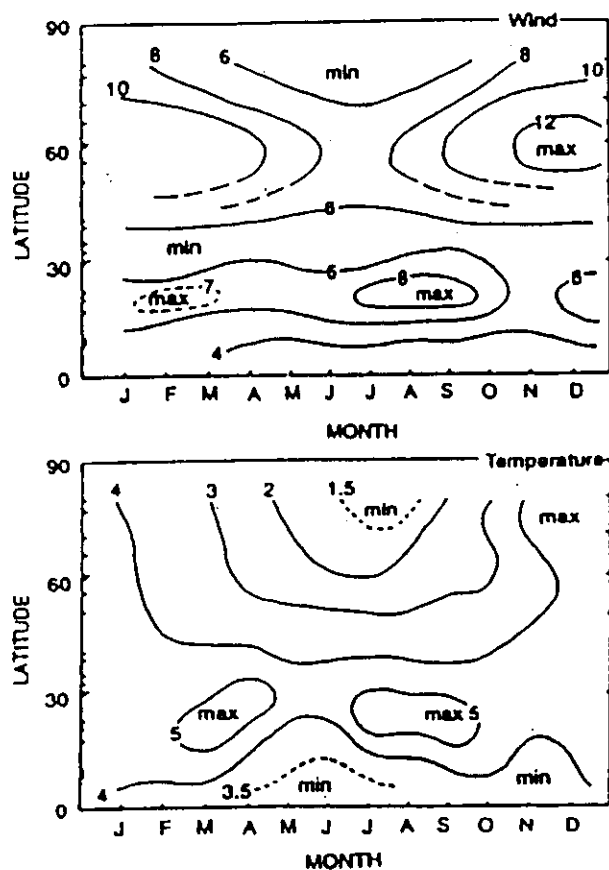


Fig. 28
 Latitude-time cross sections of wind (upper graph) and temperature (lower graph) activity. The actual numbers refer to RMS values of the second derivative, as discussed in the text. (Hirota 1985). Ticks on the left axis denote the latitudes of the rocket stations used to produce this plot

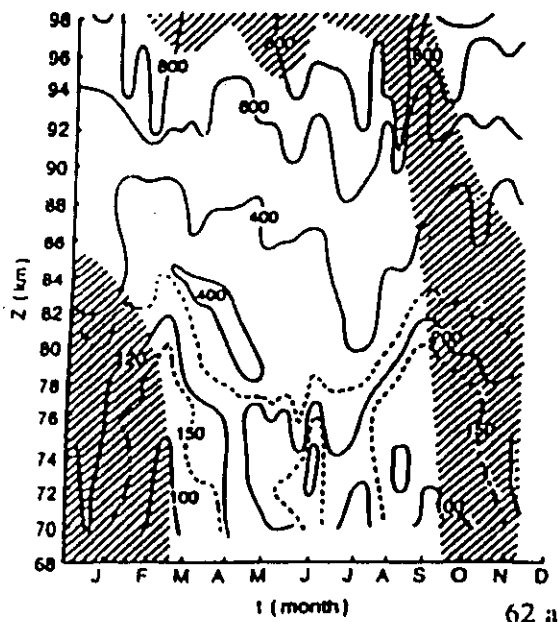


Fig. 29.

Height-time cross section of mean square east-west amplitudes of gravity waves with periods in the range 1-8 h observed at Adelaide Australia. (Vincent and Friis 1987) The altitude is denoted by z , and t is the time (months)

of season at high latitudes (max. in winter) with a transition to a semi-annual oscillation in the tropics and low latitudes, with a maximum at the equinoxes. It should be highlighted here however, that because of the nature of rocket profiles, it was not possible to distinguish the wave periods, and these RMS values include waves of all periods. Values are generally in the range $6 - 10 \text{ ms}^{-1} \text{ km}^{-2}$ and 2.5 K km^{-2} . [Typical vertical wavelengths are of the order of 5-10 km, so the vertical wave number m is approximately 1 rad km^{-1} , so a RMS value of the 2nd derivative of approximately $6 \text{ ms}^{-1} \text{ km}^{-2}$ refers to an RMS amplitude of $\approx 6 \text{ ms}^{-1}$, and temperature fluctuations of around 2.5 K.]. Eckermann and Vincent, (1989) have also estimated RMS wave amplitudes in the height region 30-60 km, and found horizontal RMS velocity amplitudes of around 5 ms^{-1} at 30 km altitude, rising to around 9 ms^{-1} at 55 km altitude. Typical RMS temperature fluctuations were around 3 – 6 K.

Meek et al., (1985) and Vincent and Fritts, (1987) used radars to monitor wind fluctuations as a function of time and height. They then spectrally analyzed the time series and divided the spectra into frequency bands. Fig. 29 shows a sample from Vincent and Fritts, (1987) of the mean square amplitudes in the period range 1 to 8 hours, plotted as a function of height and time of year. Typically the root-mean-square (RMS) values of the wind fluctuations are in the range 10 to 20 ms^{-1} at 60 to 100 km altitude. We note from fig. 29 that there is a semi-annual oscillation as a function of season below 80 km, and this becomes more like an annual variation at higher altitudes. Notice however that the semi-annual oscillation below 80 km is shifted in phase by 180° relative to that found by Hirota, (1984); in this case, maxima occur in summer and winter, whilst Hirota, (1984) found the maxima to occur at the equinoxes. However, we should note that the data used by Hirota, (1984) are at lower heights (stratospheric), and also there was no frequency filtering applied by Hirota, (1984). Thus the oscillations recorded may well have been dominated by near-inertial frequencies, or alternatively there may be a genuine change in seasonal characteristics at around 70 km altitude.

6.7.1.3 Momentum fluxes, Energy fluxes and drag forces

Studies of momentum fluxes as a function of height are becoming very important, since they impact on the mean wind in a very dramatic manner. To see how this arises, imagine the typical mean wind profile which would arise in radiative equilibrium, in which the eastward mean wind increases monotonically with increasing altitude up to about 100 km altitude. Rising up into this environment are gravity waves with phase velocities with all orientations, but we are interested only in those in the east-west plane. These may have phase velocities varying from say -50 ms^{-1} (westward) to say $+50 \text{ ms}^{-1}$ (eastward). As the waves rise up, the eastward propagating ones all eventually encounter an altitude where their phase speed equals that of the mean wind, and so they break and dissipate. Thus they are prevented from propagating above this level. Thus by about 70 km altitude, there are a dominance of westward propagating waves, with a significant portion of the eastward ones having been "filtered" out lower down. Above 70 km, these westward moving ones now begin to break (not necessarily by critical level interactions, but simply because they have grown to large amplitudes), and so impart westward momentum to the mean wind. As a result, this slows and even reverses the mean wind above 70 km. The drag force term which describes the acceleration on the mean wind is $\frac{1}{\rho} \frac{d}{dz}(\rho \overline{u'w'})$, or approximately $\frac{d}{dz}(\overline{u'w'})$.

This drag force also determines the mean north-south wind. In a purely radiative situation, a temperature gradient exists between the poles and the equator. This attempts to drive a north-south flow, but the Coriolis force twists this into an east-west flow. This east-west flow in turn produces a north-south Coriolis acceleration of its own which acts in the opposite direction to the temperature gradient, and so as a result no north-south flow occurs. However, once the gravity waves induce some alteration of the mean zonal wind, the north-south Coriolis force and the temperature gradient force no longer balance, and as a result a north-south wind results. Equilibrium occurs when

$$\frac{d}{dz} \overline{u'w'} = f\bar{v} \quad (131)$$

where \bar{v} is the mean north-south wind and f is the Coriolis parameter $= 2\Omega \sin \theta$, θ being the latitude and Ω the rotation rate of the Earth ($= 7.27 \times 10^{-5} \text{ rads s}^{-1}$). For example, to explain a 10 ms^{-1} north-south wind at 45° latitude ($f\bar{v} \approx 10^{-3} \text{ ms}^{-2}$) requires a value for $d/dz(\overline{u'w'})$ of around $1 \text{ m}^2 \text{ s}^{-2} \text{ km}^{-1}$, or about $80 \text{ ms}^{-1} \text{ day}^{-1}$. The few investigations made so far seem to measure values of this order (e.g. Vincent and Reid, 1983; Fritts and Vincent, 1987; Reid and Vincent, 1987), but these have only been occasional measurements. More are needed in order to confirm that the gravity wave drag is responsible for the observed meridional winds.

The north-south winds can also be partly balanced by other forces such as $d/dy(\overline{u'v'})$, and more studies of all these different momentum fluxes and body forces are badly needed before the dynamics of the atmosphere can be more properly understood. An appreciation of the role of gravity waves, and better measurements of the parameters outlined above, are crucial if this goal is to be attained.

Energy fluxes have been studied perhaps least of all. Vincent, (1987) has briefly reviewed a few measurements, and reported estimates between $7 \times 10^{-4} \text{ Wm}^{-2}$ for waves in the period range 50-60 mins, and $\approx 10^{-2} \text{ Wm}^{-2}$ when integrated over all wave periods, at altitudes of 80-90 km. Czechowsky et al., (1989) have made measurements of the upward and downward fluxes of gravity wave energy at the top of the troposphere in Germany, and found values in the range 0.08 to 0.1 Wm^{-2} . The upward flux exceeded the downward flux by about 0.014 Wm^{-2} . Again, more measurements are needed.

Gravity wave and equatorial wave morphology of the stratosphere derived from long-term rocket soundings

By STEPHEN D. ECKERMANN¹*, ISAMU HIROTA² and WAYNE K. HOCKING³

¹University of Oxford, UK

²Kyoto University, Japan

³University of Western Ontario, Canada

(Received 11 November 1993; revised 15 March 1994)

SUMMARY

Fluctuations in vertical profiles of atmospheric temperature and horizontal wind in the 20–60 km altitude range have been isolated from meteorological rocket measurements during 1977–87 at 15 widely separated sites. The seasonal, geographical, and vertical variability of the variance of horizontal velocities, $u'^2 + v'^2$, and relative-temperature perturbations, $\overline{T'^2}$, were studied. The bulk of the variance of both quantities in the 2–10 km and 2–20 km vertical-wavelength bands was associated with gravity-wave motions, although in-depth study of the wave polarization shows that planetary-scale equatorial wave modes contribute to the variance at equatorial sites. Annual mean variances varied widely among the 15 stations, suggesting appreciable geographical variability in stratospheric wave activity. Whereas $u'^2 + v'^2$ values generally increased significantly with altitude throughout the stratosphere, $\overline{T'^2}$ values grew less substantially and often decreased with altitude at upper heights. Rotations of wave-velocity phasors with height were always more frequently clockwise than anticlockwise in the northern hemisphere, consistent with upward-propagating wave energy, yet these percentages (>50%) showed a marked semi-annual variation, with equinoctial maxima and minima at the solstices. At high latitudes ($\sim 50^\circ\text{N}$ – 80°N) variances exhibited a strong annual variation, with the minimum in summer and a strong peak during winter at both lower (20–40 km) and upper (40–60 km) heights. The annual variance cycle attenuated somewhat at mid-latitudes ($\sim 25^\circ\text{N}$ – 40°N), and a strong peak in August dominated the $u'^2 + v'^2$ variations at 40–60 km. The peak was also evident in $\overline{T'^2}$, but was smaller relative to the winter peak. At low latitudes ($\sim 15^\circ\text{N}$ – 25°N) the wave morphology was broadly similar to that at mid-latitudes, apart from an additional upper-level peak in the variance in May. This peak in May occurred in some years but not in others at mid-latitude stations. At the equatorial stations ($\sim 10^\circ\text{N}$ – 10°S) the low-level variance showed little systematic seasonal variability, but exhibited clear modulation over a quasi-two-year period. Much of this variance was consistent with the Kelvin modes thought to drive the eastward phase of the stratospheric quasi-biennial oscillation (QBO). However, the uniform east–west alignment of waves was inconsistent with the expected polarization of the mixed Rossby-gravity wave mode which is believed to drive the westward phase of the QBO. At 40–60 km, the variance was strongly attenuated around April–May and November, when both $u'^2 + v'^2$ and $\overline{T'^2}$ decreased with height around the 40–45 km range, indicating that wave dissipation occurs here. This produced a semi-annual variation at upper heights, with maxima around January and July, which may contribute significantly to the semi-annual wave driving of the equatorial upper stratosphere. Polarization studies showed that this variance in the 2–10 km band was mostly due to gravity waves, although equatorial modes contributed during December–February.

1. INTRODUCTION

The atmosphere between about 20 and 60 km in altitude, hereafter referred to as the stratosphere, has proved to be a notoriously difficult region to probe in fine detail. For many years *in situ* measurements from rocket-borne payloads provided the majority of information on the basic dynamics and thermal structure of the atmosphere at these heights. While remote-sensing experiments aboard satellites now provide excellent global data on the background structure and on planetary-scale wave disturbances throughout the stratosphere, smaller-scale motions, such as gravity waves, are poorly resolved by these instruments at present. While ground-based radar systems now regularly measure winds in the height intervals 0–30 km and 60–100 km with high time–height resolution,

* Corresponding author. Present address: Computational Physics Incorporated, Suite 600, 2750 Prosperity Avenue, Fairfax, VA 22031, USA. e-mail: eckerman@ismap4.nrl.navy.mil.

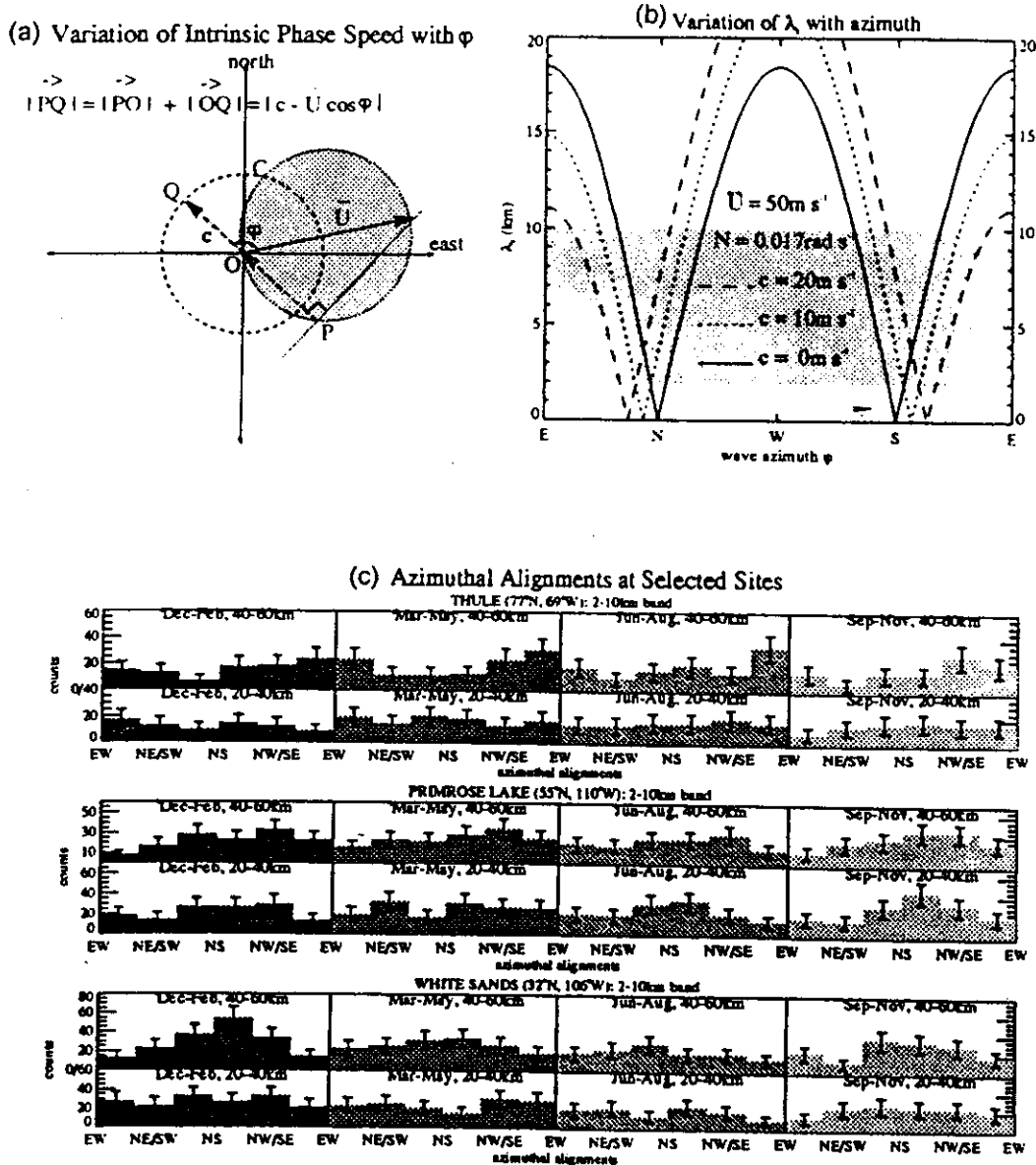


Figure 4. (a) Phasor diagram showing the geometry of the variation of intrinsic phase speed $|c - \bar{U} \cos \varphi|$ with azimuth angle between the wind and wave-propagation vectors, φ . (b) Modelled variation of vertical wavelength, λ_z , with φ for three different ground-based phase speeds c . Values of $\bar{U} = 50 \text{ m s}^{-1}$ (eastward) and Brunt-Väisälä frequency $N = 0.017 \text{ rad s}^{-1}$ were used in the calculation, and are typical of the mid-latitude winter stratosphere. (c) Histograms of the number of mean azimuthal alignments of the horizontal-velocity fluctuations, φ , within six azimuth bins, as calculated from rocket data in the 2-10 km vertical-wavelength band at three sites where earlier data were reinterpreted by Eckermann and Hocking (1989). The data are split into summer, spring, winter and autumn groupings. The lower and upper plot sequences at each site are results from a lower (20-40 km) and upper (40-60 km) height range. Error bars are 90% confidence intervals of the count as given by the Poisson distribution.

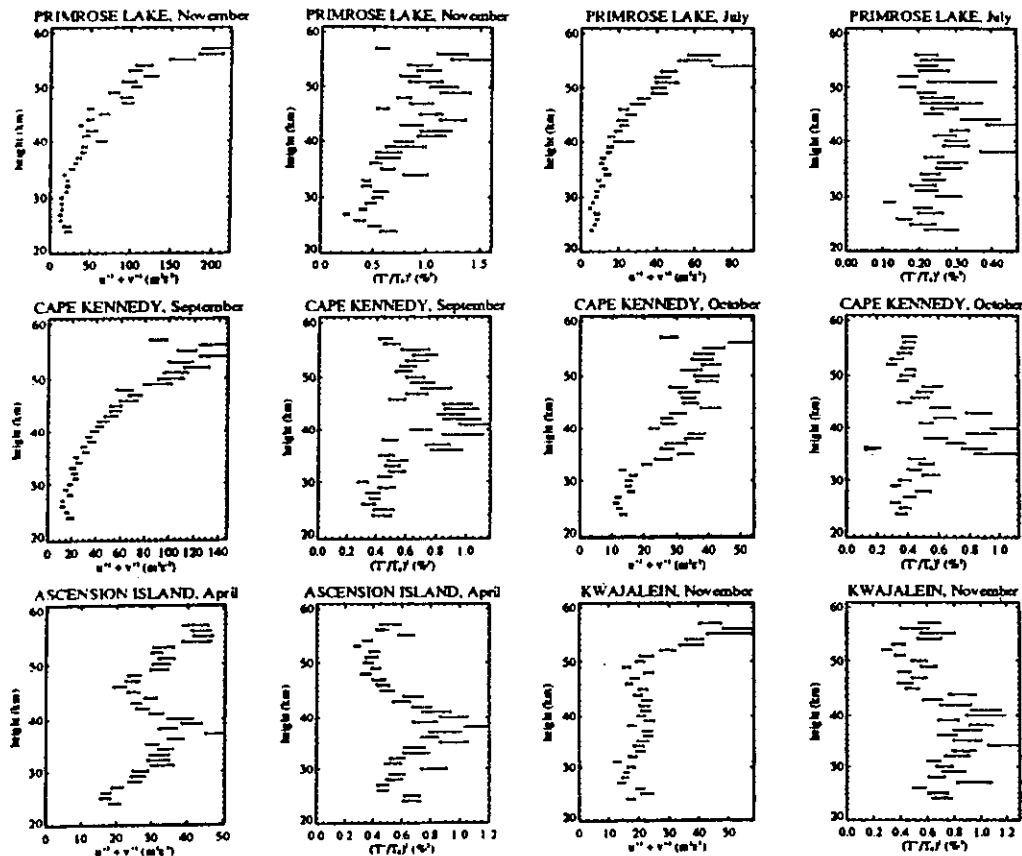


Figure 10. Plot pairs showing the values of the variance of horizontal velocities, $\overline{u'^2 + v'^2}$, and the relative temperature perturbations, $(T'/T)_f$, (2–10 km vertical-wavelength band) as a function of height at a selected site in a given month. The error bars are standard errors of the mean.

energy propagation, whereas the converse holds in the southern hemisphere (e.g. Andrews *et al.* (1987) p. 199). Therefore the sense of rotation with height of wave-induced horizontal-velocity vectors provides information on the vertical sense of propagation of the waves. Such calculations have verified that most upper-stratospheric gravity-wave energy originates from lower heights (Hirota and Niki 1985; Hass and Meyer 1987; Eckermann and Vincent 1989).

To study these features in greater depth, mean seasonal variations in the ratio of the clockwise-rotating variance to the total variance $\overline{u'^2 + v'^2}$ (equal to $(I + Q)/2I$) are plotted as percentages in Fig. 11. Complete separation of upgoing and downgoing wave energy into the clockwise and anticlockwise spectra is only possible for a circularly polarized wave, whereas the gravity waves are elliptically polarized (see, for example, Fig. 1 of Hirota and Niki (1985)), and so the partitioning is 'blurred' somewhat (Eckermann and Vincent 1989). Therefore similar ratios were also computed, using another independent technique developed by Hirota and Niki (1985), in which the change in the wind phasor angle at adjacent heights is computed, and the wind profile rotation is classified according to whichever angular change (i.e. clockwise or anticlockwise) is the more common over the 20–60 km range. The results presented are for fluctuations in the

are probably due to the inclusion of large-amplitude Kelvin-wave disturbances in this broader band (e.g. Hirota 1978; Devarajan *et al.* 1985; see also Fig. 5).

The analysis was duplicated using the data-reduction technique of Hamilton (1991), with results computed over the 28–57 km range. As for the broad-band results, these data showed a more prominent annual cycle, giving large wintertime variances. Some of this variance may be due to interannual variability in the wintertime background vertical structure due to stratospheric warming events (e.g. Labitzke 1981). Nevertheless, the qualitative seasonal variations were generally the same.

(b) Temperature fluctuations

The seasonal variations in the variance of the relative-temperature fluctuations $\overline{T'^2} = (\overline{T/T_0})^2$ are plotted in Fig. 9, again using data in the 2–10 km vertical-wavelength band. The four rows of plots correspond roughly to each of the four latitude bands defined earlier.

It is immediately apparent that $\overline{T'^2}$ does not increase substantially with altitude, in contrast to $\overline{u'^2} + \overline{v'^2}$ in Fig. 7. Additionally, monthly variations of $\overline{T'^2}$ often differ from

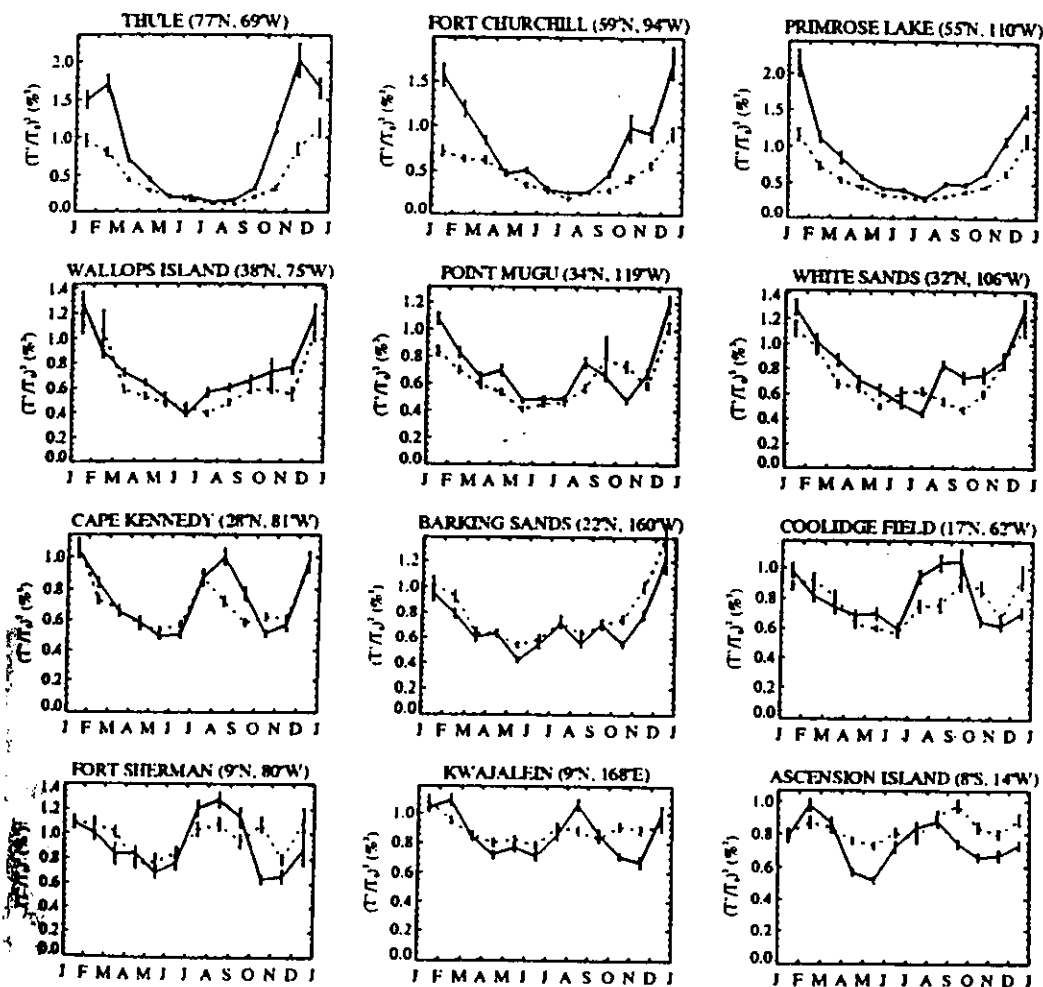


Figure 9. As Fig. 7, but for variations in the relative-temperature variance.

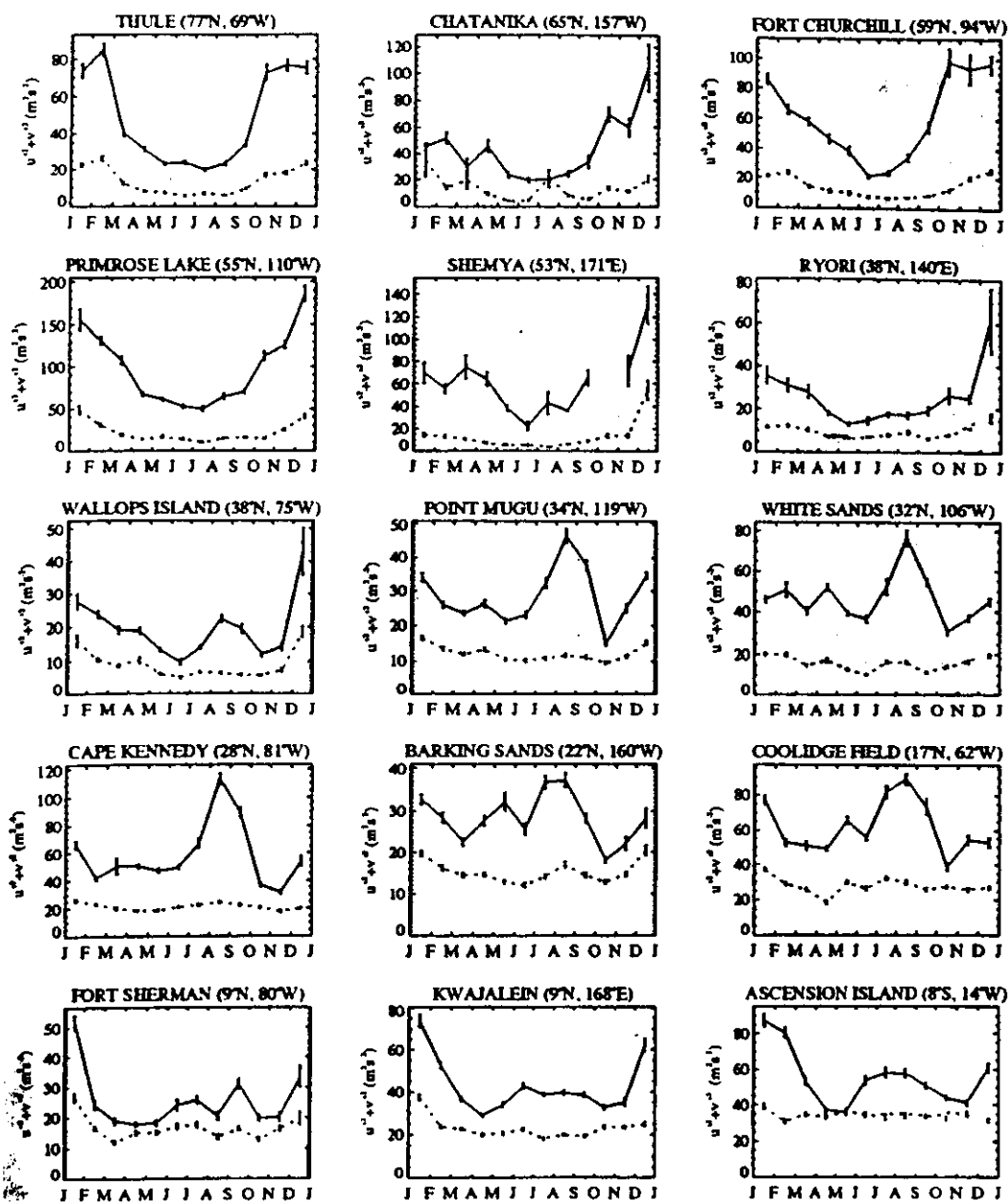


Figure 7. Mean monthly variations in the fluctuating horizontal-velocity variance $\overline{u'^2 + v'^2}$ in the 2–10 km vertical wavelength band, as calculated within two altitude ranges of 20–40 km (dashed curve) and 40–60 km (solid curve). Error bars indicate standard errors of the mean. Note: y-axis scales vary from plot to plot.

somewhat from those at the other three sites, in that the August maximum is not as large, and the winter maximum is less suppressed. These results contrast with the $(u_{zz})_{rms}$ variations from White Sands calculated by Hirota (1984), who found small maxima in April and September. The $\overline{u'^2 + v'^2}$ data at White Sands reveal that the former maximum (in April) is very weak, whereas the latter maximum is very prominent and peaks earlier (around August).

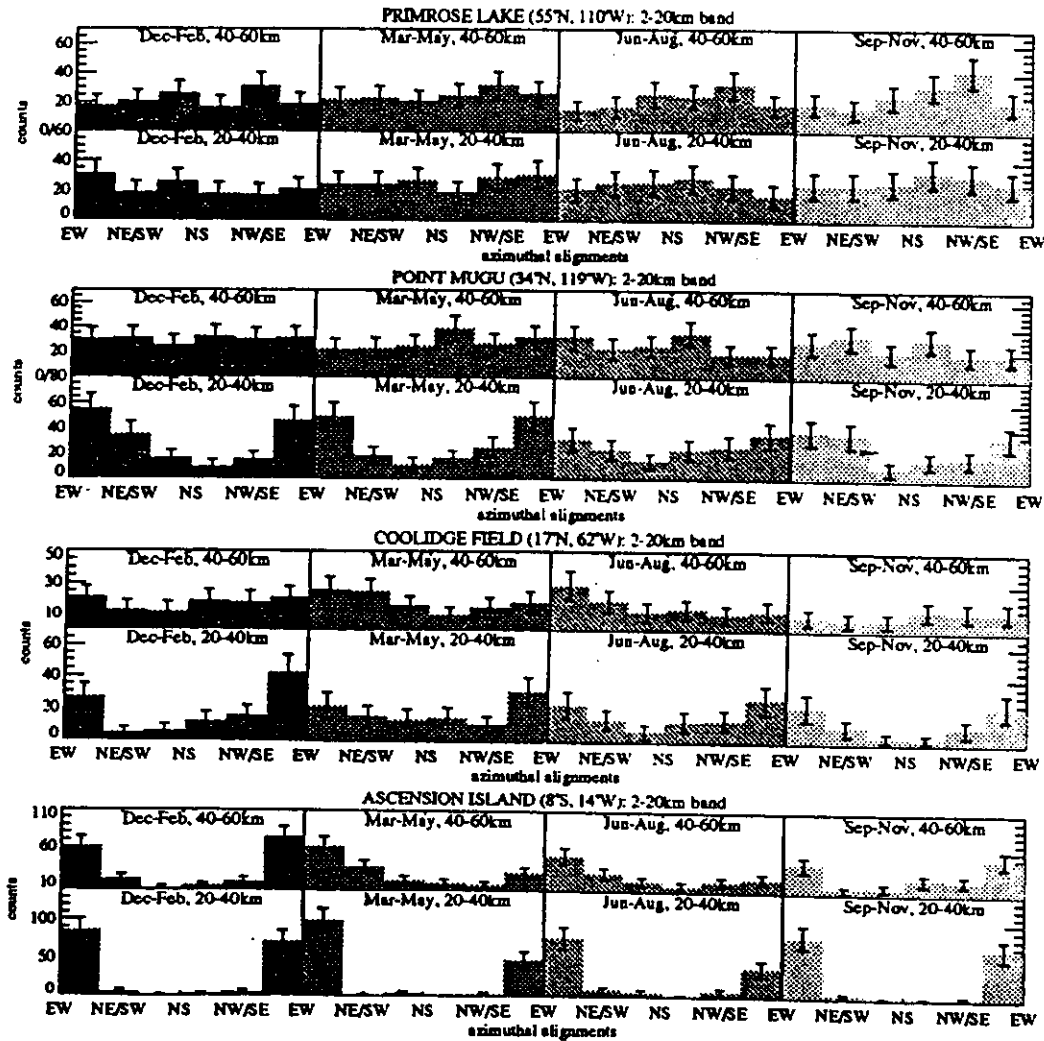


Figure 5. As for Fig. 4(c), but using data in the 2–20 km vertical-wavelength band from four representative sites.

assumption. To investigate this issue, Fig. 6 displays alignments in the 2–10 km band at the three equatorial sites. The alignments at all sites in the lower height range 20–40 km are strongly zonal in all seasons. At the uppermost heights the zonal clustering persists strongly only during December–January. In other months the zonal preference is generally much weaker.

5. MEAN SEASONAL VARIATIONS IN WAVE ACTIVITY

Hirota (1984) investigated the seasonal variations of the gravity-wave 'activity' in stratospheric rocket data by calculating the intensity of the fluctuations in various atmospheric variables, X , over the height range $z_1 \leq z \leq z_2$, using the following height-integrated formula

REFERENCES

The following references are not by any means complete, but serve as a useful starting point for further sources of information.

- Anadarao B.G., Raghavarao, R., Desai, J.N.: *J. Atmos. Terr. Phys.*, 40, 157-163, 1978.
- Barat, J.: *J. Appl. Meteorology*, 21, 1480-1488, 1982a.
- Barat, J.: *J. Appl. Meteorology*, 21, 1489-1496, 1982b.
- Barat, J.: *J. Atmos. Sci.*, 39, 2553-2564, 1982c.
- Batchelor, G.K.: *The Theory of Homogeneous Turbulence*, Cambridge University Press, 1953.
- Batchelor, G.K., Roy, J.: *Meteorol. Soc.*, 76, 133-146, 1977.
- Battaner, E. Molina, A.: *J. Geophys. Res.*, 85, 6803-6810, 1980.
- Blamont, J.E., de Jager, C.: *Ann. Geophys.*, 17, 134-143, 1961.
- Blamont, J.: *Planet Space Sci.*, 10, 89-101, 1963.
- Blamont, J.E., Barat, J.: in *Aurora Airglow*, edited by B.M. McCormac, 156-159, Reinhold Pub. Co., 1964.
- Blix, T.A., Thrane, E.V., Andreassen, O.: *J. Geophys. Res.*, 95, in press 1990.
- Blum, P., Schuchardt, K.G.H., von Zahn, U.: *J. Atmos. Terr. Phys.*, 40, 1131-1135, 1978.
- Blum, P.W., Schuchardt, K.G.A.: *J. Atmos. Terr. Phys.*, 40, 1137-1142, 1978.
- Booker, H.G., Cohen, R.: *J. Geophys. Res.*, 61, 707-733, 1956.
- Bradshaw, P.: "An Introduction to Turbulence its Measurement", Pergamon Press, 1975.
- Chakrabarty, D.K., Beig, G., Sidhu, J.S., Chakrabarty, H., Narayanan, R., Modi, N.K., Das, S.R., Chakrabarty, P.: *J. Atmos. Terr. Phys.*, 49, 975-980, 1987.
- Chakrabarty, D.K., Beig, G., Sidhu, J.S., Das, S.R.: *J. Atmos. Terr. Phys.*, 51, 19-27, 1989.
- Chandra, S.: *Planet. Space Sci.*, 28, 585-593, 1980.
- Chanin, M.L., Hauchecorne, A.: *J. Geophys. Res.*, 86, 9715-9721, 1981.
- Colegrove, F.D., Hanson, W.B., Johnson, F.S.: *J. Geophys. Res.*, 70, 4931-4941, 1965.
- Colegrove, F.D., Johnson, F.S., Hanson, W.B.: *J. Geophys. Res.*, 71, 2227-2236, 1966.
- Czechowsky, P., Ruester, R., Schmidt, G.: *Geophys. Res. Letts.*, 6, 459-462, 1979.
- Czechowsky, P., Inhester, B., Klostermeyer, J., Reid, I.M., Ruester, R., Schmidt, G.: *Handbook for MAP*, vol 28, 459-466, Scostep Secretariat, University of Illinois, U.S.A., 1989.
- Danilov, A.D.: *Adv. Space Res.*, 4, 67-78, 1984.
- Desaubies, Y., Smith, W.K.: *J. Phys. Oceanography*, 12, 1245-1259, 1982.
- Dewan, E.M.: *Science*, 211, 1041-1042, 1981.
- Dewan, E., Grossbard, N., Quesada, A.F., Good, R.E.: *Geophys. Res. Letts.* 11, 80-83, 1984 with correction in *Geophys. Res. Letts.*, 11, 624, 1984.
- Dewan, E.M., Good, R.E.: *J. Geophys. Res.*, 91, 2742-2748, 1986.
- Dong, B., Yeh, K.C.: *J. Geophys. Res.*, 93, 3729-3744, 1988.
- Driscoll, R.J., Kennedy, L.A.: *Phys. Fluids*, 28, 72-80, 1985.
- Ebel, A.: *J Atmos. Terr. Phys.*, 42, 617-628, 1980.
- Ebel, A.: *J. Atmos. Terr. Phys.*, 46, 727-737, 1984.
- Ebel, A., Manson, A.H., Meek, C.E.: *J. Atmos. Terr. Phys.*, 49, 385-401, 1987.
- Eckermann, S.D., Hocking, W.K.: *J. Geophys. Res.*, 94, 6333-6339, 1989.
- Eckermann, S.D., Vincent, R.A.: *Pure Appl. Geophys.*, 130, 509-532, 1989.
- Elford, W.G., Roper, R.G.: *Space Res.*, VIII, 42-54, 1967.
- Fellous, J.L., Frezal, M.E.: *MAP Handbook*, Vol. 2, 323-332, Scostep Secretariat, University of Illinois,

- Fritts, D.C., Rastogi, P.K.: *Radio Sci.*, 20, 1247-1277, 1985.
- Fritts, D.C., Dunkerton, T.J.: *J. Atmos. Sci.*, 42, 549-556, 1985.
- Fritts, D.C., Chou, H-G.: *J. Atmos. Sci.*, 44, 3610-3624, 1987.
- Fritts, D.C., Vincent, R.A.: *J. Atmos. Sci.*, 44, 605-619, 1987.
- Fritts, D.C., Tsuda, T., Sato, T., Fukao, S., Kato, S.: *J. Atmos. Sci.*, 45, 1741-1759, 1988.
- Fritts, D.C., Blanchard R.C., Coy, L.: *J. Atmos. Sci.*, 46, 423-434, 1989.
- Fritts, D.C., Yuan, Li.: *J. Atmos. Sci.*, 46, 2562-2568, 1989.
- Fukao, S., Sato, T., Kato, S., Harper, R.M., Woodman, R.F., Gordon, W.E.: *J. Geophys. Res.*, 84, 4379-4386, 1979.
- Fukao, S., M.D. Yamanaka, N. Ao, W.K. Hocking, T. Sato, M. Yamamoto, T. Nakamura, T. Tsuda and S. Kato, "Seasonal variability of vertical eddy diffusivity in the middle atmosphere, 1. Three-year observations by the middle and upper atmosphere radar", *J. Geophys. Res.*, 99, 18973 - 18987, 1994.
- Gage, K.S.: *J. Atmos. Sci.*, 36, 1950-1954, 1979.
- Gage K.S., Nastrom, G.D.: *Radio Sci.*, 20, 1339-1347, 1985.
- Gage K.S., Nastrom, G.D.: *J. Atmos. Sci.*, 43, 729-740, 1986.
- Garcia, R.R., Solomon, S.: *J. Geophys. Res.*, 90, 3850-3868, 1985.
- Garrett, C., Munk, W.: *Geophys. Fluid Dynamics*, 2, 225-264, 1972.
- Garrett, C., Munk, W.: *J. Geophys. Res.*, 80, 291-297, 1975.
- Gibbins, O.T., Schwartz, P.R., Thacker, D.L., Bevilacqua, R.M.: *Geophys. Res. Lett.*, 9, 131-134, 1982.
- Gordiets, B.F., Kulikov, Yu N., Markov, M.N., Marov, Ma. Ya.: *J. Geophys. Res.*, 87, 4504-4514, 1982.
- Gossard, E. D., Hooke, W.H.: *Waves in the Atmosphere*, Elsevier Scientific Publ. Co., Amsterdam, 1975.
- Greenhow J.S., Neufeld, E.L.: *J. Geophys. Res.*, 64, 2129-2153, 1959.
- Greenhow, J.S.: *J. Geophys. Res.*, 64, 2208-2209, 1959.
- Hauchecorne, A., Chanin, M-L., Wilson, R.: *Geophys. Res. Letts.*, 14, 933-936, 1987.
- Hesstvedt, E.: *Geofys. Publik.*, 27, 1-35, 1968.
- Hill, R.J., Clifford, S.F.: *J. Opt. Soc. Am.*, 68, 892-899, 1978.
- Hines, C.O.: *Canadian J. Phys.*, 38, 1441-1481, 1960.
- Hines, C.O.: *The Upper Atmosphere in Motion*, Am. Geophys. Union, Washington DC 433, 1974.
- Hines, C.O.: *J. Atmos. Sci.*, 45, 1269-1278, 1988.
- Hirota, I.: *J. Atmos. terr. Phys.*, 46, 767-773, 1984.
- Hirota, I.: *Middle Atmosphere Handbook*, vol 16, 144-148, Scostep Secretariat, University of Illinois, U.S.A., 1985.
- Hocking, W.K.: *J. Atmos. Terr. Phys.*, 45, 89-102, 1983a.
- Hocking, W.K.: *J. Atmos. Terr. Phys.*, 45, 103-114, 1983b.
- Hocking, W.K.: *Radio Sci.*, 20, 1403-1422, 1985.
- Hocking, W.K.: *J. Geophys. Res.*, 93, 2475-2491, 1988.
- Hocking, W.K., May, P., Roettger, J.: *Pure Appl. Geophys.*, 130, 571-604, 1989.
- Hocking, W.K.: *Handbook for MAP*, vol. 27, 439-442, Scostep Secretariat, University of Illinois, U.S.A., 1989.
- Hodges, R.R.: *J. Geophys. Res.*, 72, 3455-3458, 1967.
- Holton, J.R.: *J. Atmos. Sci.*, 39, 791-799, 1982.
- Holton, J.R.: *J. Atmos. Sci.*, 40, 2497-2507, 1983.
- Houghton, J.T.: *The Physics of Atmospheres*. Cambridge University, 1977.

- Hunten, D.M.: J. Geophys. Res., 79, 2533-2534, 1974.
- Johnson, F.S., Wilkins, E.M.: J. Geophys. Res., 70, 1281-1284, 1965.
- Johnson, F.S., Gottlieb, B.: Planet. Space Sci., 18, 1707-1718, 1970.
- Johnson, F.S.: J. Atmos. Sci., 32, 1658-1662, 1975.
- Jones, L.M., Peterson, J.W.: Meteorological monographs, 8, 176-189, 1968.
- Jones, W.L., Houghton, D.D.: J. Atmos. Sci., 28, 604-608, 1971.
- Justus, C.G.: J. Geophys. Res., 71, 3767-3773, 1966.
- Justus, C.G.: J. Geophys. Res., 72, 1035-1039, 1967a.
- Justus, C.G.: J. Geophys. Res., 72, 1933-1940, 1967b.
- Justus, C.G.: J. Geophys. Res., 73, 455-458, 1968.
- Justus, C.G.: J. Atmos. Sci., 26, 1137-1141, 1969.
- Kaimal, J.C., Wyngaard, J. C., Izumi, Y., Cote, O.R.: Q. J. Roy. Meteorol. Soc., 98, 563-589, 1972.
- Kelley, M.C., Farley, D.T., Roettger, J.: Geophys. Res. Letts., 14, 1031-1034, 1987.
- Kelley, M.C., Ulwick, J.C.: J. Geophys. Res., 93, 7001-7008, 1988.
- Kellog, W.W.: Space Science Revs., 3, 275-316, 1964.
- Keneshea, T.J., Zimmerman, S.P.: J. Atmos. Sci., 27, 831-849, 1970.
- Keneshea, T.J., Zimmerman, S.P., Philbrick, C.R.: Planet. Space Sci., 27, 385-401, 1979.
- Klostermeyer, J.: Middle Atmosphere Program handbook, 28, 299-308, Scostep Secretariat, University of Illinois, U.S.A., 1989.
- Kochanski, A.J.: J. Geophys. Res., 69, 3651-3662, 1964.
- Kolmogoroff, A.N.: Doklady Akad. Nauk USSR, 32, 16, 1941. German Translation in "Sammelbzur Statistischen Theorie der Turbulenz", Akademi-Verlag, Berlin, 1958.
- Korolev, S.S., Kolenik, A.G.: Geomag. Aeron., 19, 47-50, 1979.
- Kraichnan, R.H.: Phys. of Fluids, 10, 1417-1423, 1967.
- Layzer, D., Bedinger, J.F.: Planet. Space Sci., 17, 1891-1911, 1969.
- Lhermitte, R.: J. Geophys. Res., 88, 725-742, 1983.
- Lilly, D.K., Waco, D.E., Aldefang, S.I.: J. Appl. Meteorol., 13, 488-493, 1974.
- Lilly, D.K.: J. Atmos. Sci., 40, 749-761, 1983.
- Lilly, D.K.: J. Atmos. Sci., 46, 2026-2030, 1989.
- Lindzen, R.S.: J. Geophys. Res., 86, 9707-9714, 1981.
- Lloyd, K.G., Low, C.H., McAvaney, B.J., Rees, D., Roper, R.G.: Planet. Space Sci., 20, 761-769, 1971.
- Luebken, F.-J., von Zahn, U., Thrane, E.V., Blix, T., Kokin, G.A., Pachomov, S.V.: J. Atmos. Terr. Phys., 49, 763-775, 1987.
- Manson, A.H., Meek, C.E.: J. Atmos. Terr. Phys., 42, 103-113, 1980.
- Manson, A.H., Meek, C.E., Gregory, J.B.: J. Atmos. Terr. Phys., 43, 35-44, 1981.
- Massie, S.T.: J. Geophys. Res., 85, 2155-2164, 1980.
- Matsuno, T.: J. Meteorol. Soc. Japan, 60, 215-226, 1981.
- McAvaney, B.J.: Small Scale Wind Structure in the Upper Atmosphere, Ph.D Thesis. University of Adelaide, 1970.
- Meek, C.E., Reid, I.M., Manson, A.H.: Radio Sci., 20, 1383-1402, 1985.
- Mueller, H.G.: Planet. Space Sci., 16, 61-90, 1968.
- Muller, P., Holloway, G., Henyey, F., Pomphrey, N.: Rev. Geophys., 24, 493-536, 1986.
- Nastrom, G.D., Fritts, D.C., Gage, K.S.: J. Atmos. Sci., 44, 3087-3096, 1987.
- Noel, T.M.: J. Geophys. Res., 68, 2862-2863, 1963.

- Philbrick, C.R.: Middle Atmosphere Handbook, vol 2, 333-340. Scostep Secretariat, University of Illinois, U.S.A., 1981.
- Rastogi, P.K.: J. Atmos. Terr. Phys., 43, 511-524, 1981.
- Rees, D., Roper, R.G., Lloyd, K., Low, C.H.: Phil. Trans. Roy. Soc., Lond, A 271, 631-666, 1972.
- Reid, I.M.: J. Atmos. Terr. Phys., 48, 1057-1072, 1986.
- Reid, I.M., Vincent, R.A.: J. Atmos. Terr. Phys., 49, 443-460, 1987.
- Reid, I.M., Ruester, R., Schmidt, G.: Nature, 327, 43-45, 1987.
- Rhines, P.B.: J. Fluid Mechanics, 69, 417-443, 1975.
- Roettger, J., Rastogi, P.K., Woodman, R.F.: Geophys. Res. Letts., 6, 617-620, 1979.
- Roper, R.G.: J. Geophys. Res., 71, 4427-4428, 1966.
- Roper, R.G.: Turbulence in the Lower Thermosphere, in "The Upper Atmosphere Magnetosphere: Studies in Geophysics", 129, 117-129, National Research Council, U.S.A., 1977.
- Rosenberg, N.W., Golmb, D., Zimmerman, S.P., Vickery, W.K., J.S. Theon, Space Res. XIII, 435-439, 1973.
- Royrvik, O., Smith, L.G.: J. Geophys. Res., 89, 9014-9022, 1984.
- Sato, T., Woodman, R.F.: J. Atmos. Sci., 39, 2546-2552, 1982.
- Sato, T., Tsuda, T., Kato, S., Morimoto, S., Fukao, S., Kimura, I.: Radio Sci., 20, 1452-1460, 1985.
- Scheffler, A.O., Liu, C.H.: Radio Sci., 20, 1309-1322, 1985.
- Shibata, T., Fukuda, T., Maeda, M.: Geophys. Res. Letts., 13, 1121-1124, 1986.
- Shimazaki, T.: J. Atmos. Terr. Phys., 33, 1383-1401, 1971.
- Sidi, C., Teitelbaum, H.: J. Atmos. Terr. Phys., 40, 529-540, 1978.
- Sidi, C., Lefrere, J., Dalaudier F., Barat, J.: J. Geophys. Res., 774-790, 1988.
- Smith, S.A., Van Zandt, T.E.: Radio Sci., 20, 1331-1338, 1985.
- Smith, S.A., Fritts, D.C., Van Zandt, T.E.: J. Atmos. Sci., 44, 1404-1410, 1987.
- Strobel, D.F., Summers, M.E., Bevilacqua, R.M., DeLaud, M.T., Allen, M.: J. Geophys. Res., 92, 6691-6698, 1987.
- Strobel, D.: Pure Appl. Geophys., 130, 533-546, 1989.
- Tatarski, V.: Wave Propagation in a Turbulent Medium translated from Russian by Silverman, McGraw-Hill, N.Y., 1961.
- Tchen, C.M.: Phys. Rev., 93, 4-14, 1954.
- Teitelbaum, H.: Space. Res. VI, 438-447, 1966.
- Teitelbaum, H., Sidi, C.: J. Atmos. Terr. Phys., 38, 413-421, 1976.
- Teitelbaum, H., Blamont, J.E.: Planet. Space Sci., 25, 723-734, 1977.
- Thrane, E.V., Andreassen, O., Blix, T., Grandal, B., Brekke, A., Philbrick, C.R., Schmidlin, F.J., Widdel, H.V., Von Zahn, U., Luebken, F.-J.: J. Atmos. Terr. Phys., 47, 243-256, 1985.
- Tsuda, T., Inoue, T., Fritts, D.C., Van Zandt, T.E., Kato, S., Sato, T., Fukao, S.: J. Atmos. Sci., 46, 2440-2447, 1989.
- Van Zandt, T.E.: Geophys. Res. Letts., 9, 575-578, 1982.
- Van Zandt, T.E.: Handbook for MAP, vol 16, 149-156, Scostep Secretariat, University of Illinois, U.S.A., 1985.
- Van Zandt, T.E.: Radio Sci., 20, 1323-1330, 1985.
- Van Zandt, T.E., Fritts, D.C.: J. Geophys. Res., 9273-9732, 1987.
- Van Zandt, T.E., Fritts, D.C.: Pure Appl. Geophys., 130, 400-420, 1989.
- Vincent, R.A., Ball, S.: J. Atmos. Terr. Phys., 39, 965-970, 1977.
- Vincent, R.A., Stubbs, T.J.: Planet. Space Sci., 25, 441-455, 1977.

- Vincent, R.A., Ball, S.M.: J. Geophys. Res., 86, 9159-9169, 1981.
- Vincent, R.A., Reid, I.M.: J. Atmos. Sci., 40, 1321-1333, 1983.
- Vincent, R.A.: J. Atmos. Terr. Phys., 46, 119-128, 1984.
- Vincent, R.A.: Adv. Space Res., 7, 163-169, 1987.
- Vincent, R.A., Fritts, D.C.: J. Atmos. Sci., 44, 748-760, 1987.
- Von Zahn, U., Herwig, T.: Proc. NATO Advanced Study Institute, Spatind, Norway, April 12-22, eds B. Grandal, J.A. Hostet, Reidel Publ. Co., 1977.
- Weinstock, J.: J. Atmos. Sci., 35, 634-649, 1978a.
- Weinstock, J.: J. Atmos. Sci., 35, 1022-1027, 1978b.
- Weinstock, J.: J. Atmos. Sci., 38, 880-883, 1981.
- Weinstock, J.: Geophys. Res. Letts., 9, 863-865, 1982.
- Weinstock, J.: J. Atmos. Terr. Phys., 46, 1069-1082, 1984.
- Widdel, H.-U.: J. Atmos. Terr. Phys., 49, 723-741, 1987.
- Wofsy, S.C., McElroy, M.B.: J. Geophys. Res., 78, 2619-2624, 1973.
- Woodman, R.F., Guillen, A.: J. Atmos. Sci., 31, 493-505, 1974.
- Woodman, R.F., Kugel, R.P., Roettger, J.: Radio Sci., 15, 233-242, 1980.
- Woodman, R.F.: Radio Sci., 15, 423-430, 1980.
- Woodman, R.F., Rastogi, P.K.: Geophys. Res. Letts., 11, 243-246, 1984.
- Yeh, K.C., Dong, B.: J. Atmos. Terr. Phys., 51, 54-50, 1989.
- Zimmerman, S.P., Champion, K.S.W.: J. Geophys. Res., 68, 3049-3056, 1963.
- Zimmerman, S.P.: J. Geophys. Res., 71, 2439-2444, 1966.
- Zimmerman, S.P.: Space Res. VI, 425-437, 1966.
- Zimmerman, S.P.: J. Geophys. Res., 73, 463-454, 1968.
- Zimmerman, S.P., Trowbridge, C.A., Kofsky, I.L.: Space Res., XI, 907-914, 1971.
- Zimmerman, S.P., Rosenberg, N.N.: Space Res., XIII, 623-628, 1972.
- Zimmerman, S.P., Trowbridge, C.A.: Space Res., XIII, 203-208, 1973.
- Zimmerman, S.P.: J. Geophys. Res., 78, 3927-3938, 1973.
- Zimmerman, S.P., Pereira, G.P., Murphy, E.A., Theon, J.: Space Res., XIII, 209-215, 1973.
- Zimmerman, S.P., Murphy, E.A.: in Proc. NATO Advanced Study Institute, Spatind, Norway, April 12-22, eds. B. Grandal, J.A. Hostet, Reidel Publ. Co., 1977.
- Zimmerman, S.P., Keneshea, T.J.: MAP Handbook, Vol.2, 311-322, Scostep Secretariat, University of Illinois, U.S.A., 1981.
- Zimmerman, S.P., Keneshea, T.J.: J. Atmos. Terr. Phys., 48, 491-507, 1986.

258

Non-linearities, order and dis-order.

In the previous sections we presented a picture of disorganized motion - at small scales (turbulence), and organized - even linear - motion at larger scale (gravity waves).

In truth, this is not entirely realistic.

Non-linearities take place at larger scales, and there can be considerable order at small scales. The following articles demonstrate some ~~of these~~ examples which show how true this is.

I am not including the case of gravity wave break-down into turbulence, although this is also clearly an important area for study. Modern computer calculations are playing important roles in this regard (eg Frith, Wern, Peltier etc.)

The following
article discusses some peculiar
features about gravity waves
— and specially, their ability to
produce a type of diffusion which
looks a lot like turbulent diffusion.

THE ROLE OF STOKES DIFFUSION IN MIDDLE-ATMOSPHERIC TRANSPORT.

W.K. HOCKING

Physics Dept.,
University of Western Ontario,
London, Ontario, N6A 3K7, Canada.

and

R.L. WALTERSCHEID

Space Sciences Laboratory,
The Aerospace Corporation,
El Segundo, California, U.S.A.

ABSTRACT. Although turbulence occurs regularly throughout the middle atmosphere, it's appearance is sporadic both in time and space. It is certainly not possible to visualize the upper atmosphere as a homogeneous turbulent medium; laminar regions often appear to exist between the turbulent ones. Although localized occurrences of turbulence can be quite intense, this intermittency restricts the capability of small scale turbulence to cause large scale diffusion. In this paper, we discuss an alternative model for large scale atmospheric diffusion, which allows large scale diffusion to proceed even in the presence of very localized turbulence. We propose that large scale diffusion need not be entirely due to small scale turbulent eddies, but that an ensemble of gravity waves may act in a diffusive sense. This is possible because of the accumulated effects of the Stokes' drifts of an ensemble of gravity waves. We discuss the mechanism by which this occurs, and quantify the level of diffusion which we expect this mechanism to produce.

1. Introduction.

Rather than being a homogeneous process acting uniformly throughout the middle atmosphere, it has been clearly shown through the period of the recent "Middle Atmosphere Program" that turbulence is both temporally and spatially intermittent. It occurs only for short periods of time at varying spatial locations. Examples of this intermittency have been illustrated particularly well with radar studies (e.g. Czechowsky et al., 1979; Roettger et al, 1979; Woodman 1980; Sato et al., 1985, amongst many), and this intermittency has been discussed in some detail by Hocking, (1992).

The consequences of this intermittency are important. In particular, we must revisualize how large-scale turbulent diffusion takes place. An important proposal due to Dewan (1981) and Woodman and Rastogi (1984) suggested that the random occurrence of layers acts like a Monte Carlo process gradually causing diffusion, as first one layer forms, causing diffusion, and later another forms to cause transport over the depth of that layer. Thus in this model the factors which control the large-scale diffusion are not the rates of diffusion across individual layers, but the frequency of occurrence and depth of individual layers. Any determinations of effective diffusion coefficients must take this into account. "Classical" formulae relating the mean strength of turbulence within turbulent layers to the mean diffusion coefficient, such as

$$K = c \varepsilon / \omega_B^2 \quad (1)$$

would no longer be valid at large scales.

In this paper, we will discuss an alternative proposal, based around the concept of the "Stokes' Drift" of a gravity wave. The model has been reported in detail by Walterscheid and Hocking, (1991), but in this review we summarize its salient features and discuss it's implications for visualization of turbulent transport in the middle atmosphere. We should note here that we are not claiming that this is the sole cause of large scale atmospheric diffusion; we do, however, claim that it is an important one.

We choose to first give a discussion of the basic ideas inherent in the model, drawing on the results of Walterscheid and Hocking (1991). In this way, we hope to portray the salient concepts involved in the model, free of any mathematical encumbrances; we also make some statements without proof in this introductory discussion, and leave their actual justification until later in the paper. Only after this descriptive discussion do we turn to a more mathematical description.

2. A physical description of the principle of the model

A single monochromatic gravity wave in a compressible atmosphere carries a parcel of air in an elliptical orbit and returns it (almost) to its start position after one cycle. But it does not in fact return exactly to its start position. In fact (at least in the compressible case) the particle drifts slightly from its start position, and this constitutes a so-called "Stokes drift". A pictorial example is shown in fig. 1. This is true even for nondissipating waves, but more so for dissipating ones. When a spectrum of waves exists, the Stokes' drifts of the waves can add in a random-like manner to produce a sort of random walk. This results in dispersion of an initially compact cloud of particles, although it should be noted that the process will only be important over time scales of several hours and more. Walterscheid and Hocking (1991) used numerical procedures to examine the magnitude of this effect, and in due course we will summarize the results obtained in that earlier work.

However, before doing so, we now wish to take the concept of Stokes' diffusion a little further, and discuss gravity waves in a somewhat simpler atmosphere.

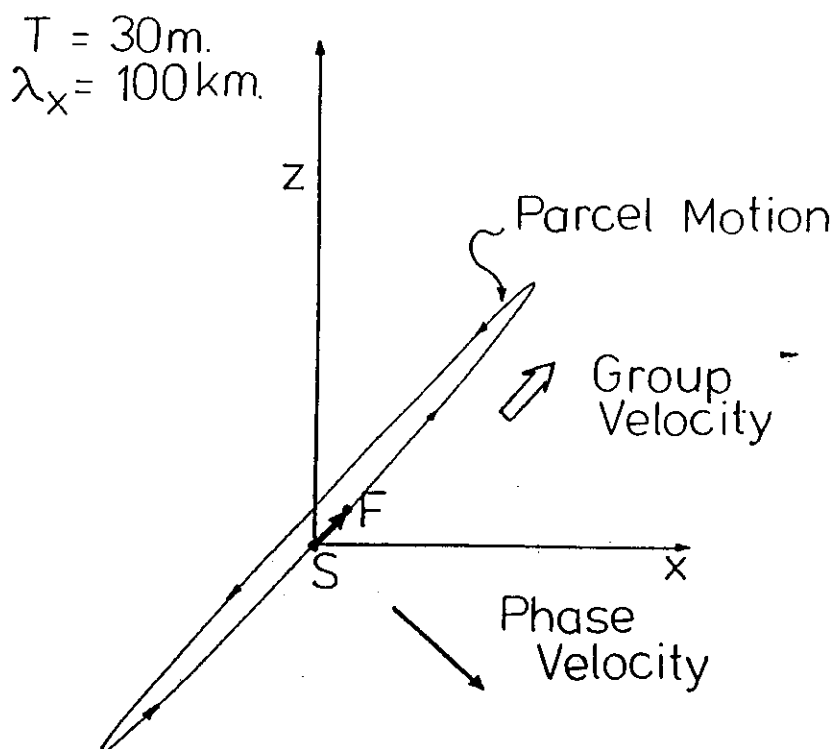


Figure 1. Schematic diagram of a typical parcel orbit when driven by a monochromatic, compressible gravity wave. The points S and F represent the parcel location at the start and finish of 1 full cycle, and the distance SF represents the "Stokes' drift".

Consider for simplicity one of the simplest types of buoyancy waves; namely the Boussinesq case. Individually, waves of this type suffer no Stokes' drift, and according to the above description they will therefore not exhibit the type of diffusion just described. However, when one considers a spectrum of waves, which may exhibit motions which decorrelate over some (as yet unspecified) spatial and temporal scales, then the picture changes. The relation between the velocity of a displaced parcel and its position becomes more complex, and the nett wave propagation vector may no longer be normal to the nett velocity. In such circumstances, even a spectrum of Boussinesq waves may exhibit a form of diffusion. In brief, a Stokes' drift may occur when one wave displaces a parcel along the direction of phase propagation of another wave.

The above description considers a special case of a random collection of monochromatic waves. However, we can also view the wave

field as a succession of wave packets. it is true that such a series of packets can be represented as a Fourier sum, and therefore in the same spectral manner as that just discussed, but it can sometimes be useful to visualize the wave field as such as sequence of packets. We can now look at the effects of our special diffusion in terms of such a description.

Consider an array of marked parcels subject to the passage of a random succession of dissipating wave packets. Because the packets are dissipating, parcels will suffer a net displacement as a result of the passage of a packet. If the parcels are separated by a distance that is large compared to the localization of wave packets, then parcels may be displaced with respect to each other in random walk fashion. As time goes on, the root-mean-square separation measured from the center of mass of the array will increase. This increasing separation in time is diffusive, and in this respect is similar to the separation that occurs as a result of the action of turbulent eddies. Wave packets are viewed as localized entities, and the diffusion that occurs is akin to scattering (Herterich and Hasselmann, 1982).

Eventually, the monochromatic waves making up the packets lose coherency in a dispersive medium and degenerate into a more or less random superposition of waves. We therefore now return to our discussions concerning a general spectrum of waves. The wave field in the mesosphere is apt to be dominated by such waves, and we now consider parcels subject to a random superposition of a large number of these waves. The motion of the parcels consists of a cycle-averaged drift and an intracycle disturbance velocity relative to the drift. The intracycle variations due to superposition of all of the waves are essentially uncorrelated for locations sufficiently far apart; i.e., for locations separated by a correlation length or greater. The correlation length in a given direction \underline{n} is $\ell_c = (\Delta k_n)^{-1}$, where Δk_n is the bandwidth of the wave-number spectrum in the direction \underline{n} . However, diffusion is the product of the cycle-averaged drift. This drift may be strongly inhibited by nonacceleration constraints (see Walterscheid and Hocking, 1991) and the degree of correlation in drift motions may be greater than that implied by ℓ_c , but it still occurs nevertheless.

We note that our model does not contravene any of the conditions of non-transport theory or potential temperature conservation in a non-dissipative field. If we consider the Boussinesq case, we imagine that parcels execute a long-term "random-walk" on surfaces of constant potential temperature. They simply "slide around" on these surfaces, but nevertheless the nett result can look very much like diffusion. We will not dwell extensively on this point in this paper; Walterscheid and Hocking (1991) discussed the implications of the model with respect to non-acceleration and non-transport theorems in greater detail.

In order to see the consequences of non-transport and conservation theorems, consider fig. 2. We imagine for simplicity a group of waves with various horizontal and vertical wavelengths, but with periods which are all harmonically related. Suppose the period of the longest wave is T_0 , and all other waves have periods of $T_0/2$, $T_0/3$ etc. Then after a time T_0 , the potential surface will look exactly like it did

at time $T=0$, as shown in the second part of fig. 2. However, the parcels which were marked in the first part of fig. 2. will now have drifted to new locations on the surfaces of constant potential surface.

*Schematic Illustration of Stokes Diffusion
along Planes of Constant Potential Temperature*

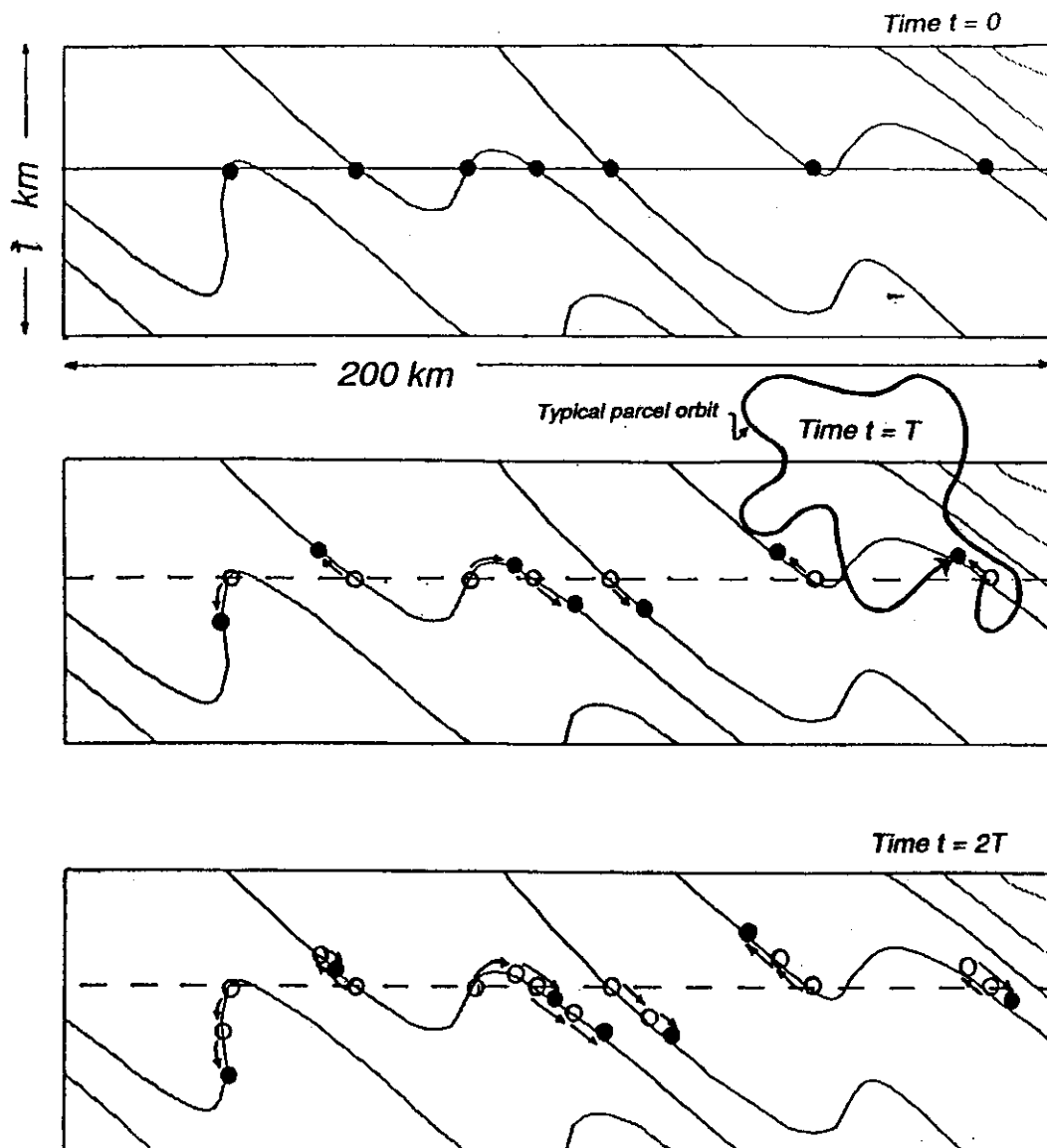


Figure 2. Illustration of the diffusive effect produced by an ensemble of gravity waves due to the Stokes' mechanism. Note that this represents only a small part of the wave field - the general slope of the isopleths up to the left is due to a larger scale wave which is not fully resolved in this diagram.

After another period T_0 , the parcels will have drifted further, as shown in the third part of fig. 2. To a distant observer, the parcels will appear to have undergone a "diffusive" spread, and this spread includes some vertical component because the original surfaces of constant potential temperature themselves had some vertical fluctuation.

Note that the spread after one cycle is much smaller than the vertical displacements which the parcel undergoes during one period of its trajectory, but the important point is that the layer never returns to a flat layer, even after all of the waves have completed integral numbers of periods. The original flat layer of parcels is now spread out vertically. After many cycles, the vertical spread can indeed be comparable with the vertical excursions of the particle during a single cycle.

However, since the parcels are still all located on surfaces of constant potential temperature, we cannot describe this as true diffusion. Certainly the motion along the surfaces of constant potential temperature is indeed true diffusion, but the apparent spread vertically is (in the non-dissipative case) an artifact. Nevertheless, from the viewpoint of a distant observer, it will appear just like vertical diffusion. The parcels can "diffuse" no further apart vertically by this mechanism than the maximum vertical excursion which the parcel undergoes during any part of its normal gravity oscillation, but in the middle atmosphere this can be several kilometres, as we will soon see. We will refer to this type of "diffusion" as "pseudo-diffusion".

The process just described will apply for any non-dissipative wave, whether it be Boussinesq or fully compressible. However, we will see that when we allow waves to be dissipative, then parcels of air can cross between lines of constant potential temperature. This, superimposed on the above "pseudo-diffusion", leads to a very real diffusion on time scales of several hours and more. In this paper, we will first treat "pseudo diffusion", and examine its magnitude and consequences as it relates to a spectrum of Boussinesq waves, and then we shall consider the case of dissipative fully compressible waves and look at the enhanced diffusion due to their dissipative nature. The actual cause of the wave dissipation will not be discussed here, but it could include non-linear interactions, critical layer interactions and turbulence production. We do however note that if the degree of wave dissipation is related to the mean energy dissipation rate, then the possibility exists that the mean strength of turbulence in individual layers might be related to the nett large scale Stokes' diffusion simply because the strength of turbulence and the Stokes' diffusion both depend on the rate of dissipation of the gravity waves. In this case it might not be so easy to dismiss relations like (1), although the functional relation between K and ϵ may not be as simple as (1) indicates.

We now turn to a more thorough mathematical discussion, in order to illustrate that what we have just said is really a valid description. Nevertheless, the discussion will be somewhat less thorough than that in Walterscheid and Hocking (1991), since this paper is intended to be a little more descriptive and less mathematically rigorous than that earlier one.

3. Theory

3.1. MATHEMATICAL DESCRIPTION OF STOKES DRIFT

Stokes drift may be viewed in terms of the drift of thin fluid tubes deformed by waves (Andrews and McIntyre 1978) or in terms of the drift of individual fluid parcels (Longuet-Higgins, 1969). In this study we adopt the latter view.

Consider a field of motion that consists at every point of an eddy contribution with zero time mean and a superposed mean flow. In general, the Lagrangian mean displacement will be different from the displacement implied by the Eulerian mean velocity. The difference between the Lagrangian mean velocity and the Eulerian mean velocity is the Stokes velocity. Thus,

$$\overline{u}^L = \overline{u} + \overline{u}_s \quad (2)$$

where \overline{u} is velocity; the overbars refer to time averages over a cycle. The quantity $()$ denotes the Eulerian time average over the locus of points traced out by the parcel's mean Lagrangian motion and $()^L$ denotes the Lagrangian average over the parcel's trajectory. Stokes drift is written in terms of parcel displacement as

$$\begin{aligned} \overline{u}_s &= \overline{u(X, t)}^L - \overline{u(\hat{X}, t)} \\ &= \overline{u\{X + \xi(\hat{X}, t)\}}^L - \overline{u(\hat{X}, t)} \end{aligned} \quad (3)$$

where X is the parcel position, $\hat{X} = X_0 + \overline{u}^L t$, $\xi = X - \hat{X}$, X_0 is the initial parcel position and 't' is time. Thus,

$$\xi = \int \overline{u(X, t')} Dt' - \overline{u}^L t \quad (4)$$

where Dt denotes integration following a parcel (Andrews and McIntyre, 1978). The quantity \overline{u}^L is that value of the mean drift velocity which gives $\xi = 0$. Stokes drift is nil for any motion for which $\overline{u(X + \xi, t)} = \overline{u(\hat{X}, t)}$; e.g., purely transverse waves. The quantity \overline{u} consists of contributions owing to mean background motion and eddy-induced Eulerian motion

$$\overline{u} = \overline{u}_B + \overline{u}_e \quad (5)$$

where \overline{u}_B is the background part and \overline{u}_e is the eddy-induced part. Henceforth, we set $\overline{u}_B = 0$.

If the parcel displacements during an averaging period are not too great, we can show (e.g. Walterscheid and Hocking, 1991)

$$\underline{u}_s = \overline{\xi \cdot \nabla \underline{u}'}(\hat{\underline{X}}, t) \quad (6)$$

correct to second order in disturbance amplitude.

This formula was determined with the requirement that $\overline{\xi} = 0$. However, it is also convenient to refer the evaluation of \underline{u}_s to the fixed point \underline{X}_0 rather than the moving point $\hat{\underline{X}} = \underline{u}^L t$ (Longuet-Higgins, 1969). Ignoring mean Eulerian motions gives

$$\left(\overline{\underline{u}}_s \right)_0 = \overline{\xi_0 \cdot \nabla \underline{u}'}_0 + O(a^3)$$

where $\xi = \underline{X} - \underline{X}_0$, $\underline{u}'_0 = \underline{u}(\underline{X}_0, t) - \underline{u}(\underline{X}_0, t)$, and 'a' is a measure of wave amplitude. We define

$$\xi_0 = \xi_0' + \delta \xi_0' \quad (7)$$

where

$$\xi_0' = \int_0^t \underline{u}'(\underline{X}_0, t') dt'$$

and where dt denotes integration at the fixed point \underline{X}_0 . Thus

$$\left(\overline{\underline{u}}_s \right)_0 = \overline{\xi_0 \cdot \nabla \underline{u}'}_0 + \overline{\delta \xi_0' \cdot \nabla \underline{u}'}_0 + O(a^3) \quad (8)$$

The vertical Stokes velocity is just the z component of this equation i.e.

$$\left(\overline{w}_s \right)_0 = \overline{\xi'_0 \cdot \nabla w'}_0 + \overline{\delta \xi'_0 \cdot \nabla w'}_0 + O(a^3) \quad (9)$$

where w is the vertical component of \underline{u} .

For small values of ξ_0/ℓ_c , the second term on the right hand side can be ignored in both (8) and (9).

3.2. SOURCES OF STOKES' DRIFT FROM A MATHEMATICAL PERSPECTIVE.

For monochromatic waves $\xi'_0 \cdot \nabla \underline{u}'_0 = i(\xi'_0 \cdot \underline{k}) \underline{u}'_0$, where \underline{k} is the wavenumber vector. Thus, Stokes drift by monochromatic waves on a background state of rest can be induced by any process that produces a longitudinal component to the wave motion. Steady, conservative, monochromatic Boussinesq wave motion, which is purely transverse, does not induce a Stokes drift, while monochromatic compressible wave motion, which has a longitudinal component, does (Coy et al. 1986). Dissipative processes also induce Stokes drift (Andrews and McIntyre 1978; Andrews et al. 1987).

Superposition effects can also generate a Stokes drift, and we have already discussed this qualitatively. However, it is unlikely that the first term on the right-hand side of (8) and (9) contributes very much to vertical diffusion. Sanderson and Okubo (1988) found that the vertical Lagrangian displacement was nil to second order for a spectrum of Boussinesq internal waves with vertical modal structures. In Walterscheid and Hocking (1991) we showed that the first term on the right-hand side is nil for a spectrum of vertically propagating Boussinesq waves for the special case where the waves comprising the spectrum are harmonically related. These results indicate that superposition effects should not contribute a significant vertical Stokes drift through the first term on the right. Thus, there is a tendency for ξ'_0 to be orthogonal to $\nabla w'_0$, even for a superposition of waves. In a non-Boussinesq atmosphere this term might contribute a significant upward drift through Stokes drifts induced by compressibility, irrespective of superposition effects (Coy et al. 1986). However, these drifts should not contribute to diffusion. They vary systematically rather than randomly and should be cancelled by induced Eulerian drifts; otherwise the Stokes drifts would result in a global long-term accumulation of mass above a given level.

This means that the diffusive action of Stokes drift is apt to originate in the second term on the right-hand side of (9) [which we denote $(\delta \bar{w})_0$] and possibly higher-order terms. This is a major point to note. When $\xi_0 \gg \ell_c$, the quantity $\delta \xi_0$ might be of the order of ξ_0 and have a large component randomly orientated with respect to $\nabla w'_0$; thus, in general, $\delta \xi'_0$ will not be orthogonal to $\nabla w'_0$. We expect the diffusion due to this effect to be a major contributor to the diffusion which we will see in our model.

4. Measures of Dispersion

In order to obtain quantitative estimates of the diffusion induced by this mechanism, we need to obtain a measure of the dispersion. We have found it convenient to define 3 separate measures, each of which has its own strengths and weaknesses.

If two parcels are separated by more than a correlation length, there can be significant relative displacement of the parcels. If this motion is extended to an array of parcels, the mean-square separation between parcels should increase as the result of uncorrelated displacements caused by the random superposition of waves. The mean-square vertical separation of parcels at time 't' relative to time t_0 is

$$\sigma_z^2 = \sum_i \frac{\langle (\Delta \bar{z}_i(t))^2 \rangle}{N} - \sum_i \frac{\langle (\Delta \bar{z}_i(0))^2 \rangle}{N} \quad (10)$$

The quantity $\Delta \bar{z}_i(t) = z_i - z_m$ is the vertical displacement of the i^{th} parcel with respect to the mean vertical position z_m , N is the number of parcels, and t is again time.

The quantity σ_z^2 can be expressed in terms of the mutual diffusion of pairs of parcels as follows. Let $\delta_i = z_i - z_i(0)$, and $\overline{(\delta_i)^2} = \Sigma (\delta_i)^2 / N = (\delta^2)_m$, where the subscript i refers to the i^{th} parcel, $1 \leq i \leq N$, and $z_i(0)$ is the initial value of z_i . It is easily shown that

$$\sigma_z^2 = \overline{(\delta_i^2)}^i \quad (11)$$

and if we further define

$$\chi_z^2 = \overline{(\delta z_{ij})^2}^{i,j} \quad (12)$$

then

$$\chi_z^2 = 2 \overline{(\delta_i^2)}^i = 2 \sigma_z^2 \quad (13)$$

The angle brackets denote an ensemble average over a large number of identical configurations of $z_i(0)$, and the quantity δz_{ij} is the vertical separation between the i^{th} and j^{th} parcel with the initial separation separated out ie

$$\delta z_{ij} = [z_i(t^*) - z_i(0)] - [z_j(t^*) - z_j(0)] \quad (14)$$

The definitions (10) and (12) are not very convenient for studying the growth in the rms separation of parcels for instances when parcels are separated by less than one correlation length. When investigating the relative dispersion of parcels initially much closer together than one correlation length, a modified form of (12) proves very useful. We define

$$\{z\Delta\ell\}^2 = \overline{(\delta z_{i,i+k})^2}^i \quad (15)$$

where k is an integer, and $\Delta\ell = k$ times the separation η of adjacent parcels. In the case that $k=1$, this formulation involves summing squares of displacements of adjacent pairs of particles. It has the advantage that, whereas the rates of increase of σ_z^2 and χ_z^2 with time depend on the rms wave amplitude, the correlation length, the separations of adjacent particles, and the total size of the cloud of particles under consideration, $\{z\Delta\ell\}^2$ has no dependence on the total cloud size. It is very similar to the structure function at lag $\Delta\ell$. When the motion of adjacent parcels is uncorrelated, $\{z\Delta\ell\}^2$ reduces to χ_z^2 . In the more general case, for N vertically aligned parcels separated by a distance $\Delta\ell$,

$$\chi_z^2 = \left[\sum_{k=1}^{N-1} (N-k) \{z(k\eta)\}^2 \right] / \{N(N-1)/2\}$$

where $\{z(k\eta)\}^2$ is the structure function at lag $\Delta\ell = k\eta$, and χ_z^2 is very nearly the structure function summed over all possible lags.

Since each has its advantages, all three measures of dispersion, (10), (12), and (15), will be used. the quantity $\{z_{\Delta\ell}\}^2$ is particularly useful for examining the dispersion of closely spaced parcels. We may think of $\{z_{\Delta\ell}\}^2$ with $k=1$ as being the mean rate of dispersion of neighboring pairs of parcels having initial separation $\Delta\ell$.

Walterscheid and Hocking (1991) considered various theoretical examples which utilized applications of these various measures of dispersion. We will not do this here, but rather will turn now to a numerical model which was used to investigate in more detail the effects which have been discussed so far.

5. Trajectory model

5.1. GRAVITY WAVE DISPERSION AND POLARIZATION RELATIONS.

In order to address the issues discussed, a numerical model was developed. It was decided to first generalize the usual fluid dynamical equations by including a Rayleigh drag term, and to solve these equations for WKBJ motions as rigorously as possible. Generalized dispersion relations for buoyancy waves were then developed. In this way, it was possible to examine the particle drifts for a variety of waves, from undamped to rapidly dissipating, and at the same time allow greater confidence that any Stokes drifts were real and not due to some inadequate approximation. The dispersion and polarization relations used are developed in appendix A.

5.2. NUMERICAL MODEL

A numerical model was developed to examine the particle drifts and evaluate the degree of diffusion. Paths of individual particles were computed by solving the relation

$$\frac{d\mathbf{x}}{dt} = \mathbf{u}(\mathbf{x}, t) \quad (16)$$

using a Runge-Kutta fourth-order scheme, where the velocity field $\mathbf{u}(\mathbf{x}, t)$ was specified by one or more gravity waves. In cases in which more than one wave was used, the wave periods and horizontal wavelengths were chosen to be harmonically related, and the drift was

determined over one period of the lowest-frequency wave so that all waves executed integral numbers of cycles. the difference in the final position and the start position was then found. The particle drifts were calculated using successively smaller time steps until the results were repeatable between two successive time steps; typical time steps necessary were in the range 0.05 to 0.5 s for Boussinesq waves and between 0.05 and 0.25s for compressible waves.

In our earlier work (Walterscheid and Hocking, 1991), we were also concerned about the possible effect of a mean nett Eulerian drift, and so in some of our simulations we also subtracted out a time-averaged Eulerian drift at each point of the trajectory. This was in order to avoid the physically unrealistic circumstance of a nett vertical mass flux being implicit in the model. However, our results with respect to diffusion were largely independent of whether this was done, so we will not consider this aspect in any more detail in this report.

5.3. WAVE SPECTRUM

The spectrum chosen was based on some observational data reported by Ball (1981) and Vincent and Ball (1981), which showed frequency spectra of the type $P(f) \propto f^{-1}$. This means that the energy per decade is constant. Within each frequency band, it was assumed that the horizontal wavenumber (k) followed a law of the type k^{-2} . These choices agree reasonably well with the relations described by VanZandt (1982).

In order to obtain stable results in reasonable computer time, it was necessary to limit the number of waves in the spectrum to a fairly small set. To do this, and yet still have an adequate range of wave periods and wavelengths, only waves with upward group velocity and eastward phase progression were considered in most of the calculations. Some simulations with westward-propagating waves showed that the dispersion of particles was essentially unchanged provided that the total energy content of the waves was unchanged. Thus, these initial limitations on the spectrum do not appear to be overly restrictive.

The Stokes drifts over six cycles of the longest period wave were calculated, using the previously mentioned Runge-Kutta scheme. In some special cases, drifts over eight cycles were found. The larger the number of waves that are included in the spectrum the more complicated the flow becomes. As the complexity of the flow increases, shorter time steps and greater precision are required in order for the iterative procedure to converge. The combination of short time steps and high precision makes trajectory calculation for a large number of waves infeasible.

An ensemble of 21 waves was chosen, using periods of 15 to 240 min, and with horizontal wavelengths in the range 6.25 to 1600 km. The phases of the waves were chosen at random. A table of the parameters of the resultant waves is shown in Table 1 of Walterscheid and Hocking, (1991). Waves with a vertical wavelength less than about 2-3 km were ignored, since these should be heavily damped by viscous and radiative effects (Schoerbel et al. 1983; Fels, 1982, 1984). Periods up to 240 min were included but not beyond, because inclusion of longer periods made the simulations prohibitively lengthy.

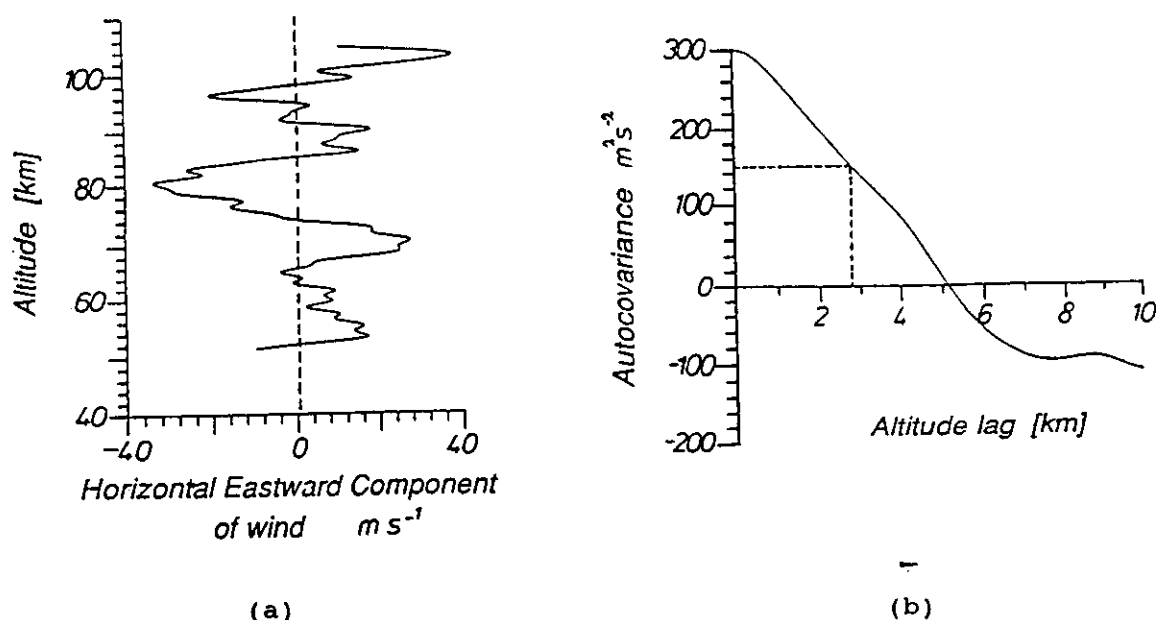


Figure 3. (a) Typical height profile of the x component of the wave velocity for the nominal spectrum of Boussinesq waves used in the trajectory simulations. (b) The vertical autocovariance function of the profile shown in (a).

Typical Parcel Trajectory

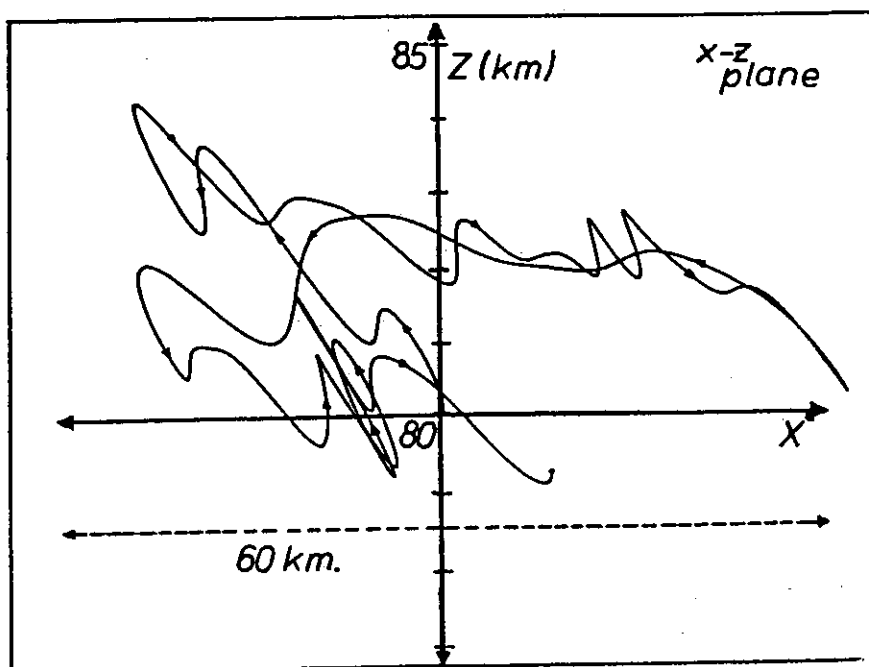


Figure 4. Typical particle trajectory for the spectrum of Boussinesq waves discussed in the text. The trajectory is for one cycle (240 mins).

6. The Simulations

Although we introduced our discussions in terms of the Stokes' drifts of compressible waves, we subsequently showed that even Boussinesq waves can cause Stokes' Diffusion, provided that a spectrum of waves is present; the drifts for individual monochromatic waves is zero. In many senses this type of diffusion is easier to model, and furthermore the diffusion inferred in this case is a useful reference point for subsequent comparisons with the compressible case. Thus we begin by studying this special case.

6.1. BOUSSINESQ SYSTEM

The Boussinesq system was obtained from the equations presented in the appendix by letting H and c_s^2 tend to infinity, except in the expression for N^2 (A4), and by setting $\hat{r} = 0$ in (A10). Potential temperature for the Boussinesq system was defined as $\theta = \theta_{ref} \hat{r}$, where θ_{ref} is taken to be 300K.

Initially, Stokes drifts were calculated for a variety of monochromatic waves, and it was confirmed that the Stokes drift in these cases were zero. In the remainder of this section we report model results for a spectrum of waves.

Fig. 3a shows a typical height profile of the x component of the velocity (u') due to the ensemble of waves chosen to represent the spectrum, and Fig. 3b shows the corresponding spatial-autocorrelation function. Notice that the vertical correlation length is about 2.8 km, since the autocorrelation function falls to 0.5 at this lag. The corresponding horizontal correlation length is ~50 km.

Fig. 4 shows a typical particle orbit over one cycle of the longest period wave for the spectrum described in Table 1 of Walterscheid and Hocking, (1991). The parcel experiences a nett drift, despite the fact that the waves are undamped Boussinesq waves. The next step was to quantify the degree of dispersion of an ensemble of particles in terms of the vertical diffusion of the ensemble. Particles were initially aligned in a vertical column and the quantity $\{z\Delta l\}^2$ [see (15)] was calculated. This was done for a variety of initial separations, including cases in which the initial separation Δl was substantially less than and substantially more than the vertical correlation length; values of Δl chosen were 4 km, 1 km, or 0.1 km.

The quantity $\{z\Delta l\}^2$ was calculated using a vertical array of 65 particles separated by 1 km, with an initial separation of 4 km. Particle pairs were successively the first and fifth, second and sixth, third and seventh, and so forth. The upper line in Fig. 5 shows the resultant variation as a function of time. One "cycle" corresponds to 240 minutes. The best-fit regression line gives

$$\log_{10} \{z\Delta l\}^2 = (1.04) \pm 0.12 \log_{10}(N_{cycle}) + (0.73 \pm 0.05) \quad (17)$$

where $t^* = N_{cycle} t_0$, and $t_0 = 240$ min.

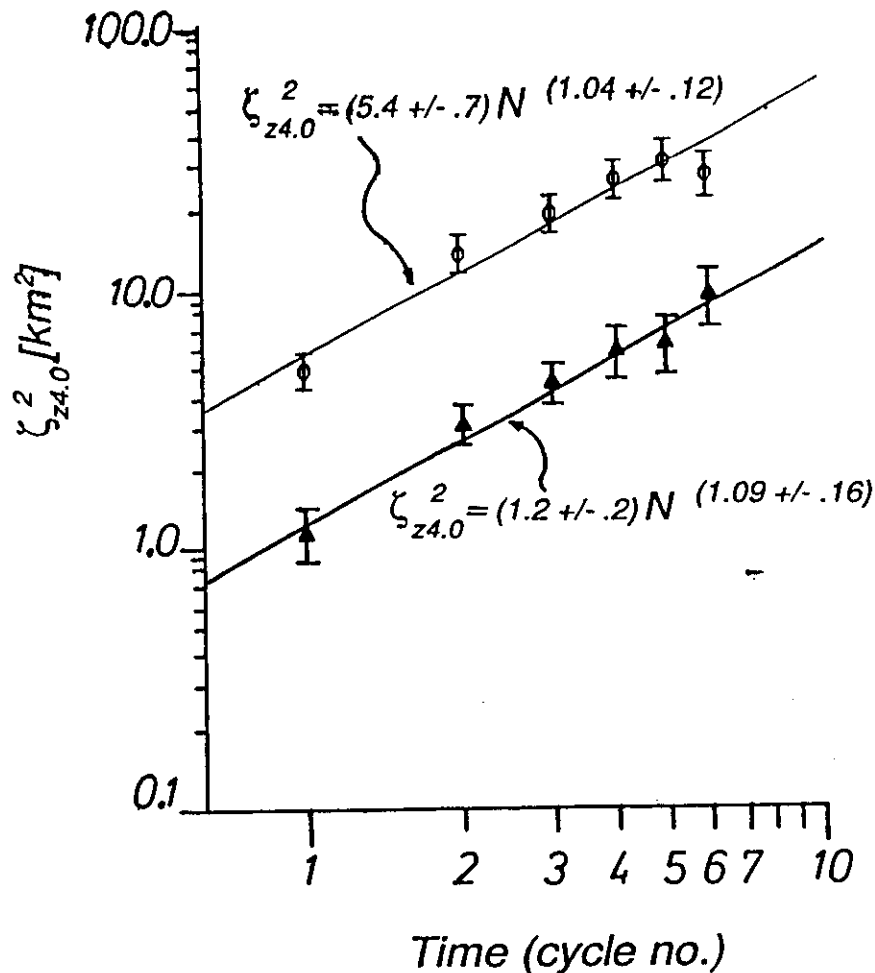


Figure 5. Mean-square separation $\zeta_{z4.0}^2$ of parcel pairs as a function of cycle number for two different sets of wave amplitudes and phases. In both cases parcel pairs were separated by 4 km vertically. The upper set of points shows the mean-square separation $\zeta_{z4.0}^2$ as a function of cycle number for one set of wave amplitudes, whereas for the lower set the wave amplitudes were halved. A different set of wave phases was used in each case. The error bars show standard errors and the solid lines show best-fit regression lines. The expressions for the best-fit lines are also indicated on the graphs, where N refers to the cycle number (N_{cycle} in the text). Both best-fit lines are statistically consistent with $\zeta_{z4.0}^2 \propto N$.

As discussed by Walterscheid and Hocking, (1991) [see their equations (29) and (30)], we expect that in the limit of large separations,

$$\sigma_z^2 = 2 D_{zz} t^*, \quad (18)$$

or

$$\chi_z^2 = 4 D_{zz} t^*. \quad (19)$$

In other words, we expect the slope to be 1.0, and our observed value is not statistically different, so we can take it as 1 exactly; if we do this and solve for D_{zz} using (19), we obtain $D_{zz} = 90 \text{ m}^2 \text{ s}^{-1}$.

The diffusion coefficient will be a function of the energy in the wave spectrum. We expect that $D_{zz} \sim (\sigma_z^2/t) \sim (\sigma_z/t)^2 t^* \sim w'^2 t^*$, so that

$$D_{zz} \propto \langle w'^2 \rangle_{t_L} \sim O(a^2) \quad (20)$$

where 'a' is a measure of wave amplitude. Thus we anticipate that D_{zz} will be proportional to the power in the spectrum.

In order to check this dependence, the above simulations were repeated with the previous wave amplitudes halved (thus reducing the total power in the spectrum by 4 times), and a new set of phases was used. For this case we found that $D_{zz} \sim 20 \text{ m}^2 \text{ s}^{-1}$ (see fig. 5). This reduction is close to the limiting value of a factor of 4 when $\xi_0 \gg l_c$.

The results presented so far refer to parcel pairs whose motions were initially uncorrelated, but it is also interesting to observe what happens when parcel motion is initially correlated. Fig. 6a shows the variation of $\xi_{z0.1}^2$ as a function of time for wave amplitudes equal to those used in the second set of calculations discussed above (i.e. reduced to one half of the original set). The smaller amplitudes were used to prevent the parcel motion from becoming uncorrelated too quickly. The most noticeable effect is that the slope of the line is much steeper than 1.0. It was found that the following equation was approximately obeyed;

$$\xi_{z0.1}^2 \propto t^{1.7 \pm 0.2} \quad (21)$$

This faster increase in $\xi_{z0.1}^2$ as a function of time arises because of the rapid increase in the decorrelation between parcels; initially the larger-scale waves do not play a dispersive role but as the parcel separations increase, the large-scale waves become involved and accelerate the dispersion of parcels.

Eventually the parcels should move so far apart that they are essentially uncorrelated, in which case there should be a transition to a relation of the type $\xi_{z\Delta t}^2 \propto t$. Parcel motion can decorrelate because of vertical and horizontal displacement. Note that in Fig. 4 the vertical and horizontal displacements both exceed their respective correlation lengths - with a somewhat greater decorrelation indicated for vertical displacement. To investigate the possibility of a transition to a diffusive limit $\xi_{z1.0}^2$ was calculated as a function of cycle number for an initial separation of 1 km and again using amplitudes equal to one-half of those used originally (i.e. the same as

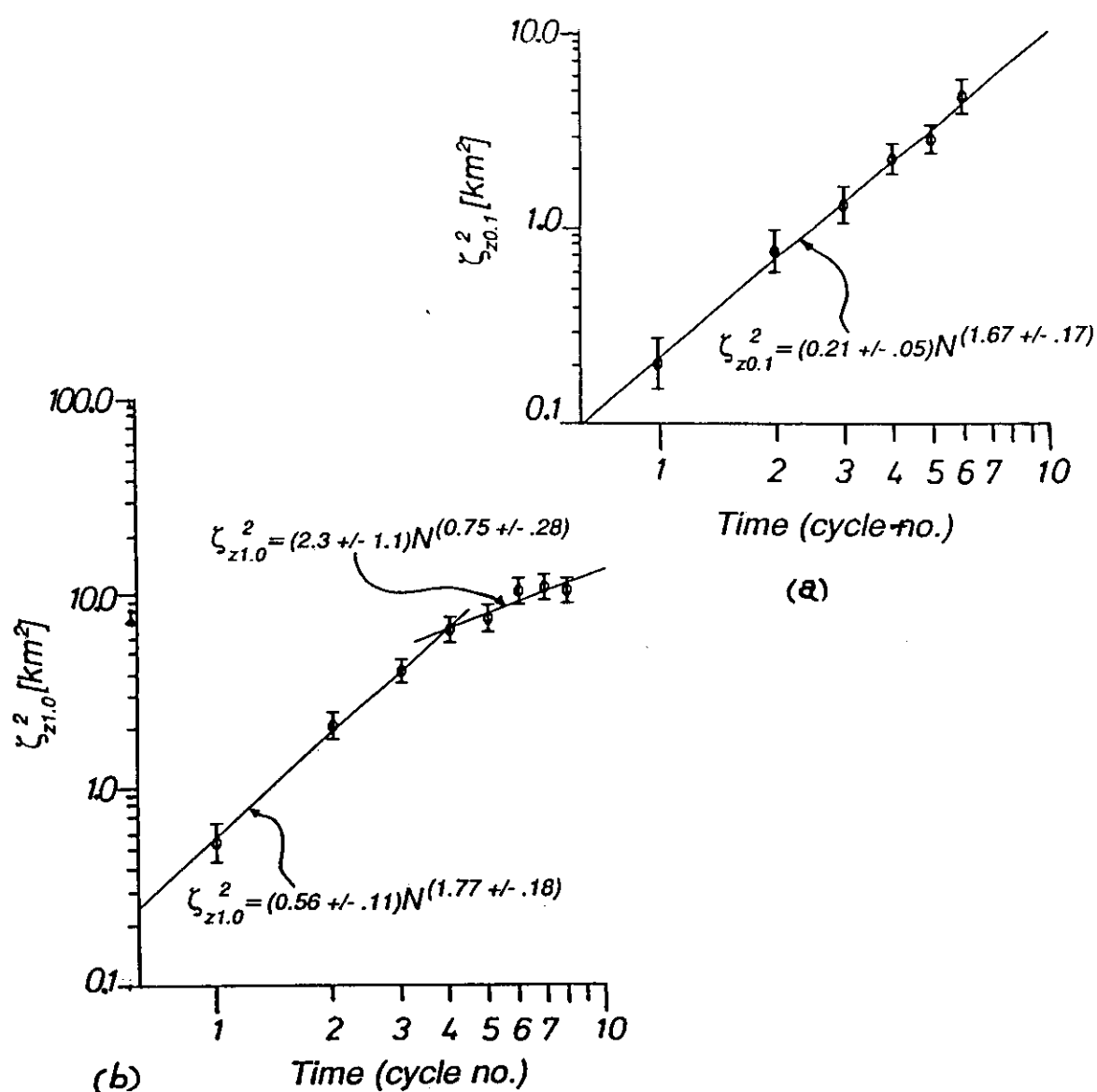


Figure 6 (a) Mean-square separation of parcels $\zeta_{z0.1}^2$ as a function of cycle number for the case in which the parcel pairs were initially 0.1 km apart. Wave amplitudes are one-half of those used in the first case discussed in fig. 5, and the same as the second case discussed in fig. 5. Note that $\zeta_{z0.1}^2$ increases much more rapidly than $\zeta_{z4.0}^2$ did in fig. 5. (b) As in (a), but with initial parcel separation equal to 1 km. Note that a break in slope occurs at about $\zeta_{z0.1}^2 \approx 7 - 8$ km². At this point the mean-square separation of particles [i.e. $(1.0)^2 + (\zeta_{z0.1}^2)$] is approximately $l_{0.5}^2$ where $l_{0.5}$ is the vertical correlation length (see fig. 3).

those used for fig. 6, and the lower line in fig. 5). A break in slope occurs at about cycle 4, when the mean square parcel separation is $[(1.0)^2 + (\delta z_{0.1})^2] \approx (2.8)^2 \text{ km}^2$, or approximately the vertical correlation length squared. It should be noted that the break shown here is slightly more pronounced than for other choices of the relative phases used, partly because of the rather low slope of 0.75 ± 0.28 beyond cycle 4. This is marginally consistent with a slope of 1.0. A break in slope was a common feature of other simulations using different phase combinations for the waves and seems to represent a real phenomenon.

We have deliberately not discussed the effects with respect to non-acceleration and non-transport theorems in this article; Walterscheid and Hocking, 1991) discussed these effects at length. We have only noted here that our model does not contravene any such theorems. However, we do note that the break in the slope of the $\delta z_{\Delta t}$ curve may also be related to constraints imposed by nonacceleration-nontransport conditions; one would expect the dispersion to tend to eventually "saturate" at large enough parcel separations—since the parcels can move no further than the maximum vertical displacement of the wave. Some evidence is seen for this in Fig. 6b at cycles greater than 6. The behavior is also seen to some extent in the upper curve shown in Fig. 5 for $N_{\text{cycle}} \geq 4$ or 5.

To be more specific, when the mean position of θ surfaces are constant as a consequence of nonacceleration-nontransport constraints, parcel displacements are limited to the maximum vertical displacement of the wave-deformed θ surface plus some drift relative to θ the surface because of nonconservation of θ . (This may be viewed, alternatively, as conservation of θ accompanied by wave transport of mean θ). The maximum excursion of a wave-deformed θ surface is $\Delta z_{\text{max}} \sim w't_0/(2\pi)$, where w' is a characteristic perturbation vertical velocity. For our nominal spectrum $\Delta z_{\text{max}} \sim 4 \text{ km}$ and is consistent with the maximum parcel displacement shown in Fig. 4.

6.2. A SPECTRUM OF COMPRESSIBLE WAVES

We now turn to some more realistic simulations, in which we allow the waves to be fully compressible. Only saturated waves are considered. We assume that saturation occurs as a result of some dissipative process (e.g., small-scale turbulence and convection), which can be modeled in idealized terms by Rayleigh friction. Rayleigh friction is chosen in such a way that m_i , the imaginary part of the vertical wavenumber, is zero. As already discussed, mean Eulerian drifts will not be discussed in this paper, although they were certainly discussed extensively in our earlier work. As for the Boussinesq case, the initial configuration of parcels was chosen to be one in which all the parcels had the same location in the x-y plane, but different vertical positions. This is because the major effect to be examined was the rate of vertical diffusion, and if different horizontal positions were used for the start positions, the horizontal spatial separation would contribute to the decorrelation of velocities and enhance the diffusion. We note that by now considering dissipative waves, there may indeed be a real diffusive effect in addition to the vertical "quasi-diffusion" discussed

in relation to the Boussinesq case.

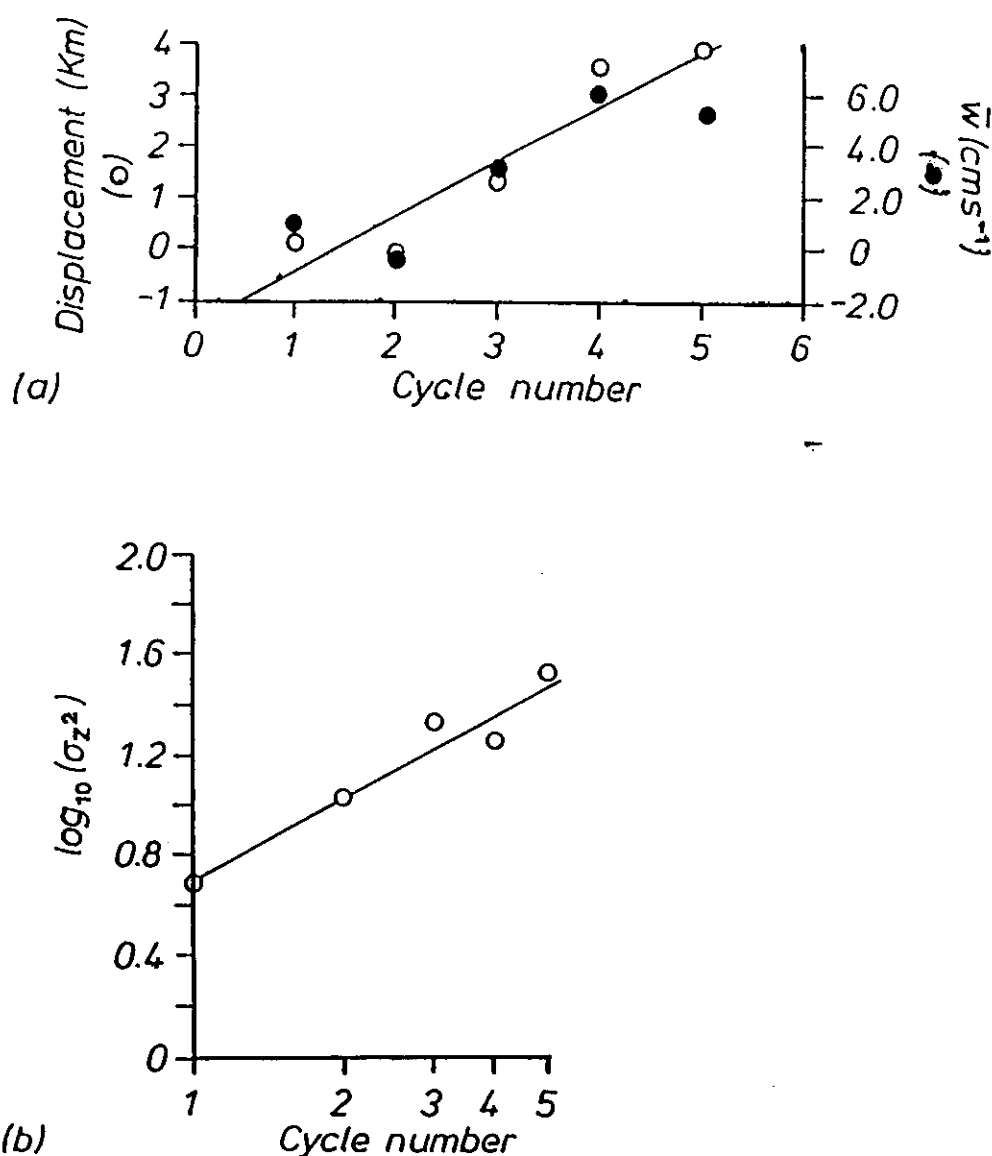


Figure 7. Mean drift and dispersion (σ_z^2) for a spectrum of saturated waves, as a function of the cycle number. Start positions were vertically aligned. Note that σ_z^2 is the dispersion from the centre of mass, and is one half of the quantity used in figs. 5 and 6.

Particles were entered with ten different start positions distributed uniformly over one full vertical wavelength of the largest wave; i.e., at (0, 0, 50), (0, 0, 56.5), etc. (units in kilometers). Typical particle orbits for a saturated wave spectrum were similar to the one shown in Fig. 4. In this case, we calculated σ_z^2 as our

measure of dispersion [see (12)], so these values should be doubled if making comparisons with figs. 5 and 6.

Results for the ensemble mean vertical Stokes drift for a saturated spectrum of waves are shown in Fig. 7. Using the quantities displayed in fig. 7 to determine D_{zz} through the relation (18) gives values for D_{zz} of about $170-200 \text{ m}^2 \text{ s}^{-1}$. We have already noted that some of this is a "quasi-diffusion" contribution, and we have also seen from our work with Boussinesq waves that this component is expected to be about $90 - 100 \text{ m}^2 \text{ s}^{-1}$. Thus we might surmise that the "real" diffusive component is the difference between D_{zz} calculated from fig. 7 and this "quasi-diffusion" component, or about $70-100 \text{ m}^2 \text{ s}^{-1}$. Such a value is quite representative of inferred diffusion rates in the middle atmosphere at $\sim 80-90 \text{ km}$ (e.g., Hocking, 1987) and suggests that this mechanism might be an important cause of diffusion in the atmosphere.

This result is the main point of this work so far, and underlines the potential importance of this mechanism as a cause of large scale diffusion in the real mesosphere.

7. Summary and conclusions

We have examined the dispersion of marked parcels by Stokes drift using the Stokes drift formalism, relations for the dispersion of marked parcels, and trajectory simulations. Our trajectory model is one in which Eulerian drifts are accounted for by simultaneously requiring the mean Lagrangian displacement to vanish for monochromatic waves when nonacceleration conditions apply and requiring that there be no long-term accumulation or depletion of mass above a given level; otherwise parcel drifts are consistent with displacements caused by a field of noninteracting waves. Trajectory simulations were performed for a spectrum of Boussinesq and saturated compressible waves.

We have found that "Stokes' Diffusion" does indeed produce long-term diffusive effects comparable to those measured in the real atmosphere, and therefore note that this process will almost certainly be important in diffusion in the Earth's middle atmosphere. Even a spectrum of waves in a Boussinesq atmosphere can cause a form of diffusion which we have labeled "quasi-diffusion", but once compressibility and dissipation are also included, we find that very substantial rates of real diffusion do indeed occur. In our case, using realistic gravity wave spectra, we obtain estimates of vertical diffusion in the range $70-100 \text{ m}^2 \text{ s}^{-1}$. We note however that this diffusion process will only be important on time scales of a few hours and more, and will not be important for local small scale diffusion.

We also note that even for a Boussinesq spectrum, there will be real diffusion along surfaces of constant potential temperature. It is only the vertical diffusion which needs to be considered as non-real. Indeed, if a tracer q has a gradient along a surface of constant potential temperature, then Stokes' diffusion will certainly cause real diffusive transport of q .

APPENDIX A: THE DISPERSION AND POLARIZATION RELATIONS FOR GRAVITY WAVES AS USED IN THE TEXT.

The equations considered were the standard fluid-dynamical equations viz

$$\frac{D\mathbf{u}}{Dt} + 2\rho\mathbf{\Omega}\times\mathbf{u} + \rho\mathbf{g} + \nabla p = 0 \quad (\text{A1})$$

$$\frac{D\rho}{Dt} = \frac{1}{c_s^2} \frac{Dp}{Dt} \quad (\text{A2})$$

$$\frac{D\rho}{Dt} + \rho\nabla\cdot\mathbf{u} = 0 \quad (\text{A3})$$

where D/Dt represents differentiation following the motion. The total velocity is \mathbf{u} , the density is represented by ρ , $\mathbf{\Omega}$ is the Coriolis parameter, $\mathbf{\Omega}\times\mathbf{u}$ is the cross product of $\mathbf{\Omega}$ and \mathbf{u} , \mathbf{g} is the acceleration due to gravity = $(0,0,-g)$, p is the pressure, c_s^2 is the speed of sound squared, ∇ represents the gradient differential operator and \cdot means the dot product.

Assuming that each variable can be written as the sum of a mean and fluctuating component $\langle\Phi\rangle + \Phi'$, and that WKBJ solutions of the type $\Phi'(x,y,z,t) \propto \exp\{i(kx + mz - \omega t)\}$ ($i = \sqrt{-1}$) exist for each of Φ = pressure, density, and velocity, then linearizing and solving these equations leads to dispersion relations for a single monochromatic wave. It will be assumed that the atmosphere is stratified with respect the mean quantities, that the wave propagates only in the zonal direction, and that the mean wind is zero, for ease of presentation. Let the fluctuating velocity component be (u',v',w') . We will also use the change of variables $\psi = p'/\langle\rho\rangle$, and $r' = \rho'/\langle\rho\rangle$, and define the Brunt-Vaisala frequency N by

$$N^2 = \frac{g}{\bar{T}} \frac{d\bar{T}}{dz} + \kappa \frac{g}{H} \quad (\text{A4})$$

Here, H is the scale height given by

$$H = \frac{R\bar{T}}{g} \quad (A5)$$

where $\kappa = R/c_p$ and R is the ideal gas constant and c_p is the specific heat of air at constant pressure.

Then the resultant algebraic equations are

$$-i\omega u' - fv' = -ik\psi' \quad (A6)$$

$$-i\omega v' + fu' = 0 \quad (A7)$$

$$-i\omega w' + r'g = -(im\psi' - \psi'/H) \quad (A8)$$

$$-i\omega r' - w'.N^2/g = 1/(c_s^2).(-i\omega\psi') \quad (A9)$$

$$-i\omega r' + iku' - w'/H + imw' = 0 \quad (A10)$$

The variable f represents the inertial frequency. The Rayleigh drag is now readily included by adding a drag term proportional to the velocity in the momentum equations, so that the first two equations above become

$$-i\omega u' - fv' = -ik\psi' - \alpha u' \quad (A11)$$

$$-i\omega v' + fu' = -\alpha v', \quad (A12)$$

where α is the Rayleigh drag coefficient.

Note that these equations are more general than even the anelastic approximation, as well as the Rayleigh drag terms being included.

When these equations are solved, a dispersion relation results, which is

$$\underline{m}(\underline{m} + i/H) = \frac{\underline{\omega}_*}{\omega} \cdot \frac{(N^2 - \omega^2) k^2}{(\underline{\omega}_*^2 - f^2)} + \frac{\omega^2}{c_s^2} \quad (A13)$$

where $\underline{m} = m_R + im_i$ and $\underline{\omega}_*$ is defined as $\omega + i\alpha$. It can readily be shown that this dispersion relation is identical to that of Gossard and Hooke (1975, p112) when the Rayleigh term is zero, which helps confirm its accuracy, but of course the relation just derived is more general. Note that the scale-height term $(-1/2H)$ has not been separated out from m_i , and if $\alpha = 0$, then $m_i = -1/2H$.

The associated polarization relations are listed below, viz;

$$v' = (-f\alpha - if\omega)/(\omega^2 + \alpha^2) \cdot u' = -if/\underline{\omega}_* \cdot u' \quad (A14)$$

$$w' = - \left[\frac{\omega(\omega_*^2 - f^2)}{\omega_*(N^2 - \omega^2)k} \cdot \left(\underline{m} + i \left(\frac{1}{H} - \frac{g}{c_s^2} \right) \right) \right] \cdot u' \quad (A15)$$

$$\psi' = (\omega_*^2 - f^2) / (\omega_* k) \cdot u' \quad (A16)$$

$$r' = \frac{k}{\omega} u' + \left(\frac{\underline{m}}{\omega} + \frac{i}{\omega H} \right) w' \quad (A17)$$

The diffusive action of gravity waves was simulated by calculating the displacements of parcels subject to the influence of an ensemble of gravity waves obeying these relations.

REFERENCES

- Andrews, D.G., and M.E. McIntyre, Planetary waves in horizontal and vertical shear: the generalized Eliassen-Palm relation and the mean zonal acceleration, *J. Atmos. Sci.*, 33, 2031-2048, 1976.
- Andrews, D.G., and M.E. McIntyre, An exact theory for nonlinear waves on a Lagrangian-mean flow, *J. Fluid Mech.*, 89, 609-646, 1978.
- Andrews, D.G., J.R. Holton and C.B. Leovy, *Middle Atmosphere Dynamics*, Academic Press, 489 pp, 1987.
- Ball, S.M., "Upper atmosphere tides and internal gravity waves at mid- and low-latitudes", Ph.D. thesis, *University of Adelaide, Australia*, 1981.
- Batchelor, G.K. "The application of similarity theory of turbulence to atmospheric diffusion", *J. Roy. Meteorol. Soc.*, 76, 133-146, 1950.
- Coy, L., D.C. Fritts and J. Weinstock, The Stokes' drift due to vertically propagating internal gravity waves in a compressible atmosphere, *J. Atmos. Sci.*, 43, 2636-2643, 1986.
- Czechowsky, P., R. Rueter, and G. Schmidt, Variations of mesospheric structure in different seasons, *Geophys. Res. Letts.*, 6, 459-462, 1979.
- Dewan, E.M., Turbulent vertical transport due to thin intermittent mixing layers in the stratosphere and other stable fluids, *Science*, 211, 1041-1042, 1981.

- Gossard E.D. and W.H. Hooke, "Waves in the Atmosphere", 456 pp, Elsevier, NY, 1975.
- Herterich, K., and K. Hasselmann, The horizontal diffusion of tracers by surface waves, *J. Phys. Oceanography*, 12, 704-711, 1982.
- Hocking W.K., Turbulence in the region 80-120 km., *Advances in Space Res.*, 7, no. 10, 171-181, 1987.
- Hocking, W.K., Two years of continuous measurements of turbulence parameters in the upper mesosphere and lower thermosphere made with a 2-MHz radar, *J. Geophys. Res.*, 93, 2475-2491, 1988.
- Hocking, W.K. "The effects of middle atmosphere turbulence on coupling between atmospheric regions", *J. Geomag. and Geoelectricity*, in press, 1992.
- Longuet-Higgins, M.S., On the mass transport by time-varying ocean currents, *Deep-sea Res.*, 16, 431-447, 1969.
- Roettger, J., P.K. Rastogi, and R.F. Woodman, High resolution VHF radar observations of turbulence structures in the mesosphere, *Geophys. Res. Letts.*, 6, 617-620, 1979.
- Sato, T., T. Tsuda, S. Kato, S. Morimoto, S. Fukao, and I. Kimura, High resolution observations of turbulence by using the MU radar, *Radio Sci.*, 20, 1452-1460, 1985.
- VanZandt, T.E., "A universal spectrum of Buoyancy waves in the atmosphere", *Geophys. Res. Letts.*, 9, 575-78, 1982
- Vincent, R.A. and S.M. Ball, "Mesospheric winds at low- and mid-latitudes in the Southern hemisphere", *J. Geophys. Res.*, 86, 9159-9169, 1981
- Walterscheid R.L. and W.K. Hocking, Stokes diffusion by atmospheric internal gravity waves, *J. Atmos. Sci.*, 48, 2213-2230, 1991.
- Woodman, R.F., High-altitude-resolution stratospheric measurements with the Arecibo 2380-MHz radar, *Radio Sci.*, 15, 423-430, 1980.
- Woodman, R.F. and P.K. Rastogi, Evaluation of effective eddy diffusive coefficients using radar observations of turbulence in the stratosphere, *Geophys. Res. Letts.*, 11, 243-246, 1984

Continuing our theme of
destroying the myth that small scales
relate to disorder, and larger scales to greater
order, here are two examples of ~~complex~~
models which involve organized motion
even at very small scales.

① VISCOSITY WAVES

② PST

Viscosity waves and thermal-conduction waves as a cause of "specular" reflectors in radar studies of the atmosphere

W. K. Hocking,¹ S. Fukao, M. Yamamoto, T. Tsuda, and S. Kato

Radio Atmospheric Science Center, Kyoto University, Kyoto, Japan

(Received June 29, 1990; revised May 18, 1991; accepted May 14, 1991.)

We present a new theory to explain the cause of the atmospheric structures which are responsible for specular reflection of radar signals from the atmosphere. Evidence recorded with the middle and upper atmosphere (MU) VHF radar at Shigaraki in Japan, as well as previous reports of specular reflections from other radars and at other frequencies, is used to support our assertions. The theory postulates that the reflectors are produced by a form of highly damped wave which arises in a fluid as a result of the effects of viscosity and thermal conduction. They occur at altitudes where gravity waves are partially reflected and in the vicinity of gravity wave critical levels but are particularly prevalent when such reflections and critical level interactions occurs in a laminar region of the atmosphere. The typical scales of the waves, their reflection efficiency, and their likely location are all considered and found to be consistent with what is currently known about specular reflectors in the atmosphere. Some predictions which will allow further tests of the model are also presented.

INTRODUCTION

A large number of papers have shown evidence for radar scatter at VHF, HF, and MF which is highly aspect sensitive. Generally, the observations of anisotropy take the form of strong scatter from overhead and less scatter at off-vertical angles. It is known that this implies that the scatterers are irregularities in refractive index which are stretched out horizontally and compressed in their vertical structure, but opinions vary about the cause of the atmospheric structures. Some authors have claimed that such structures are to be expected for anisotropic turbulence [e.g., Crane, 1980; Doviak and Zrnic, 1984; Woodman and Chu, 1989]. Others claim that the variation in power as a function of angle is too rapid to be explained by turbulence alone, and they cite other evidence such as very slow fading times to support their view that the scatter occurs not from irregularities generated by anisotropic turbulence, but rather from some sort of stratified step in refractive index [e.g., Roettger, 1980a, b; Roettger and Liu, 1978; Gregory and Vincent, 1970; Gage and Green, 1978; Hocking and

Vincent, 1982a, b]. The main possible physical models which have been invoked to explain such stratified reflecting layers have been (1) "steps" induced at the edges of very turbulent layers [Bolgiano, 1968] and (2) long-period gravity waves with short vertical wavelengths [Hines, 1960; Van Zandt and Vincent, 1983].

While it is likely that some of the aspect sensitivity can be explained by anisotropic turbulence, occasionally echoes of such stable, slowly fading character occur, and with such strong aspect sensitivity, that it really becomes hard to believe that the scatter is due to turbulence. In this work we present one such data set, and we quantify the degree of aspect sensitivity. We present arguments to support the view that these echoes are indeed due to some sort of horizontally stratified structure and consider the possibility that this is produced by either model 1 or 2 above. By solving the dispersion relation for waves in a viscous fluid we show that model 2 cannot explain the observation, and we argue that model 1 is also inadequate.

However, we note the existence of other wave modes apart from the usual acoustic and gravity waves and, in particular, the existence of so-called "viscosity waves," which have also been described by Klostermeyer [1972, 1980], Hooke and Jones [1986], Pitteway and Hines [1963], Yanowitch [1967a, b, 1969], and Myers and Yanowitch [1971]. By applying some quantitative analysis we show that viscosity waves may be able to explain our

¹ Currently at Department of Physics and Mathematical Physics, University of Adelaide, Australia.

Copyright 1991 by the American Geophysical Union.

Paper number 91RS01661.
0048-6604/91/91RS-01661\$08.00

observations and indeed many of the past observations of "specular reflectors." We make frequent reference to *Hooke and Jones* [1986], and hereafter this will be denoted HJ.

EXPERIMENT

The data reported in this work were collected during an experiment designed to measure and quantify the degree of aspect sensitivity of VHF radar scatterers in the stratosphere using the Japanese middle and upper atmosphere (MU) radar.

The MU radar at Shigaraki near Kyoto in Japan is a versatile system operating at a frequency of 46.5 MHz. It has fast flexible beam steering, and it is possible to use all, or subsets of, the Yagi's of the main array to form a radar beam. It also features high power, and good sidelobe suppression. The main beam formed when using the whole array for both transmission and reception has a half-power half width of 1.2° . More specific details have been described by *Fukao et al* [1985a, b].

The data were obtained as part of two special experiments performed in October and December 1988 which were designed to make studies of the aspect sensitivities of radio wave scatterers in the stratosphere over Japan. The data reported in this paper were recorded during the October run, and so only the beam configurations used in that case will be reported here. For more details about the experiments, see *Hocking et al.* [1990].

In the October experiment, eight beams were used with the configuration shown in Figure 1a. The tilt angles and azimuths were chosen so that the sampling volumes at a constant height produced a rectangular grid in the sky, as shown in Figure 1b. The beams were sampled on successive pulses, with the beams being sequenced in an eight-point cycle. Coherent integration over 16 points was performed giving an effective sampling time of 0.1638 s between successive points at any one height on any one beam. A 16-bit coded pulse was used to give 600-m resolution, and echoes were sampled at ranges between 7.95 and 26.55 km at 600-m intervals, giving 32 range samples in all. Data sets of 256 points were obtained between 2045 LT on October 17 and 0947 LT on October 18, each set having a duration of 42 s. A 3-s gap then followed while data transfer took place, and then the next set of 256 points was collected. Only data collected

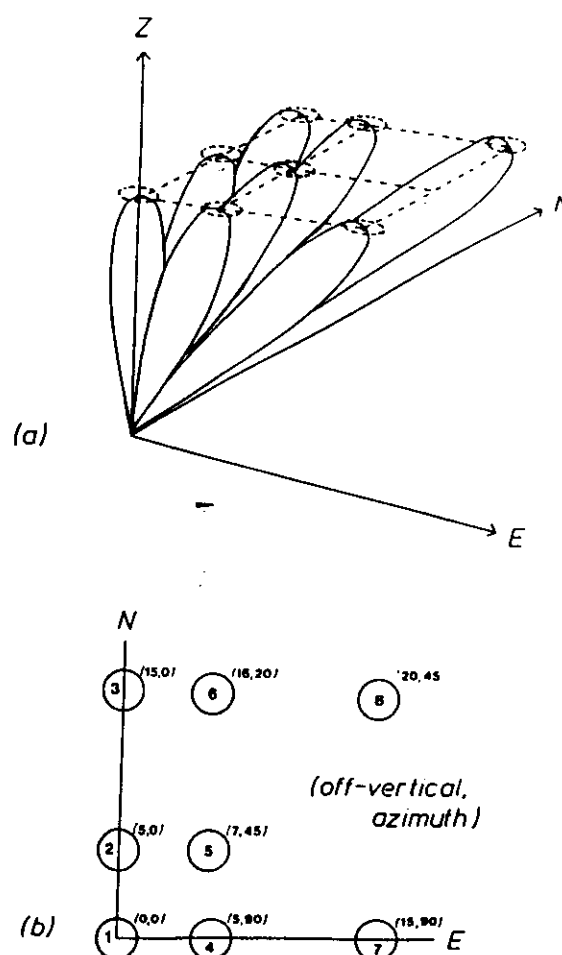


Fig. 1. Beam configurations of the MU radar used during the experiments reported in this text. (a) An artist's impression of the radar beams and (b) the regions of the atmosphere covered by each beam at a fixed height.

between 2045 and 2250 LT on October 17 will be discussed here.

OBSERVATIONS

Calculations of the mean levels of aspect sensitivity recorded with the MU radar have been reported elsewhere [*Tsuda et al.*, 1986; *Hocking et al.*, 1990]. In the work by *Hocking et al.* [1990] a parameter " θ_s " was used to quantify the degree of aspect sensitivity, where it was assumed that the power received per unit steradian as a function of off-vertical angle θ for a monostatic radar with a very narrow beam would be proportional to $\exp(-\theta^2/\theta_s^2)$. It was shown in that work that hourly

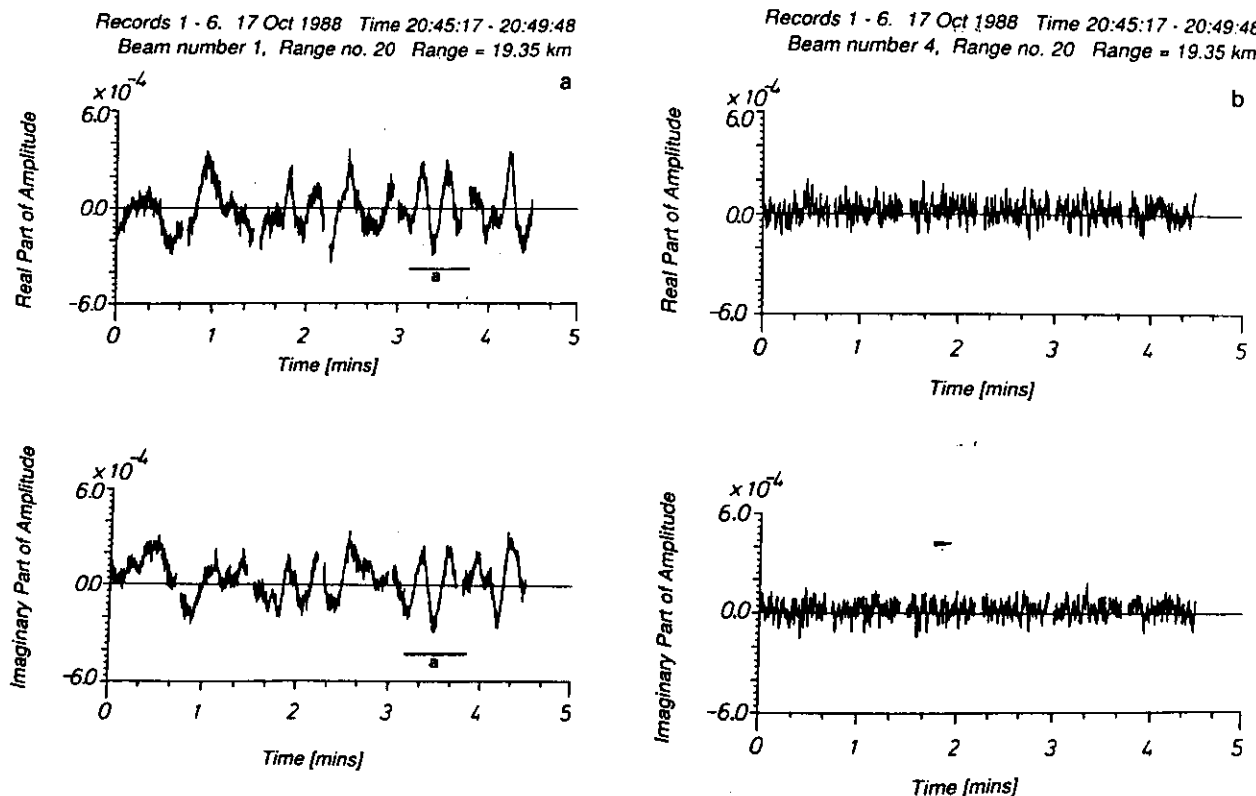


Fig. 2. (a) Inphase (real) and quadrature (imaginary) parts of the signal received by the radar for the special echo discussed in the text. The gaps represent data transfer intervals. (b) Typical amplitude variations for a "normal" signal. Note the much more rapid fading.

average values of θ_s can be as small as 1° – 2° in the stratosphere at ~ 18 km altitude, and it was noted that individual values of θ_s can be even less than this for short periods of time. This corresponds to scatterer length-to-depth ratios in excess of 20 [Hocking *et al.*, 1990]. Values for this ratio of say 5–10 can reasonably be ascribed to turbulence, but values in excess of 20 to 30 indicate some other cause for the scatterers. During a few particular intervals, θ_s became substantially less than 1° . Probably the most striking example is illustrated by the data shown in Figure 2a. This shows the variation of inphase and quadrature components recorded with the vertical beam of the MU radar at a range of 19.35 km, in the time interval 2045 to 2050 LT on October 17, 1989. There are gaps in the data at steps of about 45 s; these occurred during periods of data transfer to the host computer. Note especially the very slow changes of the inphase and quadrature components which often take a minute

to complete one cycle. Indeed, in the 1-min interval highlighted by the horizontal bar and labeled "a" the inphase and quadrature components remained in perfect phase quadrature. In contrast, Figure 2b shows the fading on an off-vertical beam (0° N; 5° E) in the same period; fading is quite clearly much faster. This is the first indication of the unique nature of the signal shown in Figure 2a. It should also be noted that under normal operating conditions the MU radar records 10-s data sets, and then these data sets are spectrally analyzed. Yet for the example shown in Figure 2a the vertical beam hardly shows any variation in signal strength over a period of 10 s, and after subtraction of the mean values these data would normally be interpreted as noise. Only by recording a full 5 min of data has it been possible to observe this remarkably slowly fading signal, and this is why such signals have not been frequently observed before.

We were careful to check that this signal was not

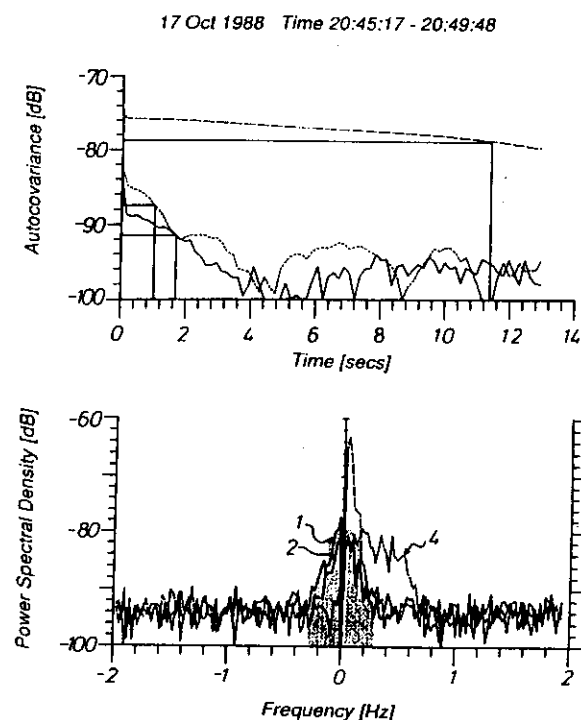


Fig. 3. (a) Mean autocorrelation functions for beams 1 (long-dashed line), 2 (solid line), and 4 (short-dashed line) for the period 2045 to 2050 LT and (b) the corresponding power spectra. In each case the ordinate is scaled logarithmically, and the numbers indicate decibels. The shaded section of Figure 3b is discussed in the text.

due to a ground reflection. This was discussed in more detail by Hocking *et al.* [1990] but will be briefly commented on here. By examining many cases of known ground reflections it was concluded that genuine ground echoes do not fade substantially over a 5-min period, so that the fading shown in Figure 2a is really due to atmospheric effects. It is of course possible that the fading was due to ground echoes ducted horizontally to the radar, with temporal variations of the duct causing the fading, but we feel this was not so. In any case the MU radar has excellent sidelobe suppression, which should effectively suppress any such horizontally propagating signals.

Figure 3a shows the autocovariance function of the signal shown in Figure 2a, where the ordinate is expressed in decibels. The function shown is the modulus of the average of the autocovariance functions for each of the six records (each of 42-s duration) in the time interval 2045:17 to 2049:48. Note that the function falls extremely slowly and

only reaches a value of 0.5 times the zero-lag value at $\tau_{0.5} = 11.4$ s. In contrast, the fading times on the other beams are generally 2–4 s. To further demonstrate the extremely slow fading associated with this echo, Figure 3b shows the power spectra recorded with the vertical beam (beam 1) and two off-vertical beams. The two off-vertical beams were a beam tilted in the northward direction at 5° from vertical (beam 2) and one tilted in the eastward direction at 5° from vertical (beam 4). Fading on the other beams (not shown) was even faster than that on these two beams. Notice the very narrow nature of the spectrum on the vertical beam near 0 Hz, although it is also noteworthy that further from 0 Hz and at low powers the spectrum matches that on beam number 2. This is highlighted by the shaded section of the plot, the outer boundary of which follows approximately the shape of both of these spectra. This suggests that the signal on beam 1 comprised a strong specular signal plus a weaker, more diffuse background. Similar deductions may be made by examining the autocorrelation function, although the log plots used do tend to suppress the effects of the weaker background signal, since the effects of the diffuse background occur as a weak peak resting on top of the slowly falling part of the curve. The typical wind speed at this height and time was 15 m s^{-1} or less, and we may use the value of the fading time of 11.4 s to estimate θ_s , giving $\theta_s = 0.3^\circ$ [Hocking *et al.*, 1990, equations (6) and (7)]. If we use far-field (Fraunhofer) theory, this suggests a horizontal correlation length of about 160 m for the irregularities. In fact, for such small values of θ_s the more general treatment of Doviak and Zrnic [1984] should be adopted, in which case the horizontal correlation length is even larger. If we assume that the scatterer is an oblate ellipsoid, then it would have had a $1/e$ full-width of about 270 m and a $1/e$ full-depth of about 2.6 m (0.4λ) [see Hocking *et al.*, 1990], giving a length-to-depth ratio of about 100. We also point out that this estimate was made using the average autocovariance function for a 5-min period; if we had just used that for the time interval denoted by "a" in Figure 2a, when the fading time was more like 60 s (the autocovariance function did not even fall below 0.5 of its maximum for this interval), then θ_s would have been even smaller and the horizontal extent even larger. It seems most unlikely that turbulence could cause such elongated structures. Furthermore, even if it could, turbulence by its nature

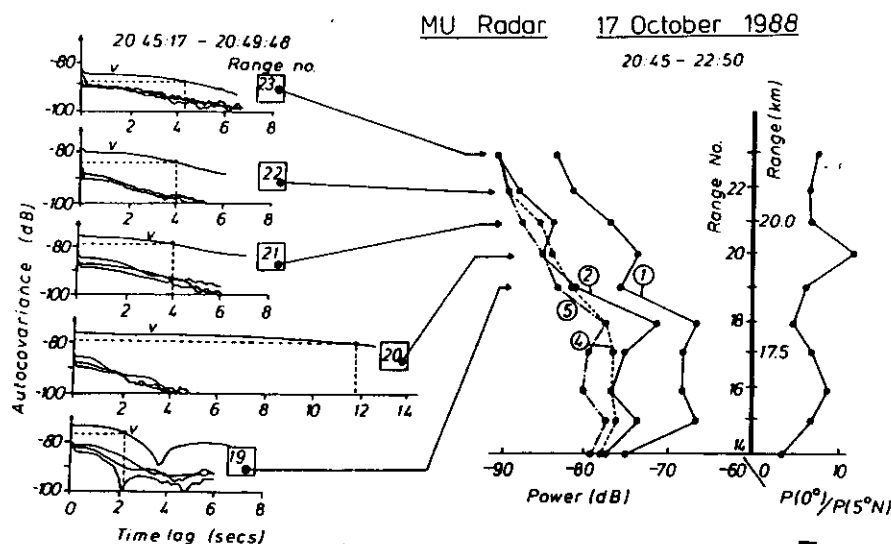


Fig. 4. The profiles to the right show both the mean power (2-hour average) and the power on the vertical beam relative to that on a beam at 5°N (beam 2), for the period 245 to 2250 LT. To the left are shown the mean autocovariance functions calculated using the first 5 min of the data set (2045–2050 LT).

involves a substantial amount of parcel motion, and this would quickly reduce the fading time. In contrast, the scattering structure here seems to be not only highly elongated horizontally but also extremely stable and very very slowly moving.

It is also worthwhile examining the environment at heights above and below this layer. Figure 4 shows 2-hour averages of the power as a function of height for a small region centered around the echo of interest, as well as the power observed with the vertical beam relative to a beam at 5° from the zenith in the northward direction. The autocovariance functions for beams 1, 2, 4, and 5 (see Figure 1) are also shown for a few heights above and below the height of interest. The autocovariance for the vertical beam is denoted by "v"; the other beams are not separately denoted because they were all fairly similar. The unique nature of the autocovariance function at height 20 stands out. It is noteworthy that the strongest powers came not from height 20, but rather heights 15–18. Thus the scatterers at the height of interest were not particularly dominant as far as backscattered power is concerned. However, the aspect sensitivity was greatest at height 20, with the power of the beam at 5°N being 12 dB less than on the vertical beam. The peaks in backscattered power do not correspond to the highest degree of aspect sensitivity; in fact, the height of strongest power (height 18) corresponds to the most

isotropic scatter, and it is likely that this was a layer of turbulence. A value of 12 dB for the ratio of the powers on the vertical beam to the beam at 5°N corresponds to a value for θ_s of 2.6° , but it should be noted that this is an upper limit and is not inconsistent with the estimate of θ_s made earlier using the fading times. This is because the spectra in Figure 2b have already suggested that the signal was due to very aspect-sensitive scatter (giving rise to the large spike) and a more isotropic "background" of scatterers which also contributed to the power on the 5°N beam. Comparison of powers on the two beams will be affected by this low-level quasi-isotropic scatter, whereas use of fading times with a vertical beam to determine θ_s is essentially only sensitive to the strong, highly aspect-sensitive scatter from overhead. Such a conclusion is also consistent with Hocking [1990], where it was shown that usually a continuum of scatterer shapes exist, from highly aspect sensitive to almost isotropic.

Until now the main models of specular reflectors have been due to Bolgiano [1968], Hines [1960], and Van Zandt and Vincent [1983]. Before examining these models, however, it is worth noting one more point. While the echo behavior on the vertical beam at height 20 suggests a very stable structure, the echo power on the off-vertical beams at that height is clearly not only due to noise. It is a real signal, with distinctly different fading times and scattering

properties to that on the vertical beam. It seems that there is some form of more isotropic scatter (possibly but not necessarily due to turbulence) being received on the off-vertical beam. Thus any successful model must not only explain the highly stratified plane reflector but also must explain how it can exist in the presence of, or at least close to, these more isotropic scatterers. Presumably, turbulence would destroy such highly elongated structures if the turbulence existed in the same physical space as the structure. It should also be noted that *Bolghiano* [1968] surmised that if the specular reflectors were due to a sharp edge of a turbulence layer, then the mixing might be so strong that the air inside the layer could become completely and adiabatically mixed, and other quantities related to the refractive index could also be mixed to constant values across the layer. Hence very little turbulent scatter from within the layer would be expected in such circumstances.

One could surmise that the turbulence might have been spatially inhomogeneous and did not exist directly over the radar. This could permit very stable conditions immediately overhead, allowing the stratified structure to exist, but elsewhere small patches of turbulence could contribute to the small amount of backscatter observed with the off-vertical beams. Nevertheless, such a model involves a rather specific and contrived set of circumstances, and it would be preferable if a more general model could be found which does not have such a degree of special requirements. The fact that other periods of such stable echoes also occurred at other times makes the above scenario even less likely. For example, similar observations were made later in the evening at 2240 at height 19 (18.75 km).

We must now turn to a more in-depth consideration of various models which might explain the observations. In order to do this, however, it is necessary to turn first to some theoretical development.

THEORY

Equations of fluid motion with viscosity and thermal conduction included

The (two-dimensional) equations of motion for small perturbations in a Boussinesq viscous fluid are (for example, HJ):

$$\frac{\partial u'}{\partial t} = -\frac{1}{\rho_0} \frac{\partial p'}{\partial x} + \nu \nabla^2 u' \quad (1a)$$

$$\frac{\partial w'}{\partial t} = -\frac{1}{\rho_0} \frac{\partial p'}{\partial z} - \frac{\rho' g}{\rho_0} + \nu \nabla^2 w' \quad (1b)$$

$$\frac{\partial u'}{\partial x} + \frac{\partial w'}{\partial z} = 0 \quad (1c)$$

$$\frac{\partial \rho'}{\partial t} + w' \frac{\partial \rho_0}{\partial z} = \kappa \nabla^2 \rho' \quad (1d)$$

where ρ is density, p is pressure, u and w are horizontal and vertical components of velocity, ν is kinematic viscosity, κ is thermal diffusivity, x and z are horizontal and vertical Cartesian coordinates, t is time, and g is acceleration due to gravity. We assume that the mean wind is zero, and primed quantities refer to perturbations about the mean. The symbol ∇^2 represents $\partial^2/\partial x^2 + \partial^2/\partial z^2$. Note that ρ' is the density difference between a displaced parcel of air and its environment.

The first two equations are the momentum equations, the third is the continuity equation for an incompressible medium, and the fourth arises from the equation of thermal transfer [e.g., *Gill*, 1982, equation (4.4.7)]:

$$\frac{D\Theta}{Dt} \approx \kappa \nabla^2 \Theta$$

with the usual Boussinesq condition $dp'/\rho_0 = -d\Theta'/\Theta_0$, Θ being potential temperature. We note also that $1/\rho_0 d\rho/dz = -1/\Theta_0 d\Theta/dz = -\omega_B^2/g$, where g is the acceleration due to gravity and ω_B is the Brunt-Vaisala frequency.

The simplest way to solve these equations is to look for solutions with variables proportional to $\exp\{i(kx + mz - \omega t)\}$. In the case that the viscous and heat conduction terms are small we may ignore the terms $\nu \nabla^2 u'$, $\nu \nabla^2 w'$, and $(\kappa/\rho_0) \nabla^2 \rho'$ and derive the usual dispersion and polarization relations for gravity waves in the atmosphere [e.g., see HJ; *Hines*, 1960].

However, the case when m is very large corresponds to short vertical wavelengths, and the terms like $\nu (\partial^2 u'/\partial z^2)$ can no longer be ignored.

In this paper we will be concentrating on solutions with near-horizontal wave fronts, which will have correspondingly small horizontal wavenumbers, so we can ignore terms like $\nu (\partial^2 u'/\partial x^2)$. Thus for very short vertical wavelengths, terms like $\nu \nabla^2 u'$ become dominant, and (1) reduces to

$$\frac{\partial u'}{\partial t} = \nu \frac{\partial^2 u'}{\partial z^2} \quad (2a)$$

$$\frac{\partial w'}{\partial t} = \nu \frac{\partial^2 w'}{\partial z^2} \quad (2b)$$

Assuming a solution of the form

$$u' = u'_0 \exp \{i(kx + mz - \omega t)\}$$

and substituting in (2a) gives

$$m = \sqrt{\frac{i\omega}{\nu}} \quad (3a)$$

or

$$m_{1,2} = \left(\frac{1}{\sqrt{2}} \sqrt{\frac{\omega}{\nu}} + \frac{i}{\sqrt{2}} \sqrt{\frac{\omega}{\nu}} \right), \quad (3b)$$

$$\left(-\frac{1}{\sqrt{2}} \sqrt{\frac{\omega}{\nu}} - \frac{i}{\sqrt{2}} \sqrt{\frac{\omega}{\nu}} \right)$$

The solution u' therefore describes a heavily damped sinusoidal variation in the vertical with wavelength

$$\lambda_z = \sqrt{8} \pi (\sqrt{\nu/\omega}) = 2\sqrt{\pi} (\sqrt{\nu T}) \quad (4)$$

and with an exponential decay. In this case, T is the period of the wave, $= 2\pi/\omega$.

Note that we will assume for the time being that ω is purely real. This is not necessarily obvious, but we shall take the view that since the waves are heavily damped, they do not grow of their own devices, but rather require forcing from other associated (gravity) waves in order to exist. Since the forcing wave has a real frequency, so will the viscosity wave. We will discuss the issue of the generation of the waves in more detail later in the text; for now we wish simply to establish the characteristics of the waves.

We will denote \hat{m} as $m_R + im_i$, where $i = (-1)^{1/2}$. An upward propagating wave ($m_R > 0$) has a positive value for m_i and dissipates with increasing height. An example is shown in Figure 5, both for a wave alone and also for a wave superimposed on a mean gradient. The abscissa can be any perturbation variable, such as temperature, velocity, density, etc. Note in the second case that the wave has an almost "steplike" appearance, and if the wave's amplitude had been a little less, it could have been

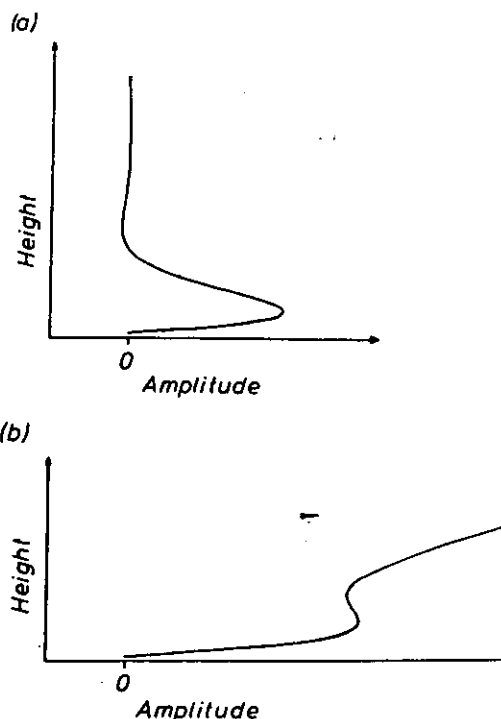


Fig. 5. (a) "Amplitude" (which may represent velocity, temperature, density, etc.) as a function of height for a typical viscosity wave. (b) A similar wave superimposed on a mean gradient.

made to look even more so. This may be important in explaining observations of "steps" in atmospheric wind and density profiles.

The wave arises because of a balance of the acceleration term and the viscous drag term and has much similarity to the well-known case of simple harmonic motion in a lossy medium, for the case that the acceleration term and loss term dominate over the force driving the motion. The motion describes the relaxation back to an equilibrium state after the medium has been perturbed. Such waves arise, for example, when sound or gravity waves reflect from any rigid surface; the conditions of no-slip and zero velocity normal to the surface, as well as the requirement for continuous velocity profiles, cannot be satisfied by the incident, reflected, and transmitted waves alone. Viscosity waves are necessary to allow all these boundary conditions to be met. The waves also have some (but not complete) similarity to the "evanescent modes" which arise in the optical case of total reflection from an interface. We will propose that

similar waves must arise even in the case of reflection from a "nonrigid" reflecting layer such as a discontinuity in the temperature gradient, as well as in the case of certain gravity wave critical level interactions.

Continuing our mathematical discussion, we note that when shears are large, (1d) can be written as

$$\frac{\partial \rho'}{\partial t} = \kappa \frac{\partial^2 \rho'}{\partial z^2}$$

giving rise to a set of waves for which

$$m = \sqrt{\frac{i\omega}{\kappa}} \quad (5)$$

HJ refer to the waves described by (3) and (5) as the "viscosity" mode and the "thermal conduction mode," respectively.

If one solves (1a)–(1d) for plane wave solutions, the following dispersion relation results;

$$\kappa \nu (m^2 + k^2)^3 - i\omega(\nu + \kappa)(m^2 + k^2)^2 - \omega^2(m^2 + k^2) + k^2 \omega_B^2 = 0 \quad (6)$$

where the term ω_B is the Brunt-Vaisala (angular) frequency. This equation is a cubic in m^2 . In the special case that $\kappa = 0$ this reduces to

$$-i\omega(\nu)(m^2 + k^2)^2 - \omega^2(m^2 + k^2) + k^2 \omega_B^2 = 0 \quad (7)$$

A similar expression, with ν replaced by κ , results if we consider the opposite extreme with $\nu = 0$ and κ nonzero.

Note that (7) differs slightly from HJ because we have assumed solutions of the form $\exp \{i(kx + mz - \omega t)\}$, whereas HJ took solutions of the form $\exp \{i(\omega t - kx - mz)\}$. The expression (7) can be rewritten as

$$m^2 = -k^2 - [i/2(\nu/\omega)] \pm \sqrt{1 + i\chi} - 1 \quad (8)$$

where

$$\chi = 4(\omega_B/\omega)^2 (\nu/\omega) k^2 (\geq 0). \quad (9)$$

This solution is exact for the case of general ν and for $\kappa = 0$; it depends only on the ratios ω_B/ω and ν/ω , and k .

We will concentrate on this special case for illustrative purposes. Of course, in the real atmosphere, κ and ν are comparable ($\nu/\kappa = 0.7$, the Prandtl number), so it is unrealistic to take $\kappa = 0$. Nevertheless, it is much easier to solve the special

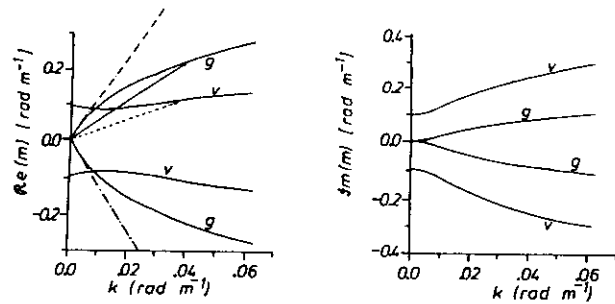


Fig. 6. Dispersion relations between m and k for a viscosity wave with $\nu/\omega_B = 12$ and $\nu/\omega = 57.3 \text{ m}^2$. The gravity wave branch is denoted by "g" and the viscosity wave branch by "v." The two arrows show typical wave vectors. The dashed-dotted line shows the gravity wave dispersion relation for Boussinesq waves in the absence of viscosity.

cases of $\kappa = 0$ or $\nu = 0$; the dispersion relation for the general case is a cubic in m^2 and is more difficult to solve. We can illustrate all the principles we wish to discuss with this simpler case; the effect of taking both κ and ν as nonzero will simply alter some of the scales discussed by small amounts. Therefore henceforth we will consider the case of $\kappa = 0$. We could have equally taken ν as zero and left $\kappa \neq 0$.

HJ discussed various special limiting cases of this dispersion relation, but it is in fact easy to solve it by computer. Figure 6 shows a sample plot of m as a function of k for the four different wave solutions which satisfy (8) and (9), for the case that $\omega_B/\omega = 12$ and $\nu/\omega = 57.3 \text{ m}^2$. The exact conditions chosen were for a wave period of 60 min ($\omega = 1.75 \times 10^{-3} \text{ rad s}^{-1}$), a Brunt Vaisala period of 5 min ($\omega_B = 0.021 \text{ rad s}^{-1}$), and a kinematic viscosity of $0.1 \text{ m}^2 \text{ s}^{-1}$. The four solutions formed represent upward and downward propagating gravity waves and upward and downward propagating viscosity waves. The dispersion relation for gravity waves in the absence of viscosity are shown by the dashed-dotted line of Figure 6. Note that the vertical wavenumber of the viscosity wave is almost constant [$\text{Re}(m) \approx (1/2)^{1/2}(\omega/\nu)^{1/2}$] over a wide range of k values. The viscous mode is always much more heavily damped than the gravity wave of the same horizontal wavelength. Viscous waves can exist with any orientation given any particular value of m , in contrast to gravity waves for which there is a strong relation between k and m for any given ω . We wish to investigate whether the viscous modes might be capable of causing specular reflection.

Typical scales

It is instructive to determine typical values of λ_z for various conditions, using (4). At about 20 km altitude, $\nu \approx 2 \times 10^{-4} \text{ m}^2 \text{ s}^{-1}$; if we take the wave period as $T \approx 5\text{--}60 \text{ min}$, then $\lambda_z \approx 0.9\text{--}3.0 \text{ m}$. The vertical phase velocity will be $\sim \lambda_z/T \sim 0.001 \text{ m s}^{-1}$. An individual wave will persist for a length of time equal to or greater than the time taken for it to propagate through its own wavelength (depending on the duration of the applied forcing). In this special case the lifetime will be at least $\sim 5\text{--}60 \text{ min}$. At 30 km altitude the kinematic viscosity coefficient is about $6 \times 10^{-4} \text{ m}^2 \text{ s}^{-1}$, so $\lambda_z \approx 1.5\text{--}5 \text{ m}$ for periods in the range 5 to 60 min.

At an altitude of 70 km, $\nu \sim 0.1 \text{ m}^2 \text{ s}^{-1}$, and so if $T \sim 5\text{--}60 \text{ min}$, then $\lambda_z \sim 20\text{--}70 \text{ m}$.

Note that in considering these typical scales we have concentrated on using the molecular kinematic viscosity ν . This contrasts with HJ, who were interested only in the planetary boundary layer and so considered turbulent viscosity coefficients.

It is important to note that $\lambda_z = 3 \text{ m}$ is the Bragg backscatter scale for 50-MHz VHF radio waves incident in the atmosphere, and $\lambda_z = 75 \text{ m}$ is the Bragg scale for 2-MHz radio waves. Thus already we see that viscosity waves at 20–30 km altitude could cause “specular” reflection at 50 MHz, and viscosity waves at around 70 km altitude could cause “specular” reflection for frequencies around 2 MHz. This simple agreement between the scales of the viscous waves and the observations of the heights of strongest specularity is quite remarkable. We have yet to establish whether this reflection will be detectable, and this will be examined shortly.

For now we reiterate that the strongest degree of aspect sensitivity so far reported for radio wave reflection have been 50-MHz reflection from the stratosphere [e.g., Roettger and Liu, 1978; Gage and Green, 1978; Hocking et al., 1986, 1990] and MF (2 MHz) reflection from around 60–80 km altitude [e.g., Gregory and Vincent, 1970; Vincent and Belrose, 1978; Hocking, 1979]. Reports of aspect sensitivity at VHF in the mesosphere exist [e.g., Fukao et al., 1980; Royrvik, 1985], but the degree of aspect sensitivity was not so pronounced as at MF and could have been simply due to anisotropic turbulence.

We will address these typical scales further in due course. Nevertheless, it is clear that further study of viscosity waves is now warranted, since they at

least have the right scales to explain the observations of specular reflection. They are also permitted to have near-horizontal wave fronts.

Effect of viscosity and thermal conduction on gravity waves

We have noted above that viscosity and thermal conduction waves can have the correct scales and orientations to cause specular reflection. We have yet to discuss whether they imply strong enough density perturbations to produce significant radar backscatter, how they are generated, and indeed where the waves are most likely to be found.

It is extremely useful at this point, however, to discuss the effects of viscosity and thermal conduction on gravity waves. The inclusion of viscosity and thermal conduction alters the dispersion relation for these waves in a very significant way, especially for waves with very short vertical wavelength.

Hines [1960] and Van Zandt and Vincent [1983] proposed that gravity waves of very long period and short vertical wavelength may be responsible for the specular reflections. Van Zandt and Vincent [1983] argued that waves could exist arbitrarily close to horizontal, provided that the period was long enough and the vertical wavelength short enough. However, Hocking et al. [1990] argued that in the stratosphere the effects of viscosity would be to damp waves with phase fronts closer than $2^\circ\text{--}3^\circ$ from horizontal. In the mesosphere, phase fronts closer to horizontal than 6° should be heavily damped.

However, examination of the new dispersion relations shows that not only are such waves strongly damped, but indeed they cannot even exist. The effect of viscosity is to tilt the phase fronts to a steeper angle than would have been the case in the inviscid situation.

Let us consider a particularly useful example. Consider a gravity wave with a vertical wavelength of 3 m in the stratosphere, so that $\text{Re}(m) = 2\pi/3 \approx 2.0 \text{ rad m}^{-1}$. Consider a kinematic viscosity of $10^{-3} \text{ m}^2 \text{ s}^{-1}$ (typical of the value at about 30 km altitude). Then in the case where viscosity is not included, the angle of the wave fronts to the vertical is $\theta_B \approx \tan^{-1}(\omega/\omega_B)$, where ω_B is the Brunt-Vaisala frequency, or alternatively, $\theta_B = \tan^{-1}(T/T_B)$, where T_B is the B-V period and T is the wave period. This becomes more exact as T increases.

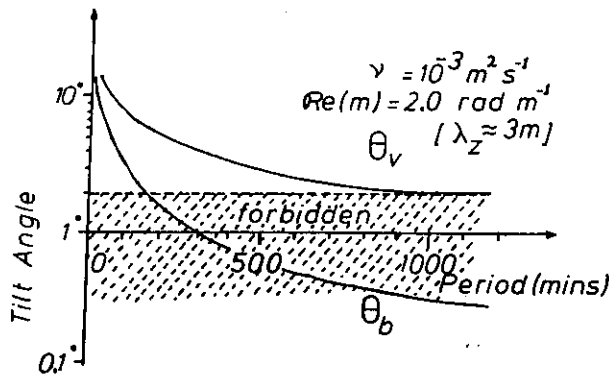


Fig. 7. Tilt angle of gravity wave wave fronts from the horizontal as a function of wave period for a vertical wavelength close to 3 m at around 30 km altitude, using both Boussinesq theory (θ_B) and the more general dispersion relation which includes the effects of viscosity (θ_v). The shaded area shows a region of "forbidden" wave front tilts. This occurs because the intrinsic periods of the waves cannot exceed 1200 min.

However, when viscosity is included, then the angle is $\theta_v = \tan^{-1} [k/\text{Re}(m)]$, where $\text{Re}(m)$ needs to be calculated from the exact dispersion relation.

We can evaluate θ_v as a function of period for a particular vertical wavelength by repeatedly plotting graphs like Figure 6 and reading off values of k for the desired value of m , and then using each (k, m) pair to deduce θ_v . When we do this and when θ_v and θ_B are calculated and plotted as a function of the period T for a value of $m_R = 2.0 \text{ m}^{-1}$, (assuming $T_B = 5 \text{ min}$) Figure 7 results. Notice that while the inviscid theory allows wave fronts as close as 0.1° to horizontal (when the period is about 20 hours) the more exact dispersion relation including viscosity shows that the wave fronts can be no closer to the horizontal than 1.8° when the period is 20 hours. The period of 20 hours is of the order of or more than the inertial period for most latitudes of the Earth, and so we must conclude that gravity waves with vertical wavelengths of 3 m cannot exist in the middle stratosphere with wave fronts closer than 2° to vertical. It is not simply a matter of their being heavily damped; they simply cannot exist because of the way that the inclusion of viscosity steepens the wave fronts. Furthermore, even those gravity waves which do exist with wave fronts close to horizontal are heavily damped. Figure 8 shows the $1/e$ depth of these waves for the same choice of ν and ω_B as for Figure 7. Note that the waves dissipate quickly, indicating that any waves which exist must be generated in situ. The waves are not

damped as heavily as the viscous waves, of course, as indicated by the arrow denoted by "v" in Figure 8. Of course, we should also have included a Coriolis forcing in (1a) and (1b), which means in fact that at very long periods θ_v will be different to the value shown in Figure 8, but even the Coriolis term is unlikely to bring θ_v back to angles less than 1° .

Reflection efficiency

It seems clear at this stage that gravity waves cannot be the cause of radar reflection from the vertical, since waves with periods less than about 10 hours and vertical wavelengths of 3 m must have tilt angles greater than about 3° – 4° from horizontal in the stratosphere. This would leave a "hole" around vertical from which no specular reflection would occur, with a half width of about 3° , and such a hole would surely have been observed experimentally if it indeed existed. It is also clear that viscosity waves can exist with the correct scales and can be aligned horizontally, so these could be the cause of the reflecting structures. We have yet to discuss the cause of the viscosity waves, since these waves represent a relaxation from a perturbed state, and something must cause the initial perturbation. We also must discuss why the viscosity waves must show a preference for horizontal alignment, as experimental studies of aspect sensitivity show, despite the fact that they are free to exist with any orientation. But before addressing these issues, it is necessary to determine whether such viscosity

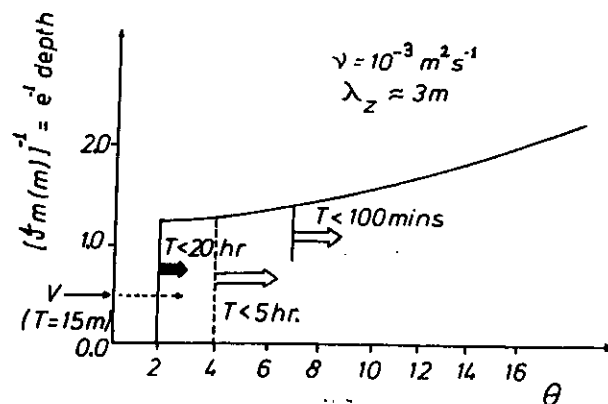


Fig. 8. The $1/e$ depth of gravity waves as a function of tilt angle for a vertical wavelength of 3 m. The arrow on the ordinate denoted by "v" shows the $1/e$ depth for a viscosity wave with vertical wavelength of 3 m, when $\nu = 10^{-3} \text{ m}^2 \text{ s}^{-1}$.

waves can in fact cause sufficient radio wave reflection to be detectable by a ground-based radar.

Density perturbations

Solving (1a)–(1c) for assumed solutions proportional to $\exp\{i(kx + mz - \omega t)\}$, it can be shown that the density perturbations for viscosity waves are related to the horizontal perturbation velocity through the relation

$$\frac{\rho'}{\rho_0} = -i \frac{\omega}{g} \left[1 + i \left(\frac{\nu}{\omega} \right) (m^2 + k^2) \right] \left(\frac{m}{k} + \frac{k}{m} \right) u' \quad (10)$$

Generally, we are interested in the case where $m \gg k$ (i.e., horizontal wavelengths much larger than vertical wavelengths), so

$$\frac{\rho'}{\rho_0} \approx -i \frac{\omega}{g} \left[1 + i \frac{\nu}{\omega} (m^2 + k^2) \right] \frac{m}{k} u' \quad (11)$$

As $k \rightarrow 0$, $1 + i(\nu/\omega)(m^2 + k^2) \rightarrow 0$ for the viscosity wave branch (by equation (3a)) and in fact approaches zero faster than k , so purely horizontal wave fronts imply no density perturbations in the vertical direction. This is reasonable, since density perturbations arise because the vertical velocity carries air at lower heights adiabatically up to regions of lesser density, and when $k = 0$, $w' = 0$. Note that although $m \gg k$, we could not replace $(m^2 + k^2)$ by m^2 alone, because then (11) would be identically zero. For the gravity wave branch, $i\nu\omega(m^2 + k^2) \ll 1$, so (9) becomes

$$\frac{\rho'}{\rho_0} = -i \frac{\omega}{g} \frac{m}{k} u' \quad (12)$$

and using $m/k \approx \omega_B/\omega$ gives

$$\frac{\rho'}{\rho_0} \approx -i \frac{\omega_B}{g} u' \quad (13)$$

a result which is well known. For $\omega_B = 0.02 \text{ rad s}^{-1}$, $\rho'/\rho_0 \approx 2 \times 10^{-3} u'$.

However, for the viscosity wave branch, no such simplification is possible. Although $1 + i(\nu/\omega)m^2 = 0$ for $k = 0$, the term is nonzero for $k > 0$. Therefore we have taken a particularly interesting case and calculated ρ'/ρ_0 numerically. The results are shown in Figure 9. A wave period of 60 min was assumed, with a Brunt-Vaisala period of 5 min and a kinematic viscosity coefficient of $2 \times 10^{-4} \text{ m}^2 \text{ s}^{-1}$. This

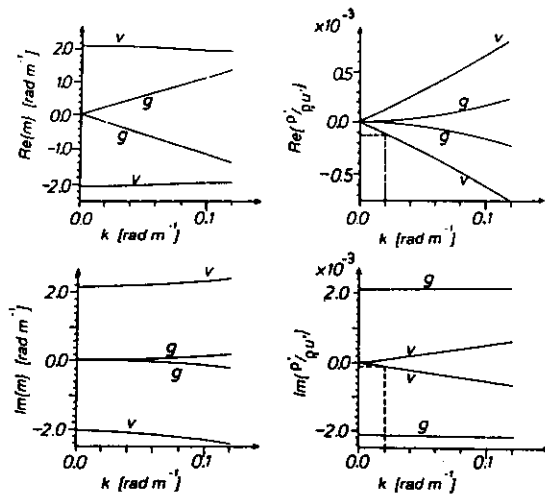


Fig. 9. Plots of dispersion relation between m and k , as well as plots of the density fluctuations as a function of k , for the case $\nu = 2 \times 10^{-4} \text{ m}^2 \text{ s}^{-1}$, $\omega_B = 0.02 \text{ rad s}^{-1}$ ($T_B = 5 \text{ min}$) and a wave period T of 60 min. The particular case of $k = 0.02 \text{ rad m}^{-1}$ ($\lambda_x = 315 \text{ m}$) is highlighted.

B-V period and viscosity coefficient apply at an altitude of 20 km, and the choice of wave period produces a viscosity wave with vertical wavelength equal to 3 m. The resultant plots for $\text{Re}(m)$, $\text{Im}(m)$, and $\text{Re}[\rho'/(\rho_0 u')]$ and $\text{Im}[\rho'/(\rho_0 u')]$ are shown in Figure 9. Notice that the gravity wave branch produces density perturbations of about 0.2% of u' (SI units), as expected, with the fluctuation being about 90° out of phase with u' . However, for the viscosity wave branch we note that the real and imaginary components are comparable, suggesting a phase difference of $\sim 45^\circ$ relative to u' . The magnitude of $(\rho'/\rho_0 u')$ is $\sim 0.1\%$ at $k = 0.14$ ($\lambda_x = 45 \text{ m}$) and $\sim 0.02\%$ at $k = 0.02$ ($\lambda_x = 315 \text{ m}$). In the first case the phase fronts are tilted at 3.5° to the horizontal and in the second at 0.5° . We shall discuss whether such a wave is capable of causing detectable VHF radar reflection shortly, but it is worth noting that since $|T'/T| = |\rho'/\rho|$ (where T is temperature) a 0.1% density fluctuation corresponds to a temperature fluctuation of about 0.3°C .

Another important example is that of a 75-m wave at around 70 km altitude, since these waves would cause "specular reflection" at 2 MHz. However, in that case it is not the neutral density perturbation which is required, but rather the electron density perturbation. Let N denote electron density, and N' the perturbation from the back-

ground. The displacement of a parcel of air or electrons due to a wave is

$$s' = \int w' dt = \frac{w'}{-i\omega} = \frac{-ik}{\omega m} u'. \quad (14)$$

Note that because the real and imaginary parts of \hat{m} for the viscosity wave branch are very nearly equal and have the same sign, the real and imaginary parts of s' will also have equal magnitudes and the same signs. The parcel of air will expand adiabatically, which will contribute to N' . Furthermore, if there is an electron density gradient, then the parcel of electrons is moved to a new height where the background electron density is different. Therefore the relevant density gradient depends not only on the degree of adiabatic expansion during displacement but also on the mean electron density gradient. The new difference in electron density between the parcel and the "normal" background electron density is thus [Hocking, 1985]:

$$N' = s' M_e \quad (15a)$$

where

$$M_e = \left[N \frac{\omega_B^2}{g} - \frac{dN}{dz} + \frac{N}{\rho} \frac{d\rho}{dz} \right]. \quad (15b)$$

N can in fact be the density of any tracer, including air. It is in fact more common to express the gradient in terms of the difference of the background minus the parcel densities, which is $-M_e$, so

$$N' = -s' M_N \quad (16)$$

where $M_N = -M_e$ is the potential electron density gradient. In the case that $N = \rho$, $M_N = M_\rho = -\rho \omega_B^2/g$. For the gravity wave branch, $w'/\omega \approx -u'/\omega_B$, and so

$$\rho' \approx \frac{w'}{-i\omega} \left(\rho \frac{\omega_B^2}{g} \right) \approx \frac{-i\rho u' \omega_B}{g} \quad (17)$$

which is consistent with (13).

However, in the ionosphere the electron density gradients can be quite steep and dominate over $N\omega_B^2/g$ and $N/\rho(d\rho/dz)$, so we must use the more general formula

$$N' = \frac{w'}{i\omega} M_N = \frac{-u'k}{im\omega} M_N \quad (18)$$

Indeed, we could have used this formula earlier to derive typical density fluctuations at 20 km; taking $N \equiv \rho$, $M_N \equiv -\rho \omega_B^2/g$, $|m| \approx 2(2^{1/2})$, $\omega = 2\pi/3600$, and $k = 0.14$ gives $\rho'/\rho_0 u' = -k\omega_B^2/(im\omega g)$ or $\rho'/\rho_0 u' \approx 0.001$, consistent with our graphical value of 0.1%.

Using an electron density profile obtained from rocket experiments and reported by Mechtly *et al.* [1972], Hocking [1981] has evaluated values of M_N at around 70–80 km. A typical value for $|M_N|$ at 70 km altitude is 10^{-2} – 10^{-1} m^{-1} . Taking $\nu \approx 0.1 \text{ m}^2 \text{ s}^{-1}$ and a wave period of 75 min ($\omega = 1.4 \times 10^{-3}$) gives a viscosity wave with a vertical wavelength, λ_ν , of 75 m, which is the Bragg scale for backscatter of 2-MHz radiation. We are interested mainly in waves with near-horizontal wave fronts, so taking $k/m = 0.02$ (phase fronts tilted at about 1° to horizontal) and $u' = 1 \text{ m s}^{-1}$ gives a value for N' of about 0.1 – 1 cm^{-3} , or about a 0.1–1% fluctuation relative to the background. The value of u' has been chosen somewhat arbitrarily at this stage; even larger fluctuations may be possible if u' is larger. These amounts of fluctuation are comparable to observed fluctuations of around 1 to 5% reported by Manson *et al.* [1969].

Backscatter reflection coefficients

For a refractive index profile $n(z)$ the amplitude and form of the reflected signal $r(z)$ is given by

$$r(z) = g(z) \otimes \frac{1}{2} \frac{dn}{dz} \quad (19)$$

where \otimes refers to convolution [Hocking and Vincent, 1982a, b; Hocking and Roettger, 1983] and $g(z)$ describes the radar pulse.

We must now convert the density perturbations deduced in the previous section to refractive index fluctuations, in order to determine the radar reflectivity of these structures. Previous estimates of reflection coefficients for typical electron density perturbations have assumed that the fluctuations are actually due to (often experimentally unresolved) steps in refractive index [e.g., Manson *et al.*, 1969; Hocking and Vincent, 1982a, b], but a viscosity wave "tuned" to the radar's Bragg scale could be even more efficient than a step. We will now proceed to see if this is true.

Stratospheric case: For the stratospheric case the refractive index is given by

See following errata.

$$n = 1 + 77.9 \times 10^{-6} \rho / T \quad (20)$$

where p is the pressure in ~~pascals~~ ^{millibars} and T is the temperature [e.g., Larsen, 1990]. Humidity fluctuations have been ignored since these are negligible in the stratosphere. If a layer of the atmosphere is displaced by a wave, it will have a new refractive index difference compared to the background. The difference will be $\delta n = -M_n \delta z$, where the refractive index gradient is

$$M_n = 77.9 \times 10^{-6} (K'_B) M_p = 0.02236 M_p \quad (21)$$

where $\rho(z)$ is the density in kg m^{-3} , $K'_B = 287.05$ is a modified form of Boltzmann's constant [Houghton, 1977, Appendix A], and M_p is the potential density gradient. Note that, as in (16), M_p and M_n refer to gradients of the difference of the background value less that of a displaced parcel, whereas we seek the value for the parcel less the background. (As an alternative derivation, we may note [e.g., Larsen, 1990] that the potential refractive index gradient is

$$\begin{aligned} M_n &= -77.9 \times 10^{-6} \left[\left(\frac{p}{T} \right) \left(\frac{1}{T} \right) \left(\frac{dT}{dz} + \Gamma_a \right) \right] \\ &= -77.9 \times 10^{-6} K'_B \rho \frac{1}{\Theta} \frac{d\Theta}{dz} = -77.9 \times 10^{-6} K'_B \rho \frac{\omega_B^2}{g} \\ &= 77.9 \times 10^{-6} K'_B M_p \end{aligned} \quad (22)$$

as in (21)). Thus the effective refractive index gradient produced by the wave is

$$\frac{dn}{dz} = -M_n \frac{ds'}{dz} \quad (23)$$

(see errata)

Suppose that

$$\begin{aligned} u'(z) &= \text{Re} \{ u'_A e^{i(mz + \phi)} \} \\ &= u'_A e^{-m_i z} \cos(m_R z + \phi) \end{aligned} \quad (24)$$

where we have taken u'_A as real, $\phi = kx - \omega t$, and $m = m_R + im_i$. We are only interested in the vertical profile since we treat the problem of backscatter in this case as one of reflection from a nearly horizontal reflector, and so it reduces to a one-dimensional (vertical) problem.

It has already been seen that $m_R \approx m_i$, and we will take this to be exactly true for convenience. Figure 9 showed that the density has about a $\pi/4$ phase difference with respect to u'_A , since the real

and imaginary parts of the density amplitude were about equal. Although not obvious from Figure 9, the real and imaginary components of the density fluctuation amplitude also have the same sign. We can also see this from (14), where it was seen that s' had real and imaginary components which were equal. Thus we may write that the density perturbations will be of the form

$$\rho' = |\rho'_A| e^{-m_i z} \text{Re} \{ e^{i(m_R z + \phi + \pi/4)} \} \quad (25)$$

where

$$\rho'_A = \sqrt{\rho_R'^2 + \rho_i'^2} \approx \sqrt{2} \rho_R' \approx \sqrt{2} \rho_i'$$

ρ_R' and ρ_i' being the real and imaginary parts of ρ'_A . Then using (21) and differentiating ρ' from (25) gives the gradient of the refractive index due to the wave as

$$\frac{dn}{dz} = 0.0224 |\rho'_A| \text{Re} \{ i m e^{i(mz + \phi + \pi/4)} \}$$

and since

$$m_{1,2} = m_A e^{i\pi/4}, m_A e^{i5\pi/4}$$

(where m_A is the magnitude of m), we produce the relation

$$\frac{dn}{dz} \approx -0.0224 |\rho'_A| \sqrt{2} m_R e^{-m_i z} \cos(m_R z + \phi) \quad (26)$$

where we have taken $m_i = m_R$, and $m_R > 0$ refers to an upward propagating wave (wave dissipates with increasing height).

Typical values of $\rho'_A(z)$ have been deduced earlier and were seen to be of the order of 0.02% to 0.1% of $\rho_0 u'_A$, where u'_A is the maximum horizontal perturbation velocity associated with the viscosity wave and ρ_0 is the background density.

As an illustrative example, we shall choose $\phi = \pi/2$, in which case the reflection function is

$$\begin{aligned} \frac{1}{2} \left| \frac{dn}{dz} \right| &\approx 0.0112 \sqrt{\frac{\omega}{\nu}} |\rho'_A| e^{-2\pi z/\lambda_\nu} \sin\left(\frac{2\pi}{\lambda_\nu} z\right) \\ &\approx \frac{0.1}{\lambda_\nu} |\rho'_A| e^{-2\pi z/\lambda_\nu} \sin\left(\frac{2\pi}{\lambda_\nu} z\right) \end{aligned} \quad (27)$$

where $m_R = m_i = 1/\sqrt{2} [\sqrt{(\omega/\nu)}]$, and we have denoted the vertical wavelength of the viscosity wave as λ_ν .

If we assume that the transmitted pulse expressed

in z coordinates ($z = ct/2$) is $g(z) = e^{-z^2/\Delta z^2} \cos(4\pi z/\lambda)$, where λ is the radar wavelength, then the reflected profile is

$$e^{-z^2/\Delta z^2} \cos(4\pi z/\lambda) \otimes \frac{1}{2} \left| \frac{dn}{dz} \right| \quad (28)$$

We can most easily evaluate this convolution by Fourier transforming each function, multiplying in the Fourier domain, and re-Fourier transforming [e.g., Hocking and Roettger, 1983]. For clarity, we do not present this derivation here and simply state the result. A proof can be found in the appendix, where we show that the reflection coefficient is

$$R = 0.0064 |\rho'_A| = 0.285 n'_M \quad (29)$$

The maximum excursion of $\rho(z)$ (and therefore $n(z)$) is not ρ'_A . The maximum occurs at $z = 0$, where (by (25), with $\phi = \pi/2$) $\rho'(0) = |\rho'_A|/\sqrt{2} = \rho'_M$ say. Thus we can write that the reflection coefficient is

$$R = 0.4 n'_M \quad (30)$$

where n'_M is the magnitude of the maximum deviation of the refractive index from the mean.

This compares to a reflection coefficient of $0.5 n'_M$ for a sharp step with refractive index change of n'_M . Thus the viscosity wave is indeed a reflector with an efficiency of reflection comparable to that of a step. In reality, it is likely that viscosity waves may exist in pairs, with one radiating upward from its source region and one downward, and organized so that dn/dz and $n(z)$ are both continuous across $z = 0$. Such a pair of waves would be an even more efficient reflector, by as much as twice that of a single wave, if the spacing of the two waves is right. Thus viscosity waves can indeed be quite efficient reflectors. A step in $n(z)$ has the characteristic that it reflects all radar wavelengths with similar efficiency, but a viscosity wave is "tuned" to a range of wavelengths and is more efficient over that range. It should be noted from Figure 10 that the range of wavelengths over which efficient scatter can occur is not very narrow; variations in the radar wavelength by a factor of 1.5 to 2 times still allow reasonable efficiency of reflection. In fact, the half-power half width of Figure 10 is about $0.56/\lambda_p$. Thus radars with wavelengths between $2(0.44\lambda_p)$ and $2(1.56\lambda_p)$ will all receive powers which are within a factor of 2 of those of the "best tuned" radar. A VHF radar operating at 50 MHz will receive powers

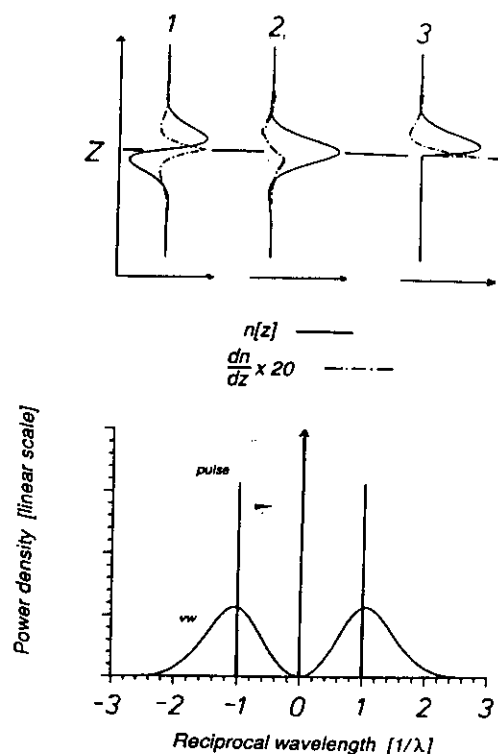


Fig. 10. Three typical refractive-index profiles used to determine the reflection efficiency of viscosity waves in the atmosphere (solid lines) and their gradients (dashed-dotted lines). The gradients have been rescaled by 20 times. In the lower figure the power spectra deduced by Fourier transforming a typical pulse (narrow line) and the reflection profile (broad curve) are shown.

which are within a factor of 2 of those of the "best tuned" radar if the viscosity waves have wavelengths in the range 1.3 to 4.7 m.

The above analytical discussion has concentrated on a particular profile of $n(z)$, but others are possible. In order to be a little more general, several different profiles were chosen, and the pulse was numerically convolved with these profiles to determine the reflection efficiency. The top three profiles in Figure 10 show three such examples. Some of these profiles consist of two viscosity waves joined (effectively radiating up and down from $z = 0$) to make dn/dz continuous across $z = 0$. In each case the efficiency of reflection was between 1 and 2.5 times that of a step. (For purposes of comparison, the change in refractive index across the step was chosen to be equal to the maximum deviation of the refractive index from the mean in the case of the viscosity wave.) Of particular interest is the middle

case, where it was found that the reflection coefficient was $0.55 n'_A = 0.78 n'_M$. This is a pair of waves radiating up and down from $z = 0$, with profiles chosen to match the case discussed in (27). We therefore expect a reflection coefficient of twice that given in (29), or about $0.57 n'_M$. This agreement confirms the accuracy of the numerical integrations.

We note here that the profiles chosen in Figure 10 are only chosen for the purposes of determining reflection coefficients. The first two at least satisfy continuity of the refractive index gradients; the third does not. In reality, we expect continuity of at least the gradient and probably the second derivative, so that these profiles may not be entirely representative of the real situation. The actual structure would need to be determined by experiment or numerical simulation, but there is scope for neither of these here. However, we are confident that these profiles are adequate choices for first-order determinations of typical reflection coefficients, and for this reason they have served their purpose adequately.

For $\lambda_p = 3$ m ($m = 2$ rad m⁻¹) and $|\rho'_A| \approx 0.02\% - 0.1\%$ of $\rho_0 u'$, (see earlier) the effective reflection coefficient at 20 km altitude (where $\rho_0 = 0.05$ kg m⁻³) is

$$R \sim 0.64 \times 10^{-7} u'_A - 3.2 \times 10^{-7} u'_A \quad (31)$$

To be useful, we need to convert this number to an "effective turbulent refractive index structure constant," C_n^2 , since most radar data are presented in terms of this parameter.

C_n^2 can be deduced from R through the relation [e.g., Hocking and Vincent, 1982b]:

$$R^2 = 0.38 \lambda^{-1/3} C_n^2 \theta_{1/2}^2 L \quad (32)$$

where L is the pulse length and $\theta_{1/2}$ is the radar polar diagram (two way) half-power half width: In our case, $L = 600$ m and $\theta_{1/2} = 1.2^\circ$.

Thus $C_n^2 = 21.5 R^2$, so

$$C_n^2 \sim 9 \times 10^{-14} (u'_A)^2 \text{ to } 2 \times 10^{-12} (u'_A)^2. \quad (33)$$

Typical values for C_n^2 at 20 km altitude are $\sim 10^{-18} - 10^{-17}$ m^{-2/3} [e.g., Hocking et al., 1986; Nastrom et al., 1982]. Thus a horizontal perturbation velocity of the order of 1 cm s⁻¹ would produce backscatter typical of that measured with a VHF radar at 20 km altitude. Such velocities are not large and can realistically be expected to occur in the

atmosphere at these heights. For example, typical gravity wave perturbation velocities at these heights are in the order of several meters per second, so a viscosity wave with a horizontal perturbation velocity of a few centimeters per second is quite reasonable. Note that a viscosity wave perturbation of 1–2 cm s⁻¹ and wavelength of around 1.5 m corresponds to a Richardson number of about $Ri = \omega_B^2 / (m_R u)^2 > 1$ and so is a stable wave.

We therefore conclude that reflections from viscosity waves can and should occur at 20 km altitude and would be detected by a VHF radar.

D region case: In this case we again apply (19) but need a new expression for dn/dz . In this case,

$$n' = \frac{\partial n}{\partial N} N' \quad (34)$$

is the perturbation refractive index. In the high-frequency limit,

$$\frac{\partial n}{\partial N} = \frac{1}{2} \frac{\lambda^2 r_e}{\pi} \quad (35)$$

where r_e is the classical electron radius [e.g., Hocking and Vincent, 1982], but in the case of frequencies around 2 MHz, $\partial n / \partial N$ must be evaluated by the Sen-Wyller equations [e.g., Sen and Wyller, 1960] (also see Hocking and Vincent [1982]). It is actually more convenient to rewrite (18) as

$$n' = \frac{-u' k}{i m \omega} M_n \quad (36)$$

where $M_n = \partial n / \partial N M_N$.

We again take the viscosity wave front to be almost horizontal, and a vertical profile of the refractive index is then

$$n'(z) = -u'_A \operatorname{Re} \left\{ \frac{k}{i m \omega} (M_n) e^{i(mz + \phi)} \right\} \quad (37)$$

The gradient of n' is then

$$\frac{dn'}{dz} = -u'_A \operatorname{Re} \left\{ \left(\frac{k}{m} \right) \frac{1}{i \omega} i m (M_n) e^{i(mz + \phi)} \right\}. \quad (38)$$

As for the stratospheric case, we choose a simple example and take $\phi = \pi/2$, so that

$$\frac{1}{2} \frac{dn}{dz} = 0.5 u'_A \frac{k}{\omega} (-M_n) e^{-m_1 z} \sin(m_R z) \quad (39a)$$

$$\frac{1}{2} \frac{dn}{dz} = 0.5 \beta \sin(\alpha_1 z) e^{-\alpha_2 z} \quad (39b)$$

where $|\beta| = |(k/\omega) M_n u'_A|$, and $\alpha_1 = \alpha_2 = 2\pi/\lambda_v$ as for the stratospheric case (appendix).

We may now follow the same discussions as for the stratospheric case, and then the effective reflection coefficient is approximately

$$R = 0.4 |\beta| / \alpha_2 = 0.4 \left(\frac{k}{\omega} \right) \frac{\lambda_v}{2\pi} (M_n) u'_A \quad (40)$$

Hocking [1981] has presented typical values for M_n (or they can be evaluated using the values of $|M_N| = 0.1\% - 1\% N$ deduced earlier), and at 70 km altitude, $|M_n| \sim 10^{-6} \text{ m}^{-1}$.

Consider a viscosity wave with a period of ~ 75 min ($\omega = 1.4 \times 10^{-3}$) and take $\nu = 0.1 \text{ m}^2 \text{ s}^{-1}$ (giving $\lambda_v = 75 \text{ m}$). If we take $k/m = 0.02$, which corresponds to a 1° tilt of the phase fronts to the horizontal, then $k = 1.7 \times 10^{-3} \text{ rad m}^{-1}$, and so

$$R = 6 \times 10^{-6} u'_A \quad (41)$$

Thus if $u'_A \sim 2 \text{ m s}^{-1}$, $R \sim 10^{-5}$. The Richardson number is again > 1 for this choice of u'_A . Reflection coefficients actually measured at 70 km altitude are typically $\sim 10^{-6} - 10^{-4}$ [e.g., Hocking, 1979; Hocking and Vincent, 1982a, b], so this value of R is quite reasonable, although the estimate of u'_A is only a guess. If the electron density gradient is steeper, M_n can be even more and therefore so can R . In the case of steep electron gradients of the order of 1 m^{-1} , as certainly occur from time to time, even values of u'_A of a few tens of centimeters per second could give measurable reflected signals. A value of $u'_A = 10 - 20 \text{ cm s}^{-1}$ is not at all unreasonable; it is only a few percent of typical gravity wave amplitudes at 70 km altitude.

Thus we again conclude that provided conditions exist which are capable of producing viscosity waves, they will generally be detectable with a 2-MHz radar.

GENERATION MECHANISMS AND LIKELY LOCATION OF WAVES

Up until this point, we have simply assumed that the viscosity waves do exist. We must now address

the issue of how they are created; clearly, they must be generated in situ, because their highly damped nature forbids propagation over large distances. There are at least two regions in which we might expect waves of this type to occur.

First, we expect that just as viscosity waves must arise in any reflection from a rigid surface in order to allow the conditions of no-slip, zero normal velocity, and continuous velocity profiles to be satisfied, so they will arise in reflection from a stratified change in Brunt-Vaisala frequency (or even mean wind speed), and we therefore expect viscosity waves to occur to some extent at places where gravity wave reflection occurs.

Second, we expect these waves to exist wherever gravity waves become highly nonlinear, and a likely candidate is a critical level. Gravity waves often break into turbulence before they actually reach a critical level, but this need not always be the case, and we will consider the case for which we have a critical level existing in an already very stable region of the atmosphere.

We shall consider the second mechanism first. Bowman *et al.* [1980] have investigated coupling between various wave modes at a critical level. They particularly studied critical levels for which the Richardson number was greater than unity, but they also assumed that the major diffusion was by turbulence. The formalization and results they developed apply directly to our model, except that we assume that the critical level takes place in a region where there is no background turbulence and the flow is purely laminar so that diffusion takes place by molecular transport. This will not be true of most critical levels, but then we only require it to be true occasionally to explain the occasional occurrences of strong specular echoes. A key result from Bowman *et al.* [1980] is that the coupling between any incident gravity wave and the resultant viscosity and thermal-conduction modes is quite strong in such a critical level interaction. The viscosity waves also play a key role in allowing some propagation of the gravity wave through the layer, but this is not the key point of our work, and the simple fact that gravity waves are capable of generating these highly damped modes is our main concern here.

Klostermeyer [1980] also performed a numerical examination of the process of critical layer interaction of a gravity in the stratosphere. He assumed a turbulent eddy diffusion coefficient of $0.5 \text{ m}^2 \text{ s}^{-1}$,

supposing that the air is always weakly turbulent. In our case, however, we assume no turbulence at all at the level of interaction, and Klostermeyer's calculations can be translated to a height of 70 km, where the molecular kinematic diffusion coefficient is around $1 \text{ m}^2 \text{ s}^{-1}$. His Figures 3 and 6 show structure which looks remarkably like Figures 5a and 5b in this text. Indeed Figure 6 from Klostermeyer's work appears to have two viscosity waves, an upward propagating one at the top of the layer and a downward propagating one at the bottom. Even the vertical wavelengths of the waves seem about right.

More recently, Hooke and Jones [1991] have studied gravity wave–viscosity wave interactions in the ocean and again found that there is substantial intermode coupling between gravity waves and viscosity waves. In their case they concentrated on regions of large velocity shear and concluded that viscosity waves could readily be generated in such regions. Hooke and Jones proposed that the gravity wave–viscosity wave interaction “bootstrapped” itself, with initial small perturbations on the shear starting the viscosity wave growth off, and then the gravity wave–viscosity wave interaction growing from that point.

In contrast, Fritts and Geller [1976] examined critical level interactions and concluded that viscosity would tend to “smooth out” the velocity perturbations around the region. However, the authors estimated accuracies of around a few percent. On the other hand, the velocity fluctuations required to explain the specular echoes in say the stratosphere are only around 1 cm s^{-1} and therefore may well be of the order of 1 or a few percent of the amplitude of the incident gravity wave. Thus while it is likely that viscosity will produce some smoothing of the velocity profile, we still anticipate that viscosity waves will exist. We do not doubt the general thrust of the work by Fritts and Geller but simply consider that it may not have the accuracy to detect the very small perturbations produced by the viscosity waves we are discussing. There may well be some room for conflict between the papers by Bowman *et al.* [1980], Hooke and Jones [1991], and Fritts and Geller [1976], but we consider that each is accurate for the regime considered therein. However, we consider the first two papers as supporting our assertion that viscosity waves will indeed be generated at critical levels and regions of large shear.

We therefore propose that a gravity wave incident at a critical level will represent a forcing which

will drive the viscosity waves with a frequency equal to its own, and this is why we have assumed a purely real frequency to date. We expect that the incident gravity wave will drive and support the viscosity waves until either the wave dies out or it grows so large that it breaks into turbulence.

We now turn to the issue of the generation of viscosity waves at reflection levels. HJ have outlined in some detail how reflection from a solid reflector like the ground generates viscosity waves. In the case of a sudden change in mean Brunt-Vaisala as a function of height a similar reflection level exists, except in this case the level is not solid and is therefore capable of being distorted by the incident gravity wave. This will reduce the efficiency of production of viscosity waves, but we do not expect it to reduce to zero. Continuity of both pressure and vertical velocity across the interface, as well as a “no-slip” condition, will require the existence of viscosity waves. Of course, for any significant reflection to occur the sudden change in Brunt-Vaisala frequency must take place in something less than a quarter of the vertical wavelength of the incident gravity wave, but once reflection does occur, the vertical wavelength of the resultant viscosity wave is dependent only on the frequency of the incident gravity wave and not its wavelength. Furthermore, at any one height all gravity waves of the same period produce viscosity waves with a single vertical wavelength, independent of the horizontal and vertical wavelengths of the gravity waves. Thus all waves of the same period act coherently to ensure that a moderately substantial viscosity wave is produced. Finally, it is important to remember that the viscosity waves need only produce small changes in refractive index, so even if the gravity waves only have reflection coefficients of a few percent, this may still be enough to produce viscosity waves with the necessary refractive index perturbations. We again emphasize that the resultant viscosity wave need only have amplitudes equal to one or a few percent of the incident wave in order to produce the observed reflection levels. It is also true that viscosity waves may not always be generated most efficiently at heights where the gravity waves are best reflected. For example, a gravity wave is reflected most efficiently at a turning level, where its vertical wavelength tends to infinity, but we do not anticipate that strong viscosity waves will be generated in this case. Viscosity waves will be generated most efficiently where the changes in Brunt-Vaisala

frequency and/or wind speed are most sudden. This is consistent with the expectation by *Hooke and Jones* [1991] that strong wind shears will be a region of substantial viscosity wave generation.

We consider that the above references support the concept of viscosity waves being forced by gravity wave nonlinearities and reflections. We have not, however, developed a model to determine the exact values of these viscosity wave amplitudes; at this stage our primary purpose is to verify that such waves may indeed be produced, and the above references illustrate that this is so. To develop a model capable of predicting the viscosity, wave amplitudes would require accuracies better than 1%, and this is not possible at present.

The viscosity waves will tend to have phase fronts aligned along the planes of the reflection level, and these reflection levels are likely to be nearly horizontally stratified, so it follows that the viscosity waves will be also. Thus the viscosity waves will tend to be aligned horizontally but not completely so. A range of waves will be produced, with differing tilts. We have already noted that there must be small tilts of the gradient discontinuity with respect to the planes of constant refractive index in order to produce backscatter; perfectly horizontal reflecting layers in a perfectly stratified atmosphere would produce no reflection.

We have also seen that the typical scales expected for viscosity waves match the Bragg scales for VHF radars at 20 km altitude and HF radars at 70 km altitude, which is consistent with our hypothesis. There is enough agreement between the wavelengths of the viscosity waves and the Bragg scale of 50-MHz radars to make the model highly plausible, but if the bandwidth of the viscosity waves had been extremely narrow, it may have been claimed that it was too much of a coincidence that 50-MHz VHF radars just "happen" to be at the correct frequency. However, the band is not very narrow; we note from Figure 10 that the bandwidth of the spectral peak of the viscosity waves is quite broad (around $\pm 50\%$ of the central wavelength), so it does not require a high level of coincidence for VHF radars to be of the correct frequency.

Thus viscosity waves can exist throughout the whole lower stratosphere with vertical wavelengths which are capable of causing radar backscatter of 50-MHz radar signals, and they will tend to exist in laminar regions. It is well known that the most stable region of the stratosphere occurs at ~ 15 – 20

km altitude (for example, see review diagram by *Chakrabarty et al.* [1987]), and the turbulent diffusion coefficient is generally least at these heights, so it may not be surprising that this is a region where these viscosity waves are frequently found. We also know that turbulence in the stratosphere tends to be a very stratified phenomenon, with layers of turbulence interspersed with layers of laminar flow. Thus it is not surprising that the specular reflectors may appear at times to occur not too far from turbulent layers, just by nature of the interleaving of turbulent and nonturbulent layers.

Explanation of the MU radar observations

At this stage we are now in a position to make a proposal to explain our observations which were discussed earlier. Figure 4 has indicated that the particularly stable region under study occurred some distance above a layer of narrow backscatter. The region of strong backscatter had some aspect sensitivity, but it was in fact the least aspect sensitive of any of the heights in Figure 4. We therefore surmise that this stronger echo was produced by a layer of turbulence, with some degree of anisotropy. Various authors [*Hocking et al.*, 1984; *Hocking*, 1985; *Woodman and Chu*, 1989; *Hocking*, 1990] have proposed that turbulence tends to be isotropic in the middle of a layer, but toward the top and bottom it is more anisotropic, and we surmise that the same is true in this case. Turbulent layers tend to oscillate with a period of the order of the Brunt-Vaisala period [*Pao*, 1973], and this results in some radiation of gravity waves. Furthermore, the turbulent motions themselves also produce (weak) radiation of gravity waves over a wide range of frequencies and wavenumbers [*Weinstock*, 1978].

We propose that the highly specular echo observed was due to viscosity waves produced in a very laminar (nonturbulent) region immediately above the localized turbulent layer discussed above. The fact that the specular echo discussed earlier occurred in a region of light winds (substantially less than 15 m s^{-1}) might be evidence that the echo was due to viscosity waves formed by orographically generated waves from below encountering a critical level region. Within the nearby turbulent layer, viscosity waves could have been produced too, but because of the larger turbulent diffusion coefficient (1 – $10 \text{ m}^2 \text{ s}^{-1}$) they would have had scales of the order of 60 – 100 m . Furthermore,

even if their scales were appropriate, the turbulence would produce corrugations on the wave fronts and prevent specular reflection. Hence we will concentrate on those viscosity waves formed in laminar regions of the atmosphere.

This proposal explains why specular reflectors occur, and why the specular reflectors occur adjacent to but not in turbulent layers. We have already seen that gravity waves are confined to have wave fronts at least 2° or more from horizontal, so these cannot explain the specular reflectors. The idea of sharp edges on the turbulent layers [Bolgiano, 1968] has been largely superseded by the idea of anisotropic turbulence on the top and bottom of the layer, and in any case cannot explain the observations shown in Figure 4, where the specular reflections occur some distance above the turbulent layer.

One feature left unexplained is the fact that even at range number 20, where the specular echoes occurred, the off-vertical beams still recorded some signal. We have already surmized that this is a region of laminar flow, so we cannot propose that there is weak turbulence. Nevertheless, we have already noted that the region is full of weak gravity waves (some perhaps radiated from the nearby turbulent layer). There are then two possible causes for this weak off-vertical scatter. First, it is unlikely that the reflecting layer will be perfectly flat. It will contain fluctuations and wobbles, so the phase fronts of the viscosity waves will contain similar such deviations. These will cause off-vertical scatter. Indeed, significant off-vertical scatter occurs even if there are "wobbles" on the scale of one eighth of the radar wavelength; in the stratosphere and for the case of 50-MHz backscatter this is less than 1 m. We propose that some of the off-vertical scatter is due to these undulations.

Second, we also propose that some of the signal observed on the off-vertical beams is due to weak Bragg reflection of the radio signals from short scale gravity waves. The waves will be fairly weak in intensity, because they will be the longest period, shortest vertical wavelength waves, and fairly heavily damped. In fact, even these gravity waves cannot have propagated far; the $1/e$ depth of gravity waves with vertical wavelengths of 3 m is only a few meters (Figure 8). More likely, they are the result of nonlinear interactions between longer wavelength waves produced by the nearby turbulent layer, and perhaps also from nonlinear breakdown of other atmospheric waves which are in the vicinity. Kloss-

termeyer [1990] has discussed how gravity waves may break down by the parametric subharmonic instability. Exactly, how these gravity waves arise here is not our direct concern; the important point is that these waves and the viscosity waves can coexist without destroying each other. Note that these gravity waves can in fact be generated at all heights, but at heights where there is any level of turbulence the enhanced diffusion will ensure that they are evenly more strongly damped, and furthermore their effects will be masked by the backscatter produced by the turbulence. They are most likely to survive and be noticed in a laminar region. Indeed, even in the laminar region, gravity waves with significant tilts will have phase fronts which pass into the nearby turbulent regions, and these waves will therefore be partly destroyed by turbulent destruction of the waves in these nearby turbulent regions. Thus these weaker gravity waves will not generally be a cause of radar backscatter and will only produce a distinguishable radar signal when they exist in nonturbulent regions.

Figure 11 summarizes the main features of this model. We note that the model explains the existence of very stable layers, and shows why VHF echoes tend to be most aspect sensitive at ~ 15 – 18 km altitude [Hocking *et al.*, 1986, 1990]. It also explains why MF echoes (~ 2 MHz) show strong aspect sensitivity at ~ 70 – 80 km altitude, and our calculated levels of backscatter have been shown to match experimental observations. We propose that the lesser degree of anisotropy observed by, for example, Fukao *et al.* [1980] and Royrvik [1985] at VHF in the mesosphere were probably due to anisotropic turbulence.

We have yet to quantify the expected ratio of vertical to off-vertical scatter, but this would require detailed model calculations to determine the nature of the spectrum of 3-m scale gravity waves in the surrounding region. This is beyond the scope of the current work.

TESTS OF THE MODEL

Possible further experimental tests of the model would include searches for more examples like that discussed in the early part of this paper. Simultaneous in situ and radar studies would be helpful to see if the specular reflections really do occur in very stable, nonturbulent regions.

Another useful prediction of the model could also

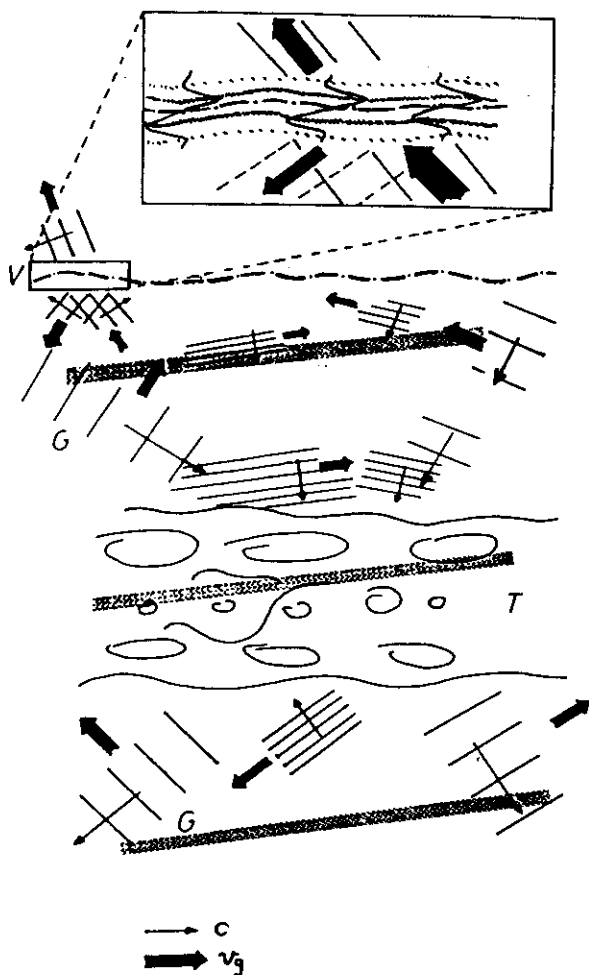


Fig. 11. Schematic picture of small-scale dynamics in a moderately stable stratified region of the atmosphere. The sets of parallel lines like those indicated by "G" represent gravity wave packets. The phase velocities (c) and group velocities (v_g) of the waves are shown by the two sets of arrows. The region "T" represents a turbulent layer, generated in this case by the longer wavelength gravity wave shown by the shaded wave fronts; elsewhere, the atmosphere is quite stable. The turbulence is statistically isotropic near the center and more anisotropic toward the edges. Some of the gravity waves shown are radiated by the turbulent layer, although the majority have propagated here from elsewhere. Adjacent to the turbulent layer is a laminar region which contains an "interface region" where the Brunt-Vaisala frequency undergoes a (stable) change, and this is indicated by the dashed-dotted line. At this level, partial reflection of gravity waves occurs, as shown by the expanded diagram of the box "V," and viscosity waves associated with these reflections are shown therein. These viscosity waves cause the "specular echoes" observed with atmospheric radars. The plane along which the Brunt-Vaisala frequency changes has a slight tilt, in order that the viscosity waves can produce density perturbations, and also contains undulations. These undulations give the surface a certain degree of "roughness" and contribute to the weaker off-vertical scatter observed.

be tested. There has been some effort dedicated to searching for radio echoes from above 30 km altitude. Our model makes some prediction about the best radar frequencies to use for such a search, assuming that the radar will receive backscatter from viscosity waves. For example, at a height of 50 km, $\nu \approx 0.016 \text{ m}^2 \text{ s}^{-1}$, and taking $\omega \sim 0.02 - 0.002 \text{ rad s}^{-1}$ we see that we expect viscosity waves with vertical wavelengths in the range 8 to 25 m. Thus frequencies in the range 6 to 20 MHz should be used to search for echoes from these heights.

Another useful prediction concerns the case of generation of viscosity waves at a critical level. The model predicts that viscosity waves will occur while the surrounding region is still laminar, but one might expect that eventually the gravity wave will grow in amplitude and break. Thus occasions should occur in which the specularly reflecting layer is observed to break up into turbulence.

Finally, it is possible that there may be a narrow "hole" around the vertical direction, from which little specular reflection occurs. This is because we have seen that if the planes of constant refractive index and the viscosity wave wave fronts are parallel, no refractive index perturbations will occur. The planes of constant refractive index tend to be near to horizontal on many occasions, so that horizontally aligned viscosity waves will produce no scatter in such circumstances. Nevertheless, there will also be occasions when the background refractive index isopleths are not horizontal, in which case reflection from overhead is possible. But as a general rule, there will always be some direction, close to vertical, from which no specular reflection occurs, and this will indicate the tilt of the contours of constant background refractive index. Interferometry would be a good means to search for such a "hole." There are just a few tests which could be applied to test our model further.

CONCLUSIONS

A model to explain the cause of specular reflection of radar signals from the atmosphere and lower ionosphere has been proposed. We suggest that these signals are due to "viscosity" and "thermal conduction" waves, these waves arising in regions of laminar flow at locations where gravity waves are reflected or critically absorbed. Provided that the flow in the region is nonturbulent, these waves will maintain their structure for lengths of time compa-

able to or greater than their period, which may be of the order of 5 to 60 min.

We have noted the following important points.

1. Viscosity waves will exist with vertical wavelengths which depend only on the viscosity coefficient and the wave period and can have any orientation. However, in the real atmosphere they will be aligned along planes where either the mean temperature gradient or the mean wind change, and such planes will tend to be near-horizontal. Typical vertical wavelengths are 1–5 m at 20–30 km altitude (i.e., around the Bragg scale for 50-MHz radars) and around 70 m at 70 km altitude (i.e., approximately the Bragg scale for 2-MHz radars). It has been noted that these scales are consistent with the fact that the highest degree of aspect sensitivity yet observed is at 50 MHz in the stratosphere and 2 MHz in the mesosphere.

2. Gravity waves cannot be the cause of the enhanced reflection from the vertical, since the effects of viscosity cause a steepening of the wave fronts compared to the inviscid theory, and gravity waves with vertical wavelengths of 3 m cannot exist any closer to about 2° – 3° from horizontal in the stratosphere. Viscosity waves can have any orientation, although in order to produce density fluctuations which can be observed with a radar, they must have a small tilt from horizontal; or, more specifically, must have a tilt with respect to the isopleths of constant mean refractive index. It is possible that this latter quantity could be tilted slightly, so in order to produce radar reflection it is only necessary that the isopleths of mean refractive index and the planes where the temperature-gradient changes occur are not the same. We have therefore proposed that viscosity waves are the cause of reflections from overhead and that these viscosity waves are produced in laminar regions in which either critical level interactions occur (prior to the breakdown of the wave at the critical level) or gravity wave reflection occurs. Off-vertical scatter may be produced by "wrinkles" at the gravity wave reflection level and by weak small-scale gravity waves.

3. Calculations of the reflection coefficients of such viscosity waves indicate that they are indeed capable of causing the observed signals.

Figure 11 summarizes the model, showing adjoining turbulent and laminar regions. The turbulent region contains scatterers which vary in aspect ratio as a function of distance from its center [e.g., Hocking et al., 1984; Hocking, 1985; Woodman and

Chu, 1989]. In the laminar region, viscosity waves are produced during partial reflection of gravity waves from gravity wave reflection levels (for example, moderately rapid changes in the Brunt-Vaisala frequency and/or the wind speed) and in the vicinity of critical level interactions; weak off-vertical reflection is produced by "wrinkles" in the phase fronts of the viscosity waves and by gravity waves of very short vertical wavelengths which exist there. These weak gravity waves may be produced by gravity waves generated by the nearby turbulent layer and also by nonlinear breakdown of other waves which exist in the region. The details of the model have been described in the previous section.

Several features are in need of further investigation but are beyond the scope of this paper. These include proper inclusion of both nonzero viscosity and thermal conductivity, which leads to a cubic dispersion relation in m^2 , and a more detailed calculation of the relative ratio of viscosity wave scatter to off-vertical scatter.

APPENDIX

In this appendix we seek to evaluate (28) in the main body of the text. We choose to Fourier transform each function of the convolution and find their product.

The Fourier transform of $e^{-z^2/\Delta z^2} \cos(4\pi z/\lambda)$ is

$$P(\xi) = \frac{1}{2} e^{-\pi^2(\Delta z)^2(\xi + 2/\lambda)^2} + \frac{1}{2} e^{-\pi^2(\Delta z)^2(\xi - 2/\lambda)^2} \quad (\text{A1})$$

where ξ is the reciprocal wavelength, and the Fourier transform of $\beta \sin(\alpha_1 z) e^{-\alpha_2 z}$ (with a value of zero for $z < 0$) is

$$V(\xi) = -\frac{\beta}{2\alpha_2} \left[\frac{1 + 2\pi i \frac{\xi + \frac{\alpha_1}{2\pi}}{\alpha_2}}{1 + \left[\frac{2\pi \left[\xi + \frac{\alpha_1}{2\pi} \right]}{\alpha_2} \right]^2} \right] + \frac{\beta}{2\alpha_2} \left[\frac{1 + 2\pi i \frac{\xi - \frac{\alpha_1}{2\pi}}{\alpha_2}}{1 + \left[\frac{2\pi \left[\xi - \frac{\alpha_1}{2\pi} \right]}{\alpha_2} \right]^2} \right] \quad (\text{A2})$$

If $\alpha_2 \ll \alpha_1$, then this function has two maxima close to $\xi = \pm[\alpha_1/(2\pi)]$, at which point $V(\xi) \approx \beta/(2\alpha_2)$, since only one of the two additive portions of (30) contributes any significant value in this case. In our case, however, $\alpha_1 = \alpha_2 = m_R$, so we cannot use this simple argument directly. The spectrum corresponding to $V(\xi)$ is shown in Figure 10 for the case of $\alpha_1 = \alpha_2 = m_R$. Note that this function is much broader than the Fourier transform of the pulse ($\alpha \exp\{-(\xi-2/\lambda)^2\}(\Delta z)^2$), which is shown in Figure 10 as the narrow "spikelike" function. The peaks of $V(\xi)$ are still close to $\pm[\alpha_1/(2\pi)]$, but substituting say $\xi = \alpha_1/2\pi$ into (A2) shows that the values of $V(\xi)$ at the peaks is about $(\beta/2\alpha_2)(-1/(1+4) + 1) = 0.4\beta/\alpha_2$. We have chosen the spectrum corresponding to the pulse to be centered at $\xi = 2/\lambda_p = \alpha_1/2\pi$, since backscatter will be most efficient in this case.

Because of the broad nature of $V(\xi)$ compared with $P(\xi)$, the product of the two Fourier transforms is approximately the same as that of the pulse alone but multiplied by $0.4\beta/\alpha_2$. Therefore the reflected pulse is the same in form as the transmitted pulse but reduced in amplitude by $0.4\beta/\alpha_2$ times, or, in other words, the reflection coefficient is $0.4\beta/\alpha_2$.

In reality, the actual reflection will be a little less than this if we properly Fourier transform the product of these two functions, because the Fourier transform of $1/2 \, dn/dz$ is not flat, but the reduction will only be a few percent, $V(\xi)$ being so much broader than the Fourier transform of the pulse.

In our case, $\beta \approx 0.1|\rho'_A|/\lambda_p$, and $\alpha_1 = \alpha_2 = 2\pi/\lambda_p$. Thus the reflection coefficient is

$$R = 0.4\beta/\alpha_2 = 0.0064|\rho'_A| = 0.285n'_A \quad (\text{A3})$$

Acknowledgments. We particularly wish to thank Colin Hines for first encouraging one of us (W.K.H.) to investigate the nature of viscosity waves. Thanks are also due to several people for proof-reading and discussions, including B. H. Briggs, T. Harris, D. Lesicar, E. Thrane, O. Andreassen, D. Fritts, and T. Sato. W.K.H. would also like to thank the Radio Atmospheric Science Center of Kyoto University for their hospitality during his visit there in 1988. The MU radar belongs to and is operated by the Radio Atmospheric Science Center of Kyoto University.

REFERENCES

- Bolgiano, R., Jr., The general theory of turbulence—Turbulence in the atmosphere, in *Winds and Turbulence in the Stratosphere, Mesosphere and Ionosphere*, edited by K. Rawer, p. 371, North-Holland, New York, 1968.
- Bowman, M. R., L. Thomas, and R. H. Thomas, The propagation of gravity waves through a critical layer for conditions of moderate wind shear, *Planet. Space Sci.*, 28, 119–133, 1980.
- Chakrabarty, D. K., G. Beig, J. S. Sidhu, H. Chakrabarty, R. Narayanan, N. K. Modi, S. R. Das, and P. Chakrabarty, Measurements of the eddy diffusion coefficient in the middle atmosphere from a balloon at low altitude, *J. Atmos. Terr. Phys.*, 49, 975–980, 1987.
- Crane, R. K., A review of radar observations of turbulence in the lower stratosphere, *Radio Sci.*, 15, 177–193, 1980.
- Doviak, R. J., and D. S. Zrnic, Reflection and scatter formula for anisotropically turbulent air, *Radio Sci.*, 19, 325–336, 1984.
- Fritts, D. C., and M. A. Geller, Viscous stabilization of gravity wave critical level flows, *J. Atmos. Sci.*, 33, 2276–2284, 1976.
- Fukao, S., T. Sato, R. M. Harper, and S. Kato, Radio wave scattering from the tropical mesosphere observed with the Jicamarca radar, *Radio Sci.*, 15, 447–457, 1980.
- Fukao, S., T. Sato, T. Tsuda, S. Kato, K. Wakasugi, and T. Makihira, The MU radar with an active phased array system, 1, Antenna and power amplifiers, *Radio Sci.*, 20, 1155–1168, 1985a.
- Fukao, S., T. Tsuda, T. Sato, S. Kato, K. Wakasugi, and T. Makihira, The MU radar with an active phased array system, 2, In-house equipment, *Radio Sci.*, 20, 1169–1176, 1985b.
- Gage, K. S., and J. L. Green, Evidence for specular reflection from monostatic VHF radar observations of the stratosphere, *Radio Sci.*, 13, 991–1001, 1978.
- Gill, A. E., *Atmosphere-Ocean Dynamics*, Academic, San Diego, Calif., 1982.
- Gregory, J. B., and R. A. Vincent, Structure of partially reflecting regions in the lower ionosphere, *J. Geophys. Res.*, 75, 6387–6389, 1970.
- Hines, C. O., Internal atmospheric gravity waves at ionospheric heights, *Can. J. Phys.*, 38, 1441–1481, 1960.
- Hocking, W. K., Angular and temporal characteristics of partial reflections from the D-region of the ionosphere, *J. Geophys. Res.*, 64, 845–851, 1979.
- Hocking, W. K., Investigations of the movement and structure of D-region ionospheric irregularities Ph.D. thesis, Univ. of Adelaide, S. Aust., 1981.
- Hocking, W. K., Measurement of turbulent energy dissipation rates in the middle atmosphere by radar techniques: A review, *Radio Sci.*, 20, 1403–1422, 1985.
- Hocking, W. K., Target parameter estimation, *Middle Atmos. Program Handb.*, 30, 228–268, 1990.
- Hocking, W. K., and J. Roettger, Pulse-length dependence of radar signal strengths for Fresnel backscatter, *Radio Sci.*, 18, 1312–1324, 1983.
- Hocking, W. K., and R. A. Vincent, A comparison between HF partial reflection profiles from the D-region and simultaneous Langmuir probe electron density measurements, *J. Atmos. Terr. Phys.*, 44, 843–854, 1982a.
- Hocking, W. K., and R. A. Vincent, Comparative observations of D-region HF partial reflections at 2 and 6 MHz, *J. Geophys. Res.*, 87, 7615–7624, 1982b.
- Hocking, W. K., R. Ruester, and P. Czechowsky, Observation and measurement of turbulence and stability in the middle atmosphere with a VHF radar, *Rep. ADP 335*, Dep. of Phys., Univ. of Adelaide, Adelaide, S. Aust., 1984.
- Hocking, W. K., R. Ruester, and P. Czechowsky, Absolute reflectivities and aspect sensitivities of VHF radio wave scatterers measured with the SOUSY radar, *J. Atmos. Terr. Phys.*, 48, 131–144, 1986.

- Hocking, W. K., P. T. May, and J. Roettger, Interpretation, reliability and accuracies of parameters deduced by the spaced antenna method in middle atmosphere applications, *Pure Appl. Geophys.*, **130**, 571–604, 1989.
- Hocking, W. K., S. Fukao, T. Tsuda, M. Yamamoto, T. Sato, and S. Kato, Aspect sensitivity of stratospheric VHF radio-wave scatterers, particularly above 15 km altitude, *Radio Sci.*, **25**, 613–627, 1990.
- Hooke, W. H., and R. M. Jones, Dissipative waves excited by gravity-wave encounters with the stably stratified planetary boundary layers, *J. Atmos. Sci.*, **43**, 2048–2060, 1986.
- Hooke, W. H., and R. M. Jones, Dissipative waves excited by internal waves in the thermocline, *J. Phys. Oceanogr.*, in press, 1991.
- Houghton, J. T., *The Physics of Atmosphere*, Cambridge University Press, New York, 1977.
- Klostermeyer, J., Numerical calculation of gravity wave propagation in a realistic thermosphere, *J. Atmos. Terr. Phys.*, **34**, 765–774, 1972.
- Klostermeyer, J., Computation of acoustic-gravity waves, Kelvin-Helmholtz instabilities, and wave-induced eddy transport in realistic atmospheric models, *J. Geophys. Res.*, **85**, 2829–2839, 1980.
- Klostermeyer, J., On the role of parametric instability in radar observations of mesospheric gravity waves, *Middle Atmos. Program Handb.*, **28**, 299–308, 1989.
- Klostermeyer, J., Gravity waves and instabilities in the lower and middle atmosphere, *Middle Atmos. Program Handb.*, **30**, 269–298, 1990.
- Larsen, M., Applications of MST radars: Meteorological applications, *Middle Atmos. Program Handb.*, in press, 1990.
- Manson, A. H., M. W. J. Merry, and R. A. Vincent, Relationship between the partial reflection of radio waves from the lower ionosphere and irregularities as measured by rocket probes, *Radio Sci.*, **4**, 955–958, 1969.
- Mechtly, E. A., S. A. Bowhill, and L. G. Smith, Changes of lower ionosphere electron concentrations with solar activity, *J. Atmos. Terr. Phys.*, **34**, 1899–1907, 1972.
- Myers, R. M., and M. Yanowitch, Small oscillations of a viscous isothermal atmosphere, *J. Comput. Phys.*, **8**, 241–257, 1971.
- Nastrom, G. D., K. S. Gage, and B. B. Balsley, Variability of C_n^2 at Poker Flat, Alaska, from mesosphere, stratosphere, troposphere (MST) Doppler radar observations, *Opt. Eng.*, **21**, 347–351, 1982.
- Pao, Y.-H., Measurements of inertial waves and turbulence in two-dimensional stratified shear flows, *Boundary Layer Meteorol.*, **5**, 177–193, 1973.
- Pitteway, M. L. V., and C. O. Hines, The viscous damping of atmospheric gravity waves, *Can. J. Phys.*, **41**, 1935–1948, 1963.
- Roettger, J., Reflection and scattering of VHF radar signals from atmospheric refractivity structures, *Radio Sci.*, **15**, 259–276, 1980a.
- Roettger, J., Structure and dynamics of the stratosphere and mesosphere revealed by VHF radar investigations, *Pure Appl. Geophys.*, **118**, 494–527, 1980b.
- Roettger, J., and C. H. Liu, Partial reflection and scattering of VHF radar signals from the clear atmosphere, *Geophys. Res. Lett.*, **5**, 357–360, 1978.
- Royrvik, O., Radar comparison of 2.66-MHz and 40.92-MHz signals scattered from the mesosphere, *Radio Sci.*, **20**, 1423–1434, 1985.
- Sen, H. K., and A. A. Wyller, On the generalization of the Appleton-Hartree magnetionic formulas, *J. Geophys. Res.*, **65**, 3931–3950, 1960.
- Tsuda, T., T. Sato, K. Hirose, S. Fukao, and S. Kato, MU radar observations of the aspect sensitivity of backscattered VHF echo power in the troposphere and lower stratosphere, *Radio Sci.*, **21**, 971–980, 1986.
- Van Zandt, T. E., and R. A. Vincent, Is VHF Fresnel reflectivity due to low frequency buoyancy waves?, in *Handbook for MAP*, vol. 9, pp. 78–80, SCOSTEP Secretariat, University of Illinois, Urbana, 1983.
- Vincent, R. A., and J. S. Belrose, The angular distribution of radio waves partially reflected from the lower ionosphere, *J. Atmos. Terr. Phys.*, **40**, 35–47, 1978.
- Weinstock, J., On the theory of turbulence in the buoyancy subrange of stably stratified flows, *J. Atmos. Sci.*, **35**, 634–649, 1978.
- Woodman, R. F., and Y.-H. Chu, Aspect sensitivity measurements of VHF backscatter made with the Chung-Li radar: Plausible mechanisms, *Radio Sci.*, **24**, 113–125, 1989.
- Yanowitch, M., Effect of viscosity on gravity waves and the upper boundary condition, *J. Fluid Mech.*, **29**, 209–231, 1967a.
- Yanowitch, M., Effect of viscosity on vertical oscillations of an isothermal atmosphere, *Can. J. Phys.*, **45**, 2003–2008, 1967b.
- Yanowitch, M., A numerical study of vertically propagating waves in a viscous isothermal atmosphere, *J. Comput. Phys.*, **4**, 531–542, 1969.
- S. Fukao, S. Kato, T. Tsuda, and M. Yamamoto, Radio Atmospheric Science Center, Kyoto University, Uji, Kyoto 611 Japan.
- W. K. Hocking, Department of Physics, University of Adelaide, G.P.O. Box 498, Adelaide, South Australia 5001.

Errata for previous paper.

82

SOME NEW PERSPECTIVES ON VISCOSITY AND THERMAL CONDUCTION WAVES AS A CAUSE OF 'SPECULAR' REFLECTORS IN RADAR STUDIES OF THE ATMOSPHERE

W.K. Hocking

Dept. of Physics, University of Western Ontario, London, Ont., N6A 3K7, Canada

Abstract

Following recent observations of sheet-like structures in the atmosphere using balloons [Luce et al., 1995], it is possible to re-examine the possibility of specular reflection being caused by viscosity and thermal conduction waves in the atmosphere. New developments in this model are presented.

1. Introduction

The concept of damped diffusive waves as a cause of specular reflections of radio signals from the middle atmosphere was first introduced by Hocking et al., [1991] - here-after referred to as H91. Since publication of that work, some new developments have occurred, which permit new perspectives on this model. In addition, there were some errors in the original paper, which will also be addressed.

First, we will attend to the errors in the original paper. One is typographical, one is conceptual but has no bearing on the results of the paper, and a third is very important and has significant bearing on the the stratospheric portion of the work - although it does not alter the final conclusions too much. This last factor causes no changes in relation to the ionospheric analyses performed in H91.

These errors are listed below, with the most significant one mentioned first.

(i) The first, and most important error, is that "p" in equation (20) of H91 should be the pressure in millibars, not Pascals.

(ii) The least significant error, which is purely typographical, is in the first line of equation (22), in which the brackets have been printed in the wrong order. The bracketed sections should appear as

$$\left[\frac{p}{T} \left(\frac{1}{T} \right) \left(\frac{dT}{dz} + \Gamma_a \right) \right]$$

(iii) Finally, equation (23) should be written as

$$\frac{dn}{dz} = -M_n \frac{ds'}{dz}$$

where s' is the vertical displacement of a parcel due to a wave at height z , and is not the same as z . s' is also given by equation (14).

Consequences

(iii) Item (iii) is not used anywhere in the paper, and so has no consequences.

(ii) Item (ii) is purely typographical and has no consequences.

(i) Item (i) is very significant, and means that a few of the constants used in the paper are in error by factors of 10^2 (and in some cases 10^4). Interestingly, as will be shown, because the comparisons with experiment were in essence "order of magnitude" only, even these changes do not permit viscosity waves to be discounted as observable entities. It has to be admitted, however, that rather more specific conditions are needed for them to be seen - although it turns out that these special conditions are not uncommon.

This error affects the following equations in the original paper. I will use the symbols 'VW' in front of equations from the original paper to emphasize their origin.

(a) Equation (VW22) - all occurrences of 77.9×10^{-6} should read 77.9×10^{-8}

(b) The second equation following (VW25) should read

$$\frac{dn}{dz} = 2.24 \times 10^{-4} | \rho'_A | \operatorname{Re}\{ime^{i(mx+\phi+\pi/4)}\}$$

(c) Equation (VW26): 0.0224 should be 2.24×10^{-4}

(d) Equation (VW27): 0.0112 should read 1.12×10^{-4} (upper line), and in the last line 0.1 should be replaced with 10^{-3} .

Equations (VW28), (VW29) and (VW30) are perfectly satisfactory as they are, but the very last line of the appendix (which relates to these equations) should read

$$R = 0.4\beta/\alpha_2 = 6.4 \times 10^{-5} | \rho'_A | = 0.285n'_A$$

Note that the term 0.285 is unchanged.

Finally, the section from equations (VW31) to (VW33), and the text up to "D-region case", needs to be re-addressed, and this will now be done. We will also examine the new developments which have placed the possibility of the existence of these damped waves in a new light.

2. Can we detect viscosity waves?

In the original paper [H91], we asked this same question, and concluded that the waves could indeed be responsible for the specular reflections observed. In view of the above corrections, these conclusions need to be re-addressed. However, rather than simply repeating the work from that paper, but with new values for the parameters, a better procedure has been developed to more clearly answer the above question. This procedure also improves our understanding of fig. VW9 and equation (VW11) in the original paper. Thus this section is not a correction, but an addition and an improvement over the original work.

First, let us return to the expressions

$$n' = M_n s' \quad \text{and} \quad \rho' = M_\rho s' \quad (1)$$

where $s' = \frac{w'}{-i\omega} = \frac{-ik}{\omega m} u'$ is the vertical excursion of a displaced parcel of air. (Note that the relation $ku' + mw' = 0$ is valid for both viscosity waves and gravity waves for an incompressible gas, since it comes directly from the continuity equation).

Then from (1), $n' = \frac{M_n}{M_\rho} \rho' = 77.9 \times 10^{-8} K'_B \rho'$ (see the modified equation (VW22)). This also means that $\frac{dn'}{dz} = \frac{M_n}{M_\rho} \frac{d\rho'}{dz}$. We have already discussed this expression in relation to the equation following (VW25) (including (VW26) and (VW27)).

But now let us look at the expression $\rho' = M_\rho s'$ in more detail. We also know that $M_\rho = \frac{-\rho_0 \omega^2}{g}$ e.g. see (VW15b) and the discussion which follows that equation.

Thus

$$\frac{\rho'}{\rho_0} = \frac{-\omega^2}{g} s' = +i \frac{\omega^2}{g} \frac{k}{m} \frac{1}{\omega} u' \quad (2)$$

Note that for fixed ω_B , m and ω , $\frac{\rho'}{\rho_0} \propto k$. This is consistent with fig. VW9, where ρ' shows an almost linear variation with k .

Note that this simple relation between ρ' and k was not recognized in the discussion following equation (VW13), and in fact is not at all evident from (VW11), since that equation does not even appear to involve ω_B !

But in fact (2) can be derived from (VW11) provided that (VW8) and (VW9) are used for m . To see this, write (VW8) as

$$m^2 = -k^2 - \frac{i\omega}{2\nu}[\pm(1 + \frac{iX}{2}) - 1] \quad (3)$$

where we have used a binomial expansion for the square root.

Then taking the negative choice of the \pm , which corresponds to the viscosity waves, we have

$$m^2 = -k^2 - \frac{i\omega}{2\nu}[-2 + \frac{iX}{2}] \quad (4)$$

Hence

$$m^2 + k^2 = \frac{i\omega}{2\nu}(2 - \frac{iX}{2}) \quad (5)$$

We wish to incorporate this information into (VW11), so multiply both sides of the previous equation by $i\frac{\nu}{\omega}$ and re-arrange to give

$$1 + i\frac{\nu}{\omega}(m^2 + k^2) = i\frac{X}{4} \quad (6)$$

Substitution into (VW11) and applying (VW9) then gives

$$\frac{\rho'}{\rho_0} = -i\frac{\omega}{g}(\frac{iX}{2})\frac{m}{k}u' = \frac{\omega}{g}(\frac{\omega_B}{\omega})^2(\frac{\nu}{\omega})k^2\frac{m}{k}u' \quad (7)$$

or

$$\frac{\rho'}{\rho_0} = \frac{\omega_B^2}{g} \frac{\nu}{\omega} \frac{k}{\omega} m u' \quad (8)$$

Finally, $\frac{\nu}{\omega} \approx \frac{1}{m^2}$ (see (VW3a)), so that

$$\frac{\rho'}{\rho_0} = i\frac{\omega_B^2}{g} \frac{k}{m} \frac{1}{\omega} u', \quad (9)$$

which is (2).

We are now in a better position to pursue the discussion following equation (VW31). We begin with our estimate of the peak reflection coefficient as $R = 6.4 \times 10^{-5} |\rho'_A|$ (via (A3) from H91), so that

$$R = 6.4 \times 10^{-5} \rho_0 \frac{\omega_B^2}{g} \frac{k}{|m|} \frac{1}{\omega} u'_A \quad (10)$$

For example, take $\rho_0 = 0.05 \text{ kg m}^{-3}$ at 20 km altitude, $\omega_B^2 = 4 \times 10^{-4} \text{ rad}^2 \text{ s}^{-2}$, $g = 9.8 \text{ ms}^{-2}$, and $|m| = 2\pi/1.5 \text{ metre}^{-1}$. If we use a period of say 60 min ($\omega = 2\pi/3600 \text{ rads}^{-1}$), and take the horizontal wavelength to be 50 m, then

$$R \approx 2.2 \times 10^{-9} u'_A \quad (11)$$

(compared to VW31). Note that using these values of m and k (vertical wavelength = 1.5 m, horizontal wavelength of 50 m) corresponds to a tilt angle for the phase fronts of 2° from horizontal.

Then using $C_n^2 = 21.5R^2$ (see just prior to (VW33) in the original paper) we have

$$C_n^2 \approx 10^{-18} u_A^2 \quad (12)$$

for our choice of radar and wave parameters.

A horizontal perturbation velocity of $u'_A = 10 \text{ cm s}^{-1}$ would then produce a value for $C_n^2 = 10^{-18} \text{ m}^{-2/3}$. However, the Richardson number in this case would be

$$R_i = \omega_B^2 / (m_R u)^2 = (4 \times 10^{-4} / ([2\pi/1.5] \times 0.1)^2) \quad (13)$$

or $R_i = 2 \times 10^{-3}$.

Thus such a wave should be unstable, so this might suggest that viscosity waves are not important in the stratosphere under normal circumstances, negating the original statements in H91.

However, new experimental data have appeared since the original paper was written, and these data allow us to re-examine these equations from a new perspective. Luce *et al.* [1995] have presented balloon data which show small step-like structures which could be related to viscosity waves. They have shown that these structures are much more prolific than was originally assumed in H91, so at any one time there may be several in a radar volume. Furthermore, in the immediate surrounding area the temperature gradient can be very high - up to 20 K km^{-1} . Thus ω_B^2 can be as high as $10^{-3} \text{ rad}^2 \text{ s}^{-1}$. These large values for the Brunt-Vaisala frequency have two effects - first, they strengthen the efficiency of backscatter of these viscosity waves, and secondly they also allow the waves to grow to larger amplitudes before becoming unstable. For example, if ω_B^2 is 10^{-3} , then (11) becomes

$$R = 5.5 \times 10^{-9} u_A' \quad (14)$$

and so $C_n^2 \approx 6 \times 10^{-16} u_A'^2$.

If in addition there are say 4 or 5 such viscosity waves within the radar pulse length, then C_n^2 could be 4 or 5 times larger (larger if the signals from some of the reflectors interfere constructively), so in this case we could have

$$C_n^2 \approx 3 \times 10^{-15} u_A'^2, \quad (15)$$

where we have assumed that all viscosity waves have approximately equal amplitudes u_A . To produce a value for C_n^2 of 10^{-18} in this case requires a typical value for the velocity amplitude of only $u_A' \approx 1.7 \text{ cm s}^{-1}$. Then the Richardson number is $R_i \approx 10^{-3} / (2\pi/1.5 \cdot 0.017)^2 \approx 0.2$.

Thus in this case the waves are close to stable. A slight increase in the horizontal wavenumber k , or a decrease in ω (see 10), or an increase in ω_B , or an increase in the number of waves, could easily permit viscosity waves which are stable to be detectable with a VHF radar.

As an interesting aside, it is interesting to contemplate the nature of the Miles-Howard stability theorem. The condition $R_i = 0.25$ is a necessary condition for turbulence, but not sufficient. This means turbulence can occur, but does not have to. Perturbations in the flow are required to trigger the turbulence. In the case of a well-organized motion like viscosity waves, existing in a very stable background, is it not possible that the perturbations necessary to initiate the turbulence may not develop? if this is true, then is it not also possible that the viscosity waves could maintain themselves even under conditions in which the Richardson number is less than 0.25 (on condition that the mean Richardson number in the surrounding area is typically much greater than 0.25)?

Regardless of the last point, we see in conclusion that viscosity waves can cause measurable radar backscatter in the stratosphere - but under more specialized conditions than proposed in the original paper. Nevertheless, the observation of very specular radio wave reflectors is itself a relatively rare event, so the need for special conditions is not a drawback for the theory.

References

- Hocking, W.K., S. Fukao, M. Yamamoto, T. Tsuda, and S. Kato, "Viscosity waves and thermal conduction waves as a cause of 'specular' reflectors in radar studies of the atmosphere", *Radio Sci.* 26, 1281-1303, 1991.
- Luce, H., M. Crochet, F. Dalaudier and C. Sidi, "Interpretation of VHF ST radar vertical echoes from in situ temperature sheet observations", *Radio Sci.*, 30, 1003-1025, 1995.

The following paper presents
a proposal by Klostermeyer that
when a gravity wave breaks down, it does
not immediately decay to chaotic turbulent
motion, but changes to small-scale, organized
structures

THE FORMATION OF LAYERED STRUCTURES BY PARAMETRIC INSTABILITY OF FINITE-AMPLITUDE GRAVITY WAVES

J. Klostermeyer

Max-Planck-Institut für Aeronomie, D-3411 Katlenburg-Lindau, Germany

ABSTRACT

VHF Doppler radars occasionally indicate the presence of almost monochromatic long-period gravity waves in the mesosphere. The radar echo intensity occurs in the form of nearly horizontally extended layers which are assumed to be generated by enhanced turbulence although the Richardson numbers are significantly larger than unity, excluding both shear and static instabilities as primary mechanisms for transition to turbulence. In good agreement with these observations, the theory of parametric instability of finite-amplitude monochromatic gravity waves predicts fast growing anisotropic small-scale disturbances whose size is limited by molecular dissipation. The disturbances form turbulent layers moving with the phase velocity of the primary wave. They are "frozen" in the primary wave flow (Taylor's hypothesis) and thus confirm the general assumption that the fluid velocity can be obtained from the Doppler shift of backscattered radar echoes.

INTRODUCTION

In recent years, sensitive VHF Doppler radars operating at frequencies near 50 MHz have provided valuable information about large-amplitude internal gravity waves in the atmosphere. In particular, the radar measurements occasionally indicate the presence of almost monochromatic long-period waves that seem to be generated in the troposphere by unidentified source mechanisms and propagate through the stratosphere with exponentially increasing amplitude up to a mesospheric breaking level above which the wave amplitude remains almost constant or decreases slightly [1]. Then the radar echo intensity at mesospheric heights reveals almost horizontally extended layers that have vertical distances equal to the apparent vertical wavelength and in general tend to move downwards with the vertical phase trace velocity of the long-period wave. Typical periods and vertical wavelengths range from 1 to 10 h and 3 to 20 km, respectively [2,3,4]. Case studies show in particular that the most intense echo layers lie well below the wave breaking level, i.e. within the statically stable wave field [5]. In addition, the wave-perturbed Richardson number at these heights is significantly larger than unity so that also shear instability cannot occur. Finally, the echo layers are sometimes at heights where both the wave-perturbed Väisälä-Brunt frequency and the Richardson number are close to local maxima excluding any explanation in terms of a linear superposition of the large-amplitude wave and other small-amplitude components of the wave spectrum giving rise to statically or dynamically unstable height intervals. In the following, we therefore consider the effect of parametric instability which is the basic instability mechanism in finite-amplitude gravity waves rather than static or shear instability. We thus adhere to the idea that enhanced radar echo power is generated by enhanced neutral air turbulence, but the transition mechanism differs from the conventional ones.

THEORY OF PARAMETRIC INSTABILITY

Since with one exception, the next section contains only results computed from a two-dimensional model, the following description is restricted to this model. Details can be found in the papers by Miel [6] and Klostermeyer [7,8] so that for brevity, we can confine ourselves to the most important aspects.

The mathematically simplest model is an unbounded inviscid Boussinesq fluid which yields a fairly faithful representation of atmospheric gravity waves with sufficiently small wavelengths [9]. We introduce the stream function Ψ and buoyancy B by

$$u = (\Psi_x, -\Psi_z), \quad B = -\frac{\rho - \rho_0}{\rho_0} g \quad (1)$$

with u , ρ and g denoting, respectively, the fluid velocity, density and gravitational acceleration. ρ_0 is the density of the reference state in which the fluid is at rest. Here and in the following, the subscripts x , z and t denote partial derivatives. The fluid motion is described by

$$\nabla^2 \Psi_t + B_x = \Psi_x \nabla^2 \Psi_x - \Psi_x \nabla^2 \Psi_x \quad (2a)$$

$$B_t - N^2 \Psi_x = \Psi_x B_x - \Psi_x B_x \quad (2b)$$

where N is the Väisälä-Brunt frequency of the reference state and is assumed to be constant. Then the finite-amplitude wave

$$\Psi = A \cos \Phi, \quad B = -N^2 l \omega^{-1} A \cos \Phi \quad (3)$$

with $\Phi = lx + mz - \omega t$ is an exact solution of (2) if the wavenumber vector $k = (l, m)$ and the angular frequency ω satisfy the dispersion equation

$$\omega^2 = N^2 \cos^2 \theta \quad (4)$$

where θ is the angle between k and the horizontal (Fig. 1).

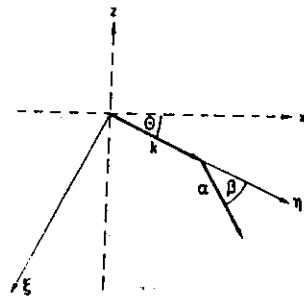


Fig. 1. Primary wavenumber vector $k = (0, 1)$ and Floquet wavenumber vector $k_0 = (\alpha \sin \beta, \alpha \cos \beta)$ in ξ, η coordinates.

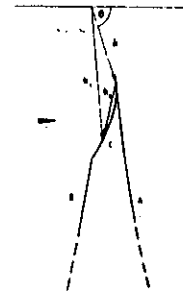


Fig. 2. Resonant sum interaction diagram for a primary wave with a propagation angle $\theta = -72^\circ$. Any point on a branch defines a resonant triad including the primary (k) and the Floquet wave (k_0). The stippled areas around branches A and C indicate triads giving rise to fast growing parametric instabilities.

To test the stability of the finite-amplitude gravity wave (3) we put

$$\Psi = A \cos \Phi + \psi, \quad B = -N^2 l \omega^{-1} A \cos \Phi + b. \quad (5)$$

The perturbation quantities ψ and b are obtained by substituting (5) into (2). After introducing the dimensionless variables

$$(\tilde{x}, \tilde{z}) = k(x, z), \quad \tilde{t} = Nt, \quad \tilde{\Psi} = k^2 N^{-1} \Psi, \quad \tilde{B} = k N^{-2} B, \quad M = k^2 (2N)^{-1} A \quad (6)$$

and a rotated coordinate system (ξ, η) such that the η axis coincides with k (Fig. 1), we get

$$\nabla^2 \psi_t + \sin \theta b_t + \cos \theta b_\eta = 2M \sin \Phi (\psi_t + \nabla^2 \psi_t) \quad (7a)$$

$$b_t - \sin \theta \psi_t - \cos \theta \psi_\eta = 2M \sin \Phi (\psi_t + b_t) \quad (7b)$$

where the tilde of the dimensionless variable has been omitted. Floquet theory yields solutions of the form

$$(\psi, b) = e^{i(\alpha \sin \beta \xi + \alpha \cos \beta \eta) + \sigma t} \sum_{j=-\infty}^{\infty} (\psi_j, b_j) e^{ij\Phi}. \quad (8)$$

We assume solutions that are bounded in space. Then the complex frequency σ and Fourier coefficients (ψ_j, b_j) can be obtained from a linear eigenproblem [7]. Equation (8) contains an infinite number of perturbation waves. The wave with $j = 0$ is called the Floquet wave and propagates with a wavenumber α at an angle β to the primary wavenumber vector k (Fig. 1). Eigensolutions with $\text{Re}(\sigma) > 0$ represent parametrically unstable modes, and it can be shown that for vanishingly small primary wave amplitudes M , parametric instability reduces to nonlinear resonant interaction (Fig. 2) [6,9].

FORMATION AND PROPERTIES OF LAYERED STRUCTURES

Next, we consider solutions of (7) for a propagation angle $\theta = -72^\circ$ (i.e. $\omega \approx 0.3N$) and a wave amplitude $M = 0.4$. Then the Richardson number is everywhere larger than 1.57 so that shear and static instabilities cannot occur in the primary wave field.

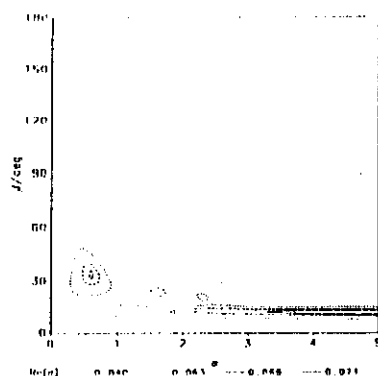


Fig. 3. Growth rate contours in the α, β plane. The contour levels are chosen such that during one primary wave period $T = 2\pi/\omega$, the amplitude increase is approximately equal to, respectively, 0.50, 0.75, 0.85 and 0.90 times the maximum amplitude increase. The restriction to $\beta \geq 0^\circ$ is possible because of the symmetry relations (14) in /8/.

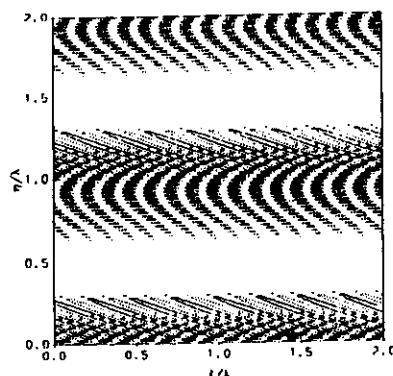


Fig. 4. Contours of the buoyancy disturbance b in the ξ, η plane for $(\alpha, \beta) = (20, 11.3^\circ)$. Both axes extend over 2λ where $\lambda = 2\pi/k$ is the primary wavelength. Continuous (dashed) contours indicate $b > 0 (< 0)$.

Figure 3 shows the growth rate $Re(\sigma)$ as a function of the wavenumber α and the propagation angle β of the Floquet wave. Besides a secondary maximum at $(\alpha, \beta) = (0.59, 34^\circ)$, large growth rates occur at $\alpha > 3$ and $\beta \approx 11^\circ$, and further computations indicate that in the absence of dissipation, the levels of strong growth rates near $\beta \approx 11^\circ$ extend to infinite α giving rise to a roughly fivefold amplitude increase during one primary wave period. The fast growing large-scale instability at $\alpha = 0.59$ and the small-scale instabilities at large α originate from triad interactions in the stippled areas of the interaction diagram in Fig. 2. Parametric instability thus gives rise to randomly superposed small-scale disturbances whose size is only limited by molecular dissipation. The energy transfer from the primary wave to all disturbance scales occurs simultaneously rather than via a turbulent energy cascade. Nevertheless, such a broad wavenumber spectrum is typical of turbulence. In particular, since parametric instabilities produce Bragg scattering of radar pulses, a finite-amplitude gravity wave makes its own appearance without needing shear or static instability as a primary mechanism for the transition to turbulence.

Figure 4 shows contours of the buoyancy disturbance in the ξ, η plane for the fastest growing mode with a Floquet wavenumber $\alpha = 20$. This value has been chosen because on the one hand, it is much larger than the primary wavenumber which is unity whereas on the other hand, the small-scale structure can still be resolved in the contour plot. Since $\theta = -72^\circ$, the ξ axis and the layers in Fig. 4 are inclined by 18° to the horizontal. Generally, the inclination is $90^\circ - |\theta|$ and therefore decreases with increasing primary wave period which is equal to $2\pi/\cos\theta$ in dimensionless units. Figure 4 indicates that the layers as a whole occur periodically in space with wavenumber vector k and in time with angular frequency ω and thus move with the phase velocity of the primary wave. It will be shown below that this is not true for the fine structure. The contour lines close to the local maxima and minima of the buoyancy disturbance resemble ellipses with the major axes almost parallel to the primary wave fronts. Therefore we expect that in the ξ, η plane, any Bragg scattering from the fine structure is highly aspect sensitive. Without going into details, we note that there is a strong decrease of $Re(\sigma)$ as the Floquet vector is rotated out of the ξ, η plane (Fig. 5) so that all small-scale disturbance modes are essentially two-dimensional. For a quantitative assessment of the aspect sensitivity of Bragg scattering, however, the refractive index disturbances have to be evaluated. For the mesosphere, this requires the solution of the ion continuity equation and, near the mesopause, has to involve the effects of a cascade mechanism that produces an inertial subrange in the electron gas extending well beyond that of the neutral gas /10/.

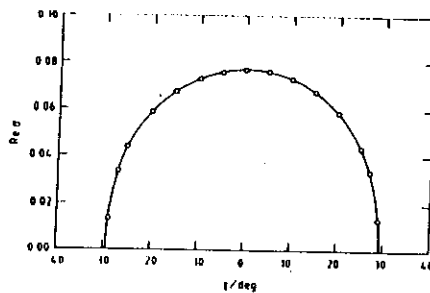


Fig. 5. Growth rate $Re(\sigma)$ vs. γ where γ denotes the angle by which the Floquet vector is rotated out of the ξ, η plane. The circles indicate results obtained from a yet unpublished three-dimensional model of parametric instability for $\alpha = 20$. The angle β was free to adjust such that $Re(\sigma)$ takes its maximum value for any given value of γ .

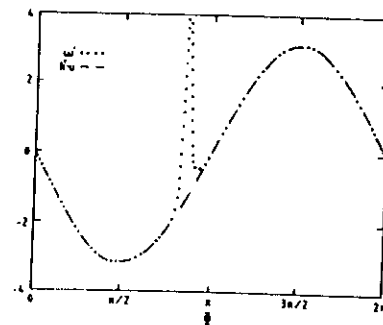


Fig. 6. Disturbance wave frequency, ω' (....), and advection by primary wave fluid velocity, $k' \cdot u$ (---), vs. primary wave phase angle Φ for $(\alpha, \beta) = (20, 11.3^\circ)$. The deviation between both curves is due to a local failure of the WKB approximation.

In atmospheric radar studies it is generally assumed that the temporal fluctuations at a fixed location are entirely due to a "frozen" field of turbulence that is advected by the mean flow (Taylor's hypothesis), i.e.

$$\frac{\partial}{\partial t} = -\mathbf{u} \cdot \nabla. \quad (9)$$

We will show that (9) also holds for the fast growing small-scale instability modes. The Floquet solution (8) indicates that for $\alpha \gg 1$, the instability modes consist of a high-wavenumber oscillation (first factor on the right of (8)) that is modulated by a Fourier series with the periodicity of the primary wave. Consequently the Floquet solution can be approximated by a WKB solution

$$a(\eta, t)e^{i\varphi(\xi, \eta, t)} \quad (10)$$

where a is a slowly varying amplitude and φ a rapidly varying phase angle so that we can define a space and time dependent wavenumber vector and angular frequency by

$$\mathbf{k}' = (\varphi_\xi, \varphi_\eta), \quad \omega' = -\varphi_t. \quad (11)$$

With the dimensionless fluid velocity of the primary wave, \mathbf{u} , we obtain approximations for the time derivative and the advective term from

$$\frac{\partial}{\partial t} = -i\omega', \quad \mathbf{u} \cdot \nabla = i\mathbf{k}' \cdot \mathbf{u}. \quad (12)$$

Figure 6 shows both ω' and $\mathbf{k}' \cdot \mathbf{u}$ as functions of the phase angle Φ in the interval $[0, 2\pi]$. There is good agreement between both quantities except near $\Phi = 0.85\pi$ where ω' tends towards very large values. Detailed investigations indicate that the strong deviations between ω' and $\mathbf{k}' \cdot \mathbf{u}$ are due to a local failure of the WKB approximation to the temporal variation of the Floquet solution. The small-scale parametric disturbances thus are "frozen" in the primary wave flow so that the space and time dependent fluid velocity can be derived from the Doppler shift of radar echoes taking into account the aspect sensitivity of the scattering process.

REFERENCES

1. Y. Muraoka, T. Sugiyama, K. Kawahira, T. Sato, T. Tsuda, S. Fukao and S. Kato, *Geophys. Res. Lett.* 15, 1349 (1988).
2. J. Klostermeyer and R. Rüster, *Adv. Space Res.* 4, # 4, 79 (1984).
3. M. Yamamoto, T. Tsuda, S. Kato, T. Sato and S. Fukao, *Physica Scripta* 37, 645 (1988).
4. R. Rüster, private communication (1990).
5. Y. Muraoka, T. Sugiyama, K. Kawahira, T. Sato, T. Tsuda, S. Fukao and S. Kato, *J. Atmos. Terr. Phys.* 50, 819 (1988).
6. R.P. Mied, *J. Fluid Mech.* 78, 763 (1976).
7. J. Klostermeyer, *J. Fluid Mech.* 119, 367 (1982).
8. J. Klostermeyer, *Geophys. Astrophys. Fluid Dyn.* 26, 85 (1983).
9. P.G. Drazin, *Proc. R. Soc. Lond. A* 356, 411 (1977).
10. M.G. Kelley, D.T. Farley and J. Röttger, *Geophys. Res. Lett.* 14, 1031 (1987).

318